Towards the Automation of Preliminary Bridge Designs with Parametric Design Software

Assessment and optimization of multiple steel-concrete bridge typologies

E.J.H. Fransen

Towards the Automation of Preliminary Bridge Designs with Parametric Design Software

Assessment and optimization of multiple steel-concrete bridge typologies

by

E.J.H. Fransen

to obtain the degree of Master of Science
at the Delft University of Technology,
to be defended publicly on Wednesday February 21, 2018 at 10:00 AM.

Student number:	4092708	
Project duration:	April 24, 2017 – February 21, 2018	
Thesis committee:	Prof. ir. R. Nijsse,	TU Delft, chairman
	Ir. J. E. P. Smits,	TU Delft
	Ir. P. Eigenraam,	TU Delft
	Ing. W. G. M. Freriks,	Movares Nederland B.V.

This thesis is confidential and cannot be made public until February 21, 2019.

TU Delft Delft University of Technology

Abstract

This thesis concerns research into the parametric modelling and optimization of steel-concrete bridge typologies typically found in the Netherlands, in order to further the automation of preliminary bridge designs. The research question posed is: "How can a parametric bridge design model be composed to fit into the overall road design process in order to get a comparative overview of structurally sound bridge designs of different typologies?". Within the literature review some background information is provided about the design of steel-concrete bridges, parametric design, finite element modelling and evolutionary solvers for optimization. With this information seven different bridges are designed according to boundary conditions and requirements posed in a fictitious case. These bridge designs cover the beam-, truss-, arch- and cable stayed bridge typologies. The designs are then parametrically modelled and converted to a finite element model in a single parametric design environment, after which they are structurally analysed and optimized for minimum costs. The result is that, for the fictitious case considered, the Warren truss without verticals is the solution with the lowest costs. This bridge design is able to carry the loads, according to load model 1 from the Euro Codes, with a lower amount of structural steel compared to the girder beam bridges, and the absence of expensive cables in the structure makes it less expensive than the arch and cable stayed bridges. Due to the scope defined at the start of the research, there are some limitations. The costs calculated for the bridges are purely based on the bridge structure itself, foundations and approach structures are not considered and this has to be kept in mind when comparing the bridges. Finally, the research into how to implement this design and optimization tool into the overall design process has not been performed, however, the model is composed in such a way that it will be compatible with minor changes to the start and end of the process.

Preface

This report is the result of my graduation research into the parametric design and optimization of steel-concrete bridge typologies with regard to the developments towards automated design of civil structures. It is the end of almost ten months of work and the final piece of my Masters in Building Engineering at the Faculty of Civil Engineering of the Delft University of Technology.

The research was performed at Movares, where I undertook an internship. Movares provided a framework for my research, and in consultation with my supervisor, Wim Freriks, I formulated the research question. The start of the research was a bit tough, but as soon as I was fully immersed I enjoyed studying and working on this topic. Working at Movares has been a pleasure and I really appreciate the friendly atmosphere and numerous activities I was invited to and participated in.

I would like to thank my supervisor from Movares, Wim Freriks, for providing the topic of this research and his useful and insightful feedback. Especially near the end some valuable improvements on the report could be made thanks to his advice.

Many thanks goes out to my other supervisors, Rob Nijsse, Joris Smits and Peter Eigenraam, who guided me at the start of the graduation and pointed me in the right direction. I also want to thank you for the feedback and discussions during the meetings we had over the course of this graduation.

Finally, I am grateful for all the questions that were answered by the employees of Movares. You provided useful insight whenever I got stuck, this really helped me to keep going.

For now, I wish you a pleasant read.

E.J.H. Fransen
Delft, February 2018

Contents

1 Introduction

In this introduction to the master thesis project the context of this project will be explained and following the problem this brings forward will be stated. With the proposition and research objective the target is defined and questions to be answered are posed. Finally, the approach and scope for this project are presented.

1.1. Subject

For the master thesis project I am doing an internship at Movares Nederland B.V., an engineering and consultancy company specialised in infrastructure. Currently Movares is setting up a new automated design process for the preliminary design of roads, including structures like underpasses and bridges to cross obstacles. The basic idea behind this new process is that large parts of the design process are automated and optimized and the total process is quicker, saving time and money.

It starts with providing input like the start and endpoint of the new road, the desired width of the road or number of lanes, but also choosing between underpasses or bridges and within this also choosing a type of underpass or bridge. An algorithm then starts retrieving information from Geographic Information System-maps (GIS-maps) to find the height of the groundwater table (GWT) and obstacles like rivers, existing buildings, roads or other structures and possibly also defines land ownerships. With all this information the algorithm then tries to find the optimal path for the new road.

From this optimal path come the locations where obstacles have to be crossed with underpasses or bridges. To design and calculate these structures a parametric design model has to be built. Pre-defined inputs for this parametric model, defined by the user or coming from the previously mentioned step, are the width of the road or the number of lanes, the start and endpoint of the structure, the depth of the underpass or the minimal clearance of the bridge with possible positions for intermediate supports. Loads like the soil- and water pressure and the traffic loads are generated automatically based on the geometry, location and functional use. The parametric inputs for the model could consist of different dimensions for different structural elements like the thickness of the outer walls, the thickness of the deck, the dimensions of columns etc. The initial dimensions of the structure are generated automatically based on the geometry, design rules and rules of thumb.

The initial design is then exported to a finite element method (FEM) analysis software program and calculations of the structure for different load cases are performed. The outcomes of these calculations will indicate whether parts of the initial design are over- or under dimensioned. With this information the parameters in the parametric design model can be changed accordingly. Preferably, these changes are performed automatically in a loop of changing the design and calculating the changed design until all parts fulfil the predefined requirements and are not over-dimensioned. The final dimensions of the structure, together with all other loads acting on it, will give the loads that will act on the foundation of the structure.

With the design of the structure ready, the total costs of the whole project can be estimated. By choosing different types of underpasses or bridges, or by changing other input parameters, different end results are obtained which can be compared to each other. The result of this new design process is that the whole design process can be quicker which leads to more information sooner in this process. By generating different designs and comparing them, more substantiated decisions can be made. In the end it is desired to create a visual presentation of the whole project to get a good impression of the complete design.

1.2. Problem Statement

My research will focus on the parametric model for bridges within the new design process. The general problem on which this research will focus is how to construct a correct parametric design model for different bridge typologies, how to optimize these typologies for changing boundary conditions, how to compare the different results and how to implement the parametric model in the overall design process. This problem can be divided into three parts which will be described below.

1.2.1. Bridges

Movares, more specifically the section 'Kunstwerken Beton', or concrete civil works, where I am doing the internship, is mainly involved in construction of in-situ concrete bridges crossing railways or roads. From personal interests and considering the software to be used, it is however decided to investigate bridges consisting of a combination of concrete and steel. In this way the benefits of both materials can be combined. The main bearing structure could for instance be constructed in steel and the deck of the bridge could be a concrete one. Steel has the advantage that it is easier to design and has more architectural freedom, concrete can provide the necessary safety and durability for the structure. Besides, concrete can be used in compression zones and steel in tension zones, exploiting the benefits of both materials' properties.

There are many different typologies for bridges. To get an extensive overview of all possibilities, as many typologies as possible should be investigated. The designs should be adapted to the Dutch environment.

1.2.2. Parametric model

Parametric design is a powerful tool to quickly change or adapt a certain design. If set-up correctly, the design can easily adapt to changing boundary conditions, a large number of different variants can be produced without a lot of effort, or the design can be changed according to the outcomes of structural analyses. However, one has to be careful not to set too many parameters as variable. This will create endless possibilities and thus the speed of the design process is reduced, losing the advantage of the parametric design. The question then arises which parameters to predefine and which to set variable.

The parametric model, which will be used to optimize the previously designed bridge typologies, should fit into the overall design process, enabling a smooth transition of data between software without loss of information. This means it should be able to read the outcomes of the road alignment process, like start and endpoint and the width of the road, and it should be possible to set certain input parameters manually. Furthermore it should be possible for the parametric model to be influenced by FEM-analysis calculations in order to optimize the bridge design.

1.2.3. Comparison

To make a decision on which design is best suited for a specific case, the different optimized designs have to be compared to one another. Each bridge typology differs a lot and to make a good comparison, a valid and consistent approach should be used which is applicable to every type.

1.3. Proposition

By investigating which parameters play a key role in the design of bridges, and therefore deciding which parameters to predefine and which to set variable, a correct parametric design of multiple different bridge typologies is created. By implementing this parametric design to fit smoothly in the overall design process, detailed information about the complete project is known sooner and substantiated decisions can be made earlier.

1.4. Research Objective

The objective of this research is to investigate what parameters are important to create a correct parametric bridge design, to investigate how to implement this parametric design into the overall design process and in the end have a complete comparative overview of different bridge typologies for the same problem.

1.5. Research Question

How can a parametric bridge design model be composed to fit into the overall road design process in order to get a comparative overview of structurally sound bridge designs of different typologies?

1.5.1. Sub Questions

- What are feasible designs for a steel-concrete composite bridge?
- What are key parameters in each type of bridge?
- How should the parametric model be composed?
- How can the results of the different typologies be compared?

1.6. Approach

To be able to answer the research question and sub questions, and therefore to complete this master thesis project, the following approach will be applied.

1.6.1. Bridge Design

This research is part of the preliminary design phase and therefore a standard design per typology will be made, which is suitable for the Dutch environment and which is applicable to many different projects. The outcome will be an advice on which typology is best suited and will be based on structural performance and material consumption. In the end more in-depth information about the typologies will be gathered by incorporating as many different types as possible and by investigating the influence of changes in size and shape. Think of changing the height of a pylon or the number of cable stays.

The environmental conditions in The Netherlands should be considered while designing the bridges. The Netherlands is a flat country with weak soil, this will have consequences on the design and means for instance that suspension bridges are no viable solution.

To make a comparison an overview has to be made of all the different typologies with their characteristics, design rules and rules of thumb. With this information simple preliminary designs will be made which will be optimized with the parametric model for specific cases.

1.6.2. Parametric Optimization

Before the parametric optimization can start, it should be investigated which software to use. The most important thing is that the software is capable of doing the task well. Preference goes to Rhinoceros in combination with Grasshopper and Karamba, these programs are good to use, work in a single environment and have many different add-ons and tools. Additionally, there are many tools to let these programs work together with other software and therefore there might be a possibility to incorporate the parametric optimization into the overall design process.

With the preliminary designs ready, the key parameters can be defined. These will largely influence the parametric design. With these parameters defined the model can be built. At first, a model of the smallest or simplest bridge will be made, before extending this model to create the other bridges. To have a good overview and to keep it as integrated as possible, all typologies will be created on a single sheet and linked to FEM-analysis software, which could be Karamba. When this is ready the bridge designs can be worked out in more detail according to calculation results and eventually be optimized for a specified case.

1.6.3. Decision

To be able to make a final decision on which typology is most suitable for a certain problem, the final designs will have to be compared to one another in a certain way. Cost comparison would be an option, but these calculations have a large variability in results and numerous factors change over time. Another option would be to compare based on influence factors for costs, like material consumption. Possibly a comparison can be made based on structural performance related to the amount of material used. The final results will be presented in a comparative overview.

1.7. Scope

The scope will define the boundaries, and with it some limitations of the research conducted for this master thesis project.

This research will focus on the structural design of steel bridges with a concrete deck. The bridge should support a two-lane road for traffic and a bicycle- and footpath. It will also focus on the parametric design and optimization of bridges together with FEM-analysis, the integration and implementation in the overall design process and on a comparative overview for decision making.

What falls out of this scope is the design of the foundations, the design of joints and bearings and other bridge related structures which are not part of the main bearing structure, like approach ramps. Maintenance and materials other than steel and concrete will not be included. Calculations for fatigue of bridge elements and dynamics will not be performed. Aesthetics of the designed bridges will not be guiding throughout this research. The influence of construction methods will not be taken into account.

2

Background Information

In this chapter the necessary background information is presented to be able to understand and follow the applied methodology and performed research. First, all different steel-concrete bridge typologies will be discussed extensively. Afterwards, information is presented about parametric design, finite element method analysis software and optimization with evolutionary solvers.

2.1. Bridge Typologies

This research will focus on bridges with a main bearing structure consisting of a combination of steel and concrete. A steel main bearing structure is light, and therefore imposes fewer loads on the substructure, and it is easier to erect compared to a concrete girder. The higher mass of a concrete slab, compared to a steel deck, reduces dynamic loads, vibrations and noise. Additionally, the concrete slab is easier to build, cheaper than a steel orthotropic deck, allows for easier paving and is more durable [16]. The disadvantages are that a steel main bearing structure is more expensive than a concrete one and due to restrained concrete shrinking cracks in the slab can occur. Furthermore, for the longest spans the concrete slab induces large additional weight.

Bridges can be classified based on their structural form, all bridges considered in this research can be categorised in the following main typologies:

- Beam bridges
- Arch bridges
- Cable stayed bridges

In the following sections the characteristics of each of these typologies will be described.

2.1.1. Beam Bridges

The basic structural form of the beam bridge is a straight line between the supports, see Figure 2.1. It carries the load mainly by means of bending and shear. When a member carries load by bending, the stresses in this member change linearly over its height from compression to tension. This means that only the outer fibres reach maximum allowable stresses, as can be seen in Figure 2.2. The rest of the material in the member is not fully used and therefore more material is used to carry the same load compared to an element which fully uses all of its material [5]. This inefficiency causes their self-weight to increase significantly with increasing span and therefore beam bridges are mainly used for short to medium spans [13]. Beam bridges can be divided into composite steel plate-girder bridges, composite steel box-girder bridges or truss bridges.

Plate-girder bridges

Composite steel plate-girder bridges are structurally the simplest and they are mostly used for short to medium spans. Figure 2.3 gives a schematic overview of a plate-girder bridge. Typically, this type of bridge consists of I-profile beams, a concrete deck and cross bracing.

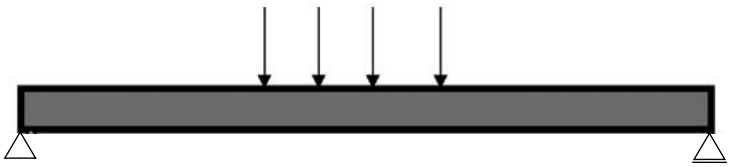

Figure 2.1: Beam in bending

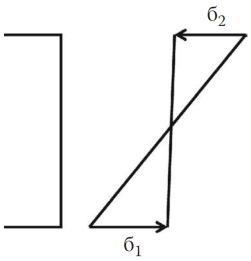

Figure 2.2: Stress for a beam in bending [5]

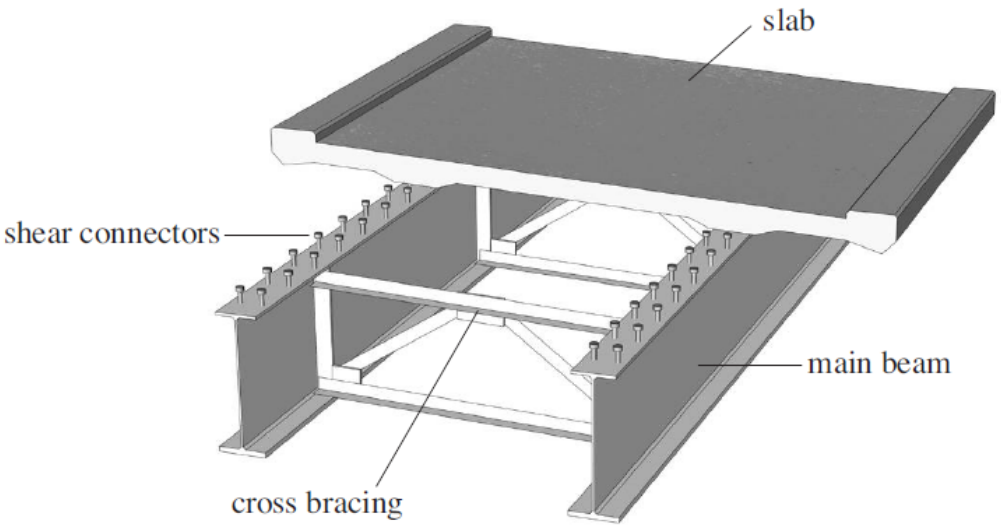

Figure 2.3: Schematic view of a main bearing structure of a composite plate-girder bridge [13]

The I-profile is used for the steel main bearing structure and is the most effective solid section to resist bending and shear. As explained earlier, the largest bending stresses occur at the top and bottom of the cross-section. Therefore the flanges carry the bending moments. The web is needed to connect the flanges and carries the shear forces. The section can be a rolled section, which is known as an I-beam, or it can be a plate-girder, which is a welded section. Rolled sections have maximum dimensions and are therefore restricted to spans of about 30 metres, while plate-girders can span up to 100 metres. Because plate-girders are welded, the dimensions, like the thickness of the flanges or height of the web, can be adjusted over the length of the girder to suit the forces they will be subject to and thus an efficient section is created. Transverse and longitudinal stiffeners might be needed to increase the post-buckling shear strength and to develop inelastic flexural buckling strength, respectively [6].

The concrete deck slab is used to provide a riding surface and to transmit the external traffic loads to the steel girders. The slab must additionally also support various bridge components like curbs, lighting masts or crash barriers and forces acting on these barriers [13]. It is normally formed from reinforced concrete and can be prestressed. The slab can be cast in-situ, cast over prefab slabs or fully precast [16]. With shear studs the slab is connected to the steel girders, ensuring composite action. In this way it also serves as plan bracing, as lateral support for the compression flanges of the main beams, increasing their lateral torsional buckling resistance, and contributes to the longitudinal bending moment resistance [13]. Due to durability requirements and minimum concrete cover of the rebars, the thickness of the concrete slab should always be larger than 240 mm [13]. When using in-situ concrete, problems could arise due to restrained shrinking. Concrete tends to shrink after hardening, and when it is firmly connected to the steel girders, which do not shrink, this shrinking is restrained and the concrete might crack due to large stresses occurring.

Cross bracing provides support against lateral torsional buckling of compression flanges during erection and concrete slab placement, and for all loading stages in negative flexure regions [6]. Lateral bracing for wind loads and participation in live load distribution is also provided. The cross bracing can be a girder, a K-frame or an X-frame, see Figure 2.4. The differential deflection of adjacent girders in skewed bridges is resisted by the cross bracing, causing them to carry significant load [6]. When the cross girders are placed in the upper part of the cross section, these can provide additional support to the slab, as can be seen in Figure 2.5. Especially for wider slabs this is advantageous. The cross girders can also cantilever from the longitudinal girders to further support wide slabs. They are structurally connected to the slab and thus contribute to the transverse bending resistance. The cross girders should be spaced at such distances that the concrete slab can have a constant thickness close to the minimum. Typically this will be around 4 metres [13].

Box-girder bridges

Composite steel box-girder bridges are bridges with a closed cross section. They are especially efficient for medium- to long-span bridges, both curved and tangent [6]. In this range of spans, box-girders can result in less steel consumption compared to plate-girders and have a more aesthetic appearance [20]. Their closed cross section is advantageous for bridges with high torsional loading since closed cross sections have a uniform torsion resistance by means of shear flow around the box. Composite steel box-girder bridges consist of either a closed steel box with a concrete deck, a quasi-closed section with a concrete deck, or a steel U-shaped section which is closed by a concrete deck [13]. Cross bracing inside the box-girder is used to limit distortions.

Open steel sections consist of a bottom flange and two webs, as can be seen in Figure 2.6. A closed section is achieved when the concrete slab is placed or poured on top, after the steel section has been placed in its final position. During erection, the steel open section is susceptible to warping, while the top flanges are also susceptible to lateral-torsional buckling. Due to the fact that the shear centre is below the cross section, eccentric vertical or horizontal loads will make the section unstable [6]. To protect the flange or webs from plate buckling due to high compression stresses that may occur during erection or in the final stage, longitudinal stiffeners can be welded to the steel box-girder [20].

Closed steel sections, Figure 2.6, have a high value of torsional rigidity, improving the stability during both the erection and the final stage. However, due to this high torsional rigidity, large torsional moments will appear. As a result, the section is susceptible to warping, which can result in unexpected failure modes during erection and the final stage. Appropriate internal stiffening should prevent these effects [20]. The same torsional rigidity may also lead to high tension forces on the shear studs connecting the corners of the box with the concrete slab. Without sufficient reinforcement, a pull-out concrete failure is possible [20].

The quasi-closed section lowers the steel consumption compared to the closed section and increases the torsional rigidity compared the open section, see Figure 2.6. The top lateral bracing closes the section while reducing the weight and cost of the cross section [6].

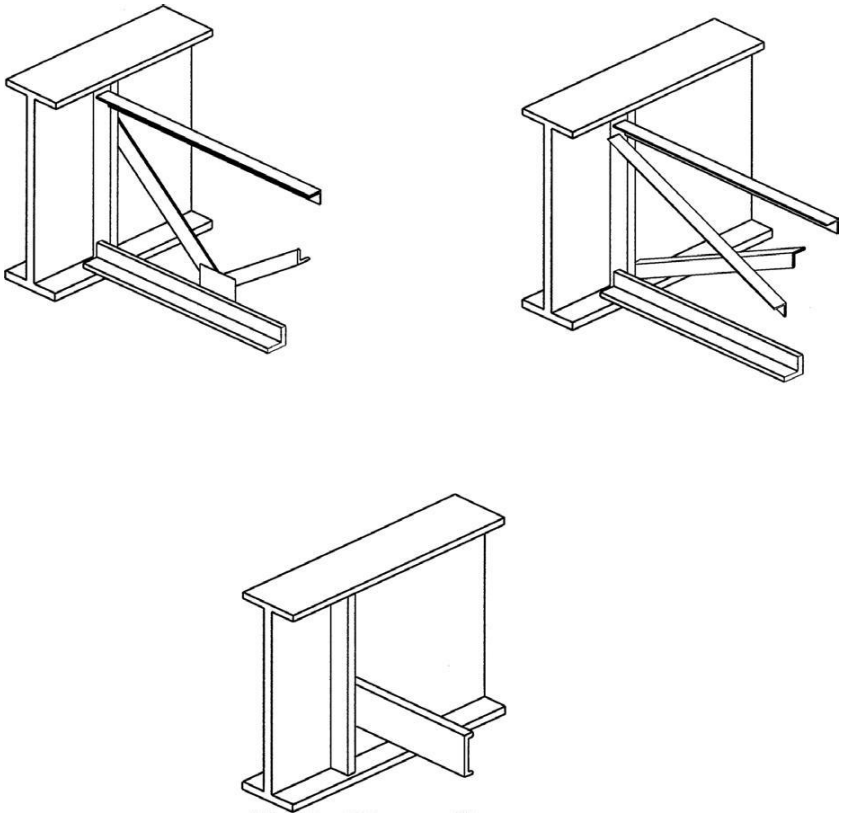

Figure 2.4: Schematic overview of cross bracing for girder bridges [6]. Top left: K-frame, top right: X-frame, bottom: girder

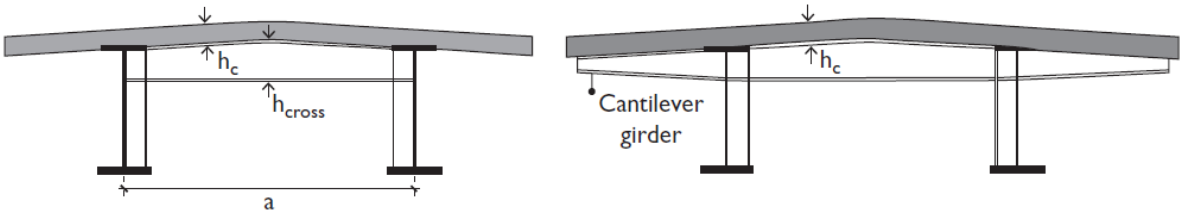

Figure 2.5: Schematic overview of cross girder supporting deck slab [13]

To prevent a spreading effect in the open steel section prior to hardening of the concrete slab, horizontal transversal bracing in the form of spreading ties is needed. To further stabilize the open tub and to limit distortions caused by temperature effects during construction, top lateral bracing is used. After hardening of the concrete, the transversal and lateral top bracing serve no further function, but do carry a locked-in force [6]. Internal K- or X-trusses or diaphragms limit distortional effects, maintaining the geometric integrity of the cross section.

Considering the dimensions of the cross section, narrower boxes are preferred to wider boxes. Narrower boxes have a larger resistance to torsional effects and distortion, and they have smaller flanges, which have a greater resistance to buckling [6]. Wider boxes need additional longitudinal and transverse stiffeners, which lead to demanding detailing and a dense net of welds. This raises the structures' cost and risk of fatigue failure [20]. Due to the shear lag effect, parts of wide flanges may be considered as ineffective and a reduced effective width must be applied. Therefore, excessive widths should be avoided [20]. Making use of the trapezoidal section, the width of the bottom flange is reduced. Whilst using the same amount of material, required for bending in the bottom flange, in a thicker plate, the stability of the bottom flange is increased, the shear lag effect is reduced as well as the need for longitudinal stiffening [6]. Additionally, the aesthetic appearance is enhanced and the trapezoidal shape reduces fatigue problems due to secondary vibrations and is more stable to fabricate and erect [6]. With narrower boxes the spacing is increased, which leads to fewer girder lines and a more economical design. The torsional stiffness of the boxes provides a fixed end support for the transverse

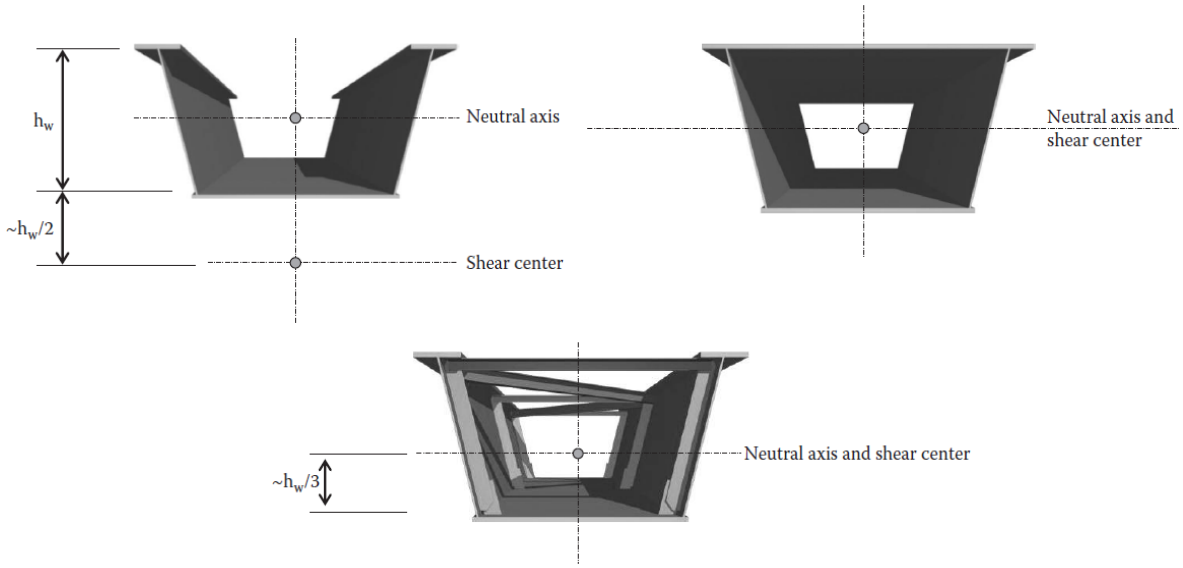

Figure 2.6: Schematic overview of different cross sections for box-girders [6]. Top left: open, top right: closed, bottom: quasi-closed

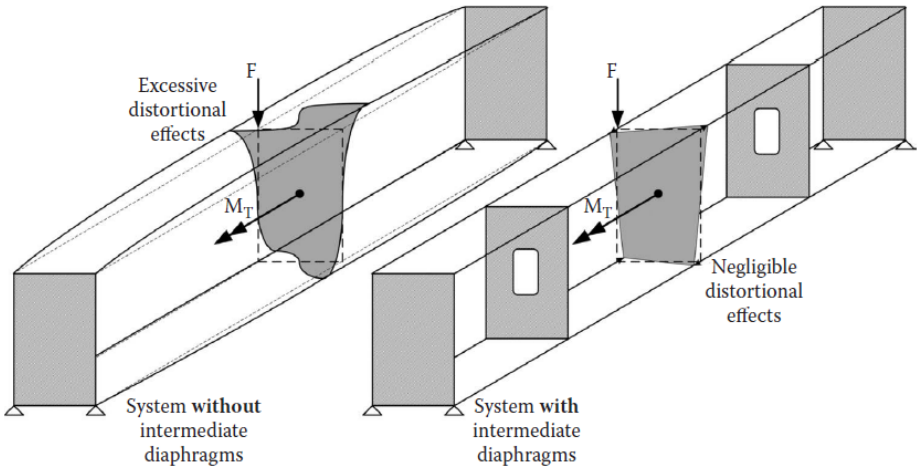

Figure 2.7: Role of intermediate diaphragms [20]

bending moments in the slab. This stiffens the superstructure transversely and provides the opportunity to increase the transverse slab spans [6].

Truss beam bridges

During the nineteenth century development and construction of truss bridges peaked. Many types were developed empirically, designed to carry heavy train loads. After the breakthrough of Squire Whipple, which is to treat all connections of the truss as frictionless pin-joints, resulting in all members being subjected only to compression or tension forces, the more complex and less functional types gradually disappeared [6]. The relatively high fabrication costs of truss members and the many joints have meant that they tend to be economic only for heavier loads or larger spans today [7]. During the end of the twentieth century the warren truss without verticals has resurfaced as an aesthetically pleasing bridge design. This is due to the parallel chord configuration, where sway frames are omitted from the design, except at locations of portals, which has led to a simplification of the truss detailing [6]. Figure 2.9 shows which truss members are under compression or tension for a Warren truss without verticals subject to a vertical load.

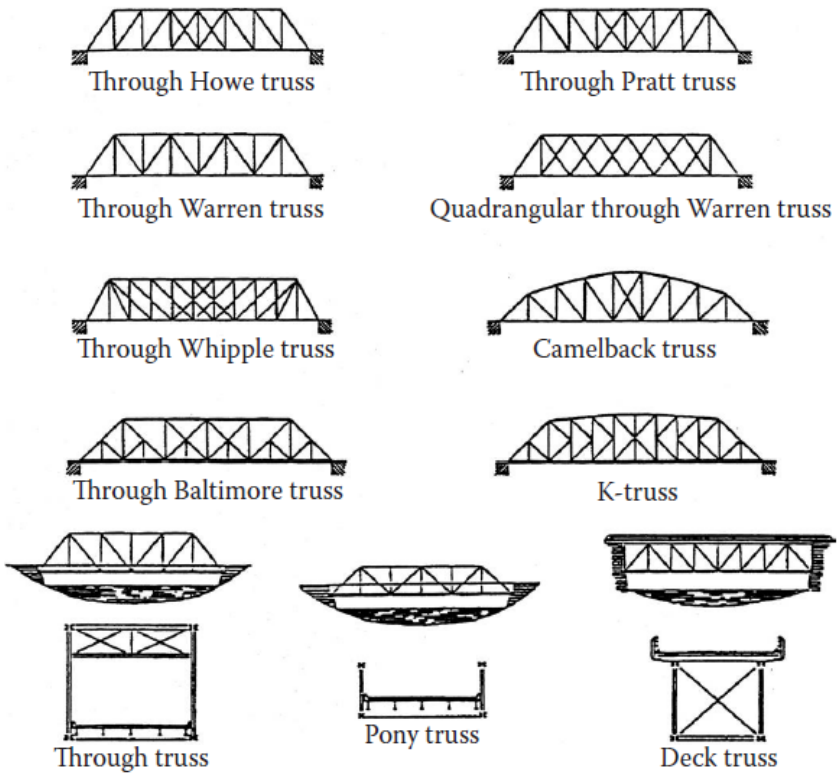

Figure 2.8: Overview of historic truss types and the different forms [6]

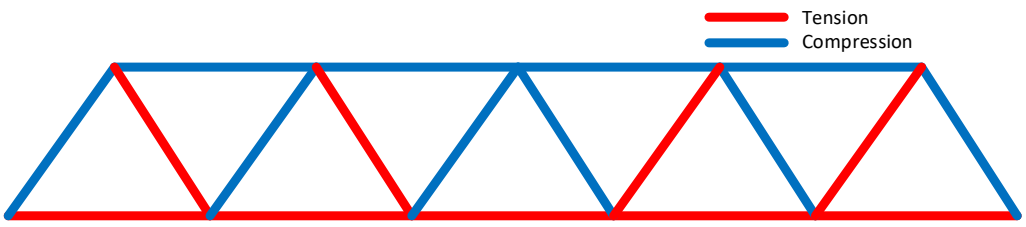

Figure 2.9: Schematic representation of forces the truss members are subject to for a Warren truss without verticals under bending

There are three basic forms of truss bridges, through trusses, deck trusses and half-through trusses. Figure 2.8 gives an overview of some historic truss types together with the three forms. With a through truss form,

the deck is supported by the lower chords of the truss. This means that the deck is in the tensile zone of the structure, and the truss design should accommodate sufficient clearance above the deck for traffic to pass. The deck is supported by the upper chords of the truss with a deck truss. In this case the concrete deck is in the compression zone of the structure, where it can act more efficiently as a composite section [7]. With a half-through truss, the deck is located somewhere in between the upper and lower chords of the truss.

With four planes capable of resisting shear and end portals sufficient to transfer the shear back into vertical loads to the supports, the truss behaves much like a closed-box structure [6]. An overview of typical truss members can be seen in Figure 2.10. The top and bottom lateral bracing brace the compression chords and resist wind loads. Sway frames increase the torsional rigidity of the truss and end portals carry torsional loads, resulting from wind loads and uneven vertical loads, into the bearings [6].

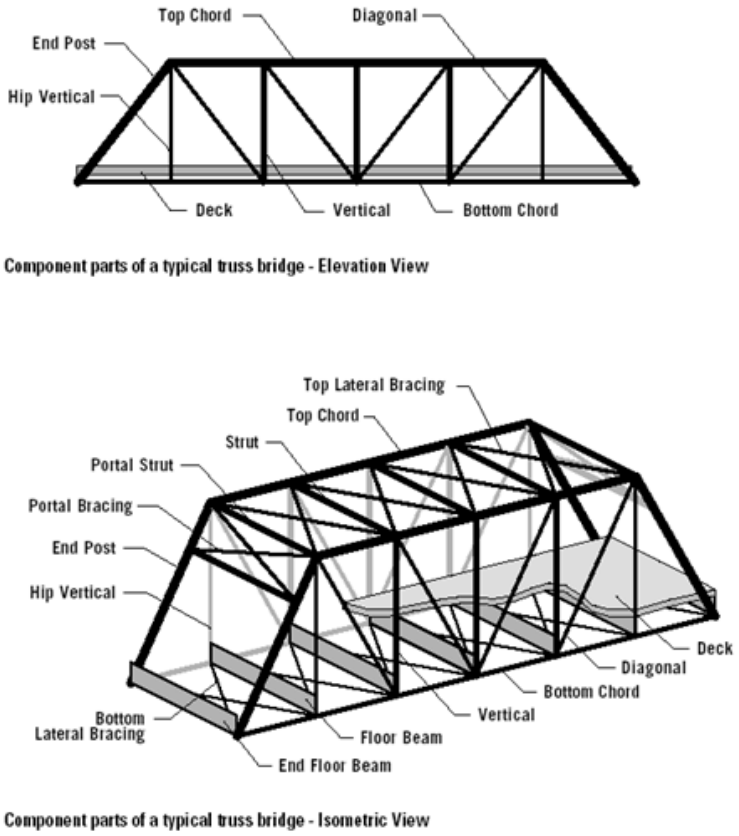

Figure 2.10: Typical truss members [10]

The most used truss members are box- or H-shaped. H-shaped members are more economical in terms of fabrication, easier to connect to the gusset plates and easier to maintain since all surfaces are accessible. The box-members are generally structurally more efficient and resist wind-induced vibrations better. The choice for members is very project specific, H-shaped members are more advantageous in case of tension members since they are easier to connect to the gusset plates, box shapes have an advantage as compression members since their slenderness ratio about the weak axis is usually lower [6].

The conventional deck system of truss bridges consists of transversal floor beams, longitudinal stringers and a concrete slab. The concrete slab is supported by the longitudinal stringers, which transfer the load through the floor beams to the truss. The floor beams are located at the joints between the chords and the diagonals.

2.1.2. Arch Bridges

Arch bridges are one of the oldest forms of bridges. Initially, arch bridges were constructed from stones or masonry with the deck on top of the arch. Nowadays, the arches are constructed either in concrete or in steel. Due to its shape, the arch transfers loads primarily by means of compression to the supports. This

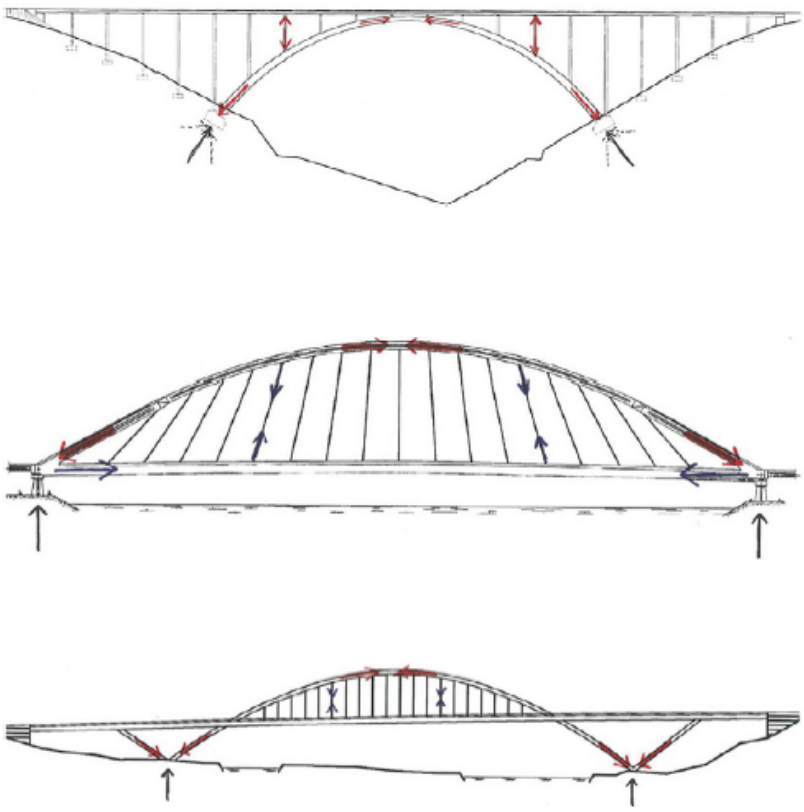

Figure 2.11: Arch bridges classified by position of the deck including flow of forces, (a) deck arch bridge, (b) through arch bridge, (c) half-through arch bridge [16]

would imply that most arches are constructed in concrete, but steel has the advantages of a lower self-weight, quicker erection, and weldability [13]. The deck of the arch bridge can be located on top of the arch, the deck arch bridge, at the location of the supports of the arch, the through arch bridge, or somewhere in between, the half-through arch bridge, see Figure 2.11. The position of the deck largely depends on the environment of the project. While spanning a river in shallow terrain, a lower deck might be more suitable, and to cross a gorge with steep walls, an upper deck would be more beneficial. In general, concrete arches tend to have an upper deck and steel arches tend to have a suspended lower deck [13]. Arch bridges are competitive for medium to long spans [13]. Figure 2.12 gives an overview of the arches' terminology.

Arch bridges can be classified in multiple manners. The first one is by the position of the deck, as discussed previously. The space between the arch and the deck of a deck arch bridge is called the spandrel. If the spandrel is filled with solid materials, like soil, it is called a solid spandrel. If the loads of the deck are transferred to the arch by means of columns, it is called an open spandrel arch bridge. In a through arch bridge the deck is located at the level of the supports of the bridge. The loads from the deck are transferred to the arch by means of tension hangers. The horizontal thrust of the arch is often absorbed with a tie, which is usually the deck of the bridge. Especially for bad soil conditions the use of a tie, which can be a steel box girder, steel plate girder or even a prestressed concrete girder, is often adopted [6].

The second method of classification is by means of connections. The arch can be hingeless, two-hinged or three-hinged, see Figure 2.13. The three-hinged arch is statically determinate and the hingeless arch is threefold statically indeterminate. With higher indeterminacy, the arches sensitivity to differential settlements, temperature variations and arch shortening increases. Adding hinges ensures that these secondary effects decrease or nearly disappear, but they increase construction and maintenance costs, especially for concrete arches, and make the arch more flexible [6]. Therefore, most modern concrete arch bridges are designed without hinges.

Through arches can be classified by the arrangement of the hangers. Most hangers consist of rolled sections or wire ropes and are usually vertical. Diagonal, truss-like hangers are also used since they result in a

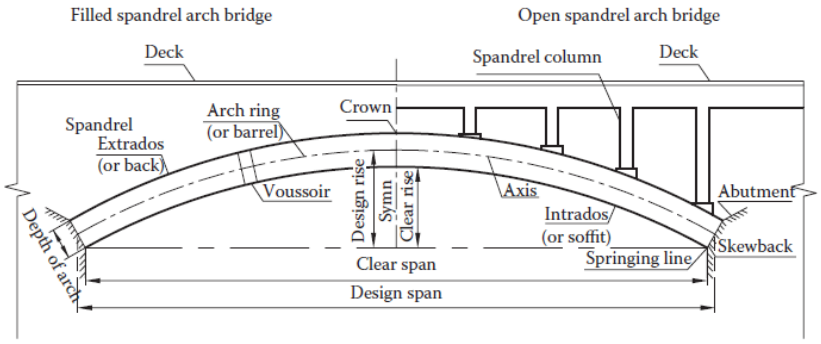

Figure 2.12: Terminology of arch bridges [6]

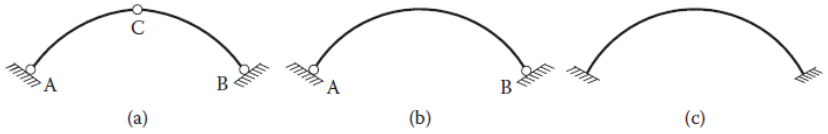

Figure 2.13: Connections of arch bridges, (a) three-hinged, (b) two-hinged, (c) hingeless [6]

reduction of the bending moments in the deck and arch rib and in smaller deflections. Additionally, diagonal hangers reduce the tendency for buckling in the arch plane. As a result, both the arch and the deck can have a more slender design [6]. Vertical hangers are, however, easier to construct [16].

The general shape of the arch can be parabolic, elliptical, circular, a catenary or even polygonal [6]. Depending on the load acting on the arch, a perfect arch shape, where only compressive forces are acting along the arch axis, is possible. However, due to the numerous changing forces and loads acting on the bridge, this perfect shape is impossible to create and therefore bending stresses will occur in the arch rib. By letting the arch axis coincide with the thrust line of the design loads, these bending moments can be kept to a minimum. Similarly, the rise-to-span ratio of the arch is of importance. A high arch, which has a high ratio, develops large bending moments due to increased arch length and self-weight. A shallow arch, with a small ratio, will have high compression forces in the arch, and therefore also large horizontal thrust at the foundations.

The cross sections used for concrete arches are usually solid rectangular, I-shaped or hollow boxes. The solid sections are mostly used for short spans while the hollow box sections are suitable for longer spans due to their higher bending and torsion resistance. The hollow box sections can have multiple cells with varying dimensions along the span. Concrete arches tend to have two individual ribs with lateral bracing in between [6].

For steel arches the cross sections usually are I-, circular- or box-shaped. To avoid local buckling under compression forces, stiffening is required [6]. The steel arch consists of solid ribs or truss ribs, with bracing. Truss ribs are usually used for larger spans, since the truss members are smaller and lighter than the ones in solid ribs. This is also advantageous for transportation and erection.

A steel concrete composite arch bridge is achieved by making use of concrete filled steel tubes (CFST). Just like the steel arch, the rib of the CFST arch consists of solid or trussed sections. For a solid section a single tube or a dumbbell form is used, see Figure 2.14. For a trussed section a multiple of the dumbbell form is used [7]. Most of these types of arch bridges are constructed by first assembling the steel framework with the help of temporary cable stays. When the arch is closed, the main tubes are filled with concrete, after which the tubes have their final strength and stiffness. Depending on the type of arch, the deck slab is then placed on top of the arch or suspended from it [7]. By filling the steel tubes with concrete, the axial and bending capacity is higher, the stiffness is increased and the members are less prone to buckling [7].

2.1.3. Cable Stayed Bridges

The cable stayed bridge consists of a deck, cable stays and one or more pylons. These elements form a number of super-imposed triangles [7]. The vertical loads acting on the bridge are transferred by the girder to the stay cables, which provide elastic supports, and through tension in the cables to the pylons [6]. The forces in these members are in equilibrium, compressive axial forces in the pylons and girders with the tension forces

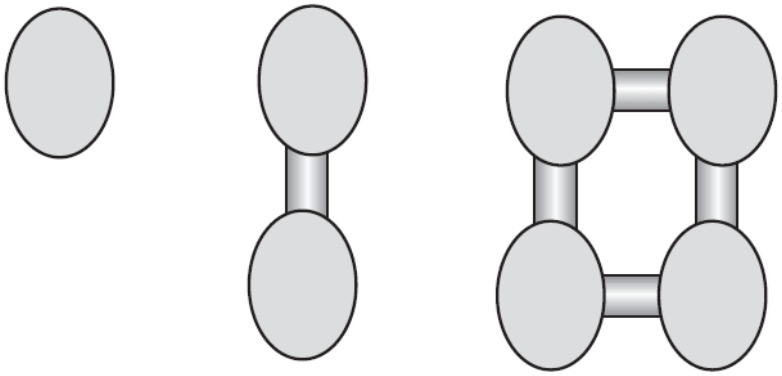

Figure 2.14: Some forms of CFST, (a) single tube, (b) dumbbell, (c) double dumbbell [7]

in the cables, and therefore the symmetric cable stayed bridge is a self-anchored structure. This means that no heavy anchor blocks are needed, which makes this type of bridge suitable for cases with bad soil conditions. This also speeds up the erection time since the construction of the superstructure, with the progressive cantilever method, can start when the height of the pylons reach the first anchor points [6]. Disadvantage of this system is the high compression force in the girder.

There are two basic cable configurations, namely the fan stay system and the harp stay system, see Figure 2.15. The fan system was used for the early designs of modern cable stayed bridges. The cable stay is anchored in the main span, passes over the pylon and anchored at the back span. In this way the cables have a maximum eccentricity from the deck and impose minimum moment to the pylon [9]. As spans became larger and the number of cables increased, there was not enough space for all the cables to pass over the pylon. With the modified fan stay system all cables are individually anchored near the top, with a vertical spacing of around two metres. As the behaviour of the cable system is dominated by the outer cable attached to the top of the pylon, the structural efficiency of this modified system will almost be the same, provided all anchor points are close to the top of the pylon [9].

The cables of the harp system are placed parallel to each other and at equal spacing over the height of the pylon. This arrangement can be aesthetically pleasing and emphasises the flow of forces. This arrangement is, however, structurally less efficient as the fan system. Under a-symmetric loading, the triangle of forces can't balance the load and the system has to rely on bending resistance of the pylon, the deck or a combination of both. To overcome this disadvantage, the back stay cables can be anchored to the approach piers [9].

The pylons are one of the most visible elements of the cable stayed bridge and therefore their aesthetic appearance has a large impact and is of high importance. The pylon should, however, be able to transmit the forces, induced by the anchoring of the cable stays, towards the foundation. Preferably it will do so by compression, minimizing any eccentricities [9]. The design must accommodate the soil conditions and topography of the site, adapt to the cable layout and carry the forces economically [9]. The pylon can be constructed in concrete, steel or a composite of both materials. Different types of pylons are illustrated in Figure 2.16.

If only one single plane of stay cables is used, the torsional rigidity has to be provided by the bridge deck. This requires more complex and heavier decks with greater depth. By using two planes of stays, the deck is suspended at the two transversal ends and will have improved torsional rigidity. Therefore, the deck can be very simple and slender. The two planes of stays can be either vertical, connected between the edge of the deck and the pylon legs located outside of the deck cross section, or inclined, connected between the edge of the deck and an inverted Y-frame or A-frame [9]. Inclined stays form a transverse frame, thus further increasing the stiffness and stability of the structure. They improve the torsion response to both aerodynamic effects and eccentric live loads [9].

There are three main types of cables in use, locked coil ropes, parallel wire cables and parallel strand cables. They are depicted in Figure 2.17. The locked coil ropes have a high density and are prefabricated. Therefore, their quality is high, but transportation and installation is difficult, especially for longer spans. Parallel wire cables are also prefabricated. Their stiffness, high resistance to fatigue and low aerodynamic resistance do make them suited for longer spans. The strands of parallel strand cables are installed one by one, which makes installation easy and tensioning light [16].

The deck of the bridge is not only carrying traffic loads, but also the horizontal component of the stay

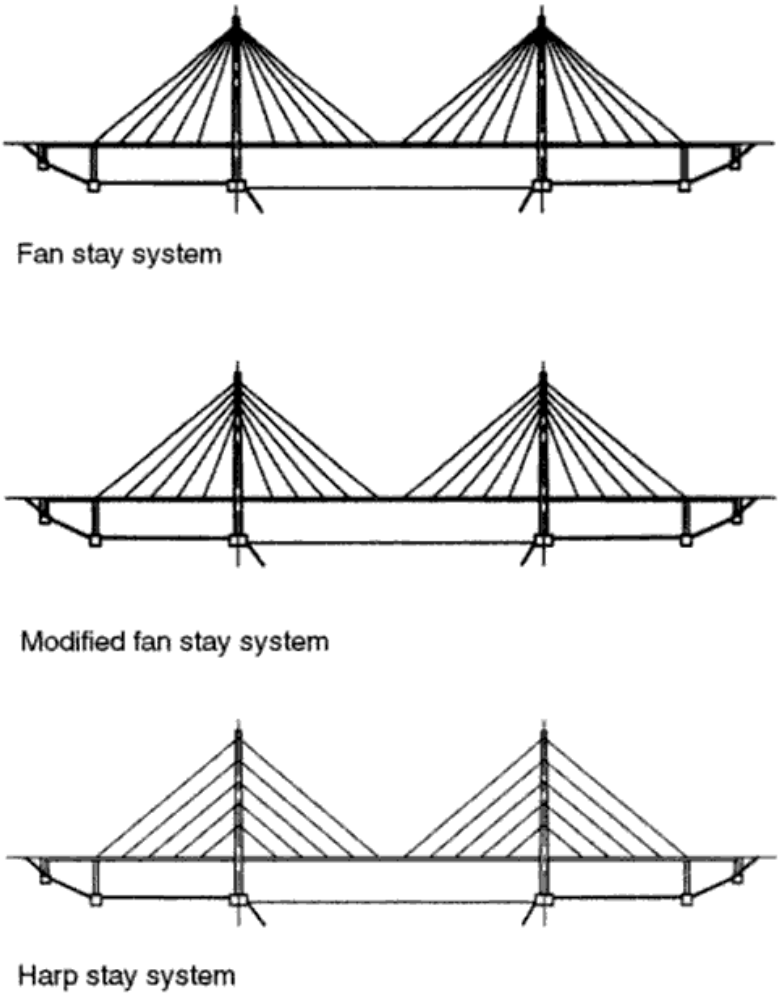

Figure 2.15: Cable stay arrangements [9]

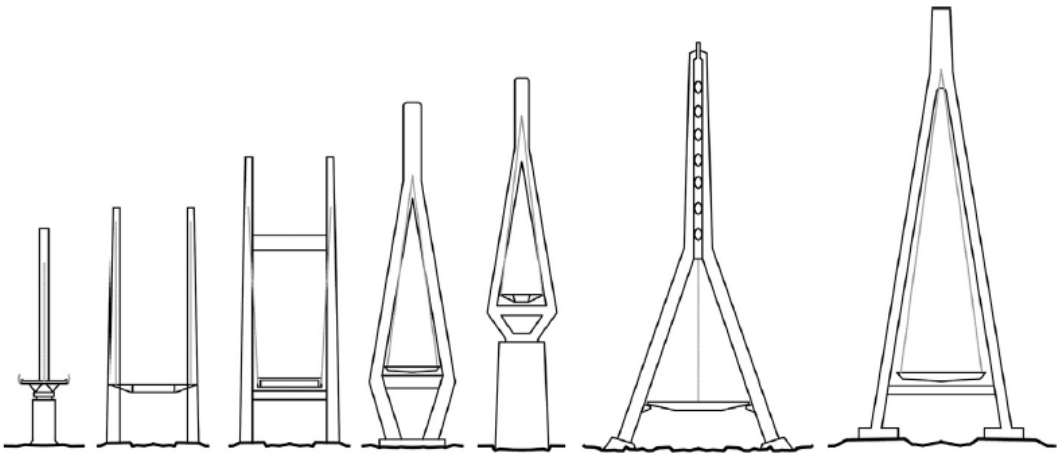

Figure 2.16: Configurations of pylons for cable stayed bridges [16]

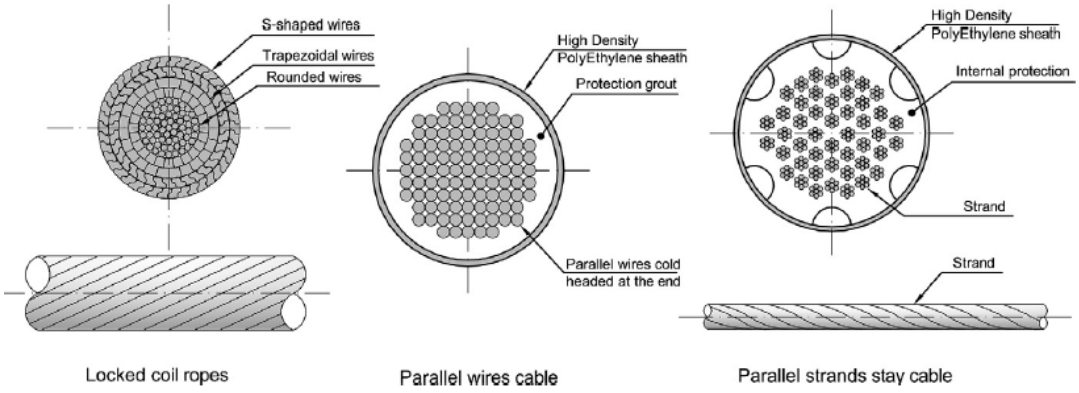

Figure 2.17: Cross section of the main stay cable types [16]

force. As such, the deck is loaded in bending and compression. It can be constructed in steel, concrete or a combination of both. Concrete is an efficient material to use for compression members, but its higher self-weight leads to larger loading of the stay cables. For long spans a steel orthotropic deck is more economical. When two planes of stays are present, the bridge deck can be constructed with longitudinal girders, cross beams at the locations where the stays are anchored to the deck, and a deck slab. For bridges with only a single plane of stays, the decks are always box girders to provide torsional rigidity [16]. Mainly for long spans, or for sites with strong winds, the deck must be streamlined, reducing drag and improving aerodynamic stability [16].

2.2. Parametric Design

With parametric design geometry is created from an initial family of parameters. These parameters are related to each other through designed associations and relations. A hierarchy of these geometric and mathematical relations is generated by the use of variables and algorithms, and the result is a certain geometric design. This geometric design is not fixed, but the whole range of possible outcomes can be explored that is allowed by the variability of the initial family of parameters [15].

Parametric design can be performed by using Textual Programming Languages (TPL) or Visual Programming Languages (VPL). TPL's are often provided by CAD applications and require some programming skills, whereas VPL's require no knowledge of scripting or programming. Programs in a VPL consist of iconic elements that can be manipulated according to some spatial grammar [14]. An example of a VPL is Grasshopper, which is a graphical algorithm editor using generative algorithms and is tightly integrated with Rhinoceros3D [2]. In Figure 2.18 an example of visual programming with Grasshopper is provided, as well as the corresponding output in Rhinoceros3D.

2.3. Finite Element Methods

Laws of physics for time- and space-dependent problems, such as reactions to forces, vibrations or heat, can be expressed in partial differential equations (PDE). These PDE's cannot be solved with analytical methods for most problems and geometries. By discretizing the problem an approximation of these PDE's can be constructed with numerical model equations. These can be solved using numerical methods, which are in turn an approximation of the real solution to the partial differential equations. Finite element methods (FEM) compute these approximations [8]. In general they break down an object into a very large number of finite elements and predict the behaviour of every element with mathematical equations. All individual behaviours are summed up to predict the actual behaviour of the object.

2.4. Evolutionary Solvers for Optimization

To optimize the bridges an evolutionary solver is used. Evolutionary solvers try to find the optimal solution by using genetic algorithms. The first introduction of this technique is in the paper "On the Organization of Intellect" by Lawrence J. Fogel in the early sixties [18].

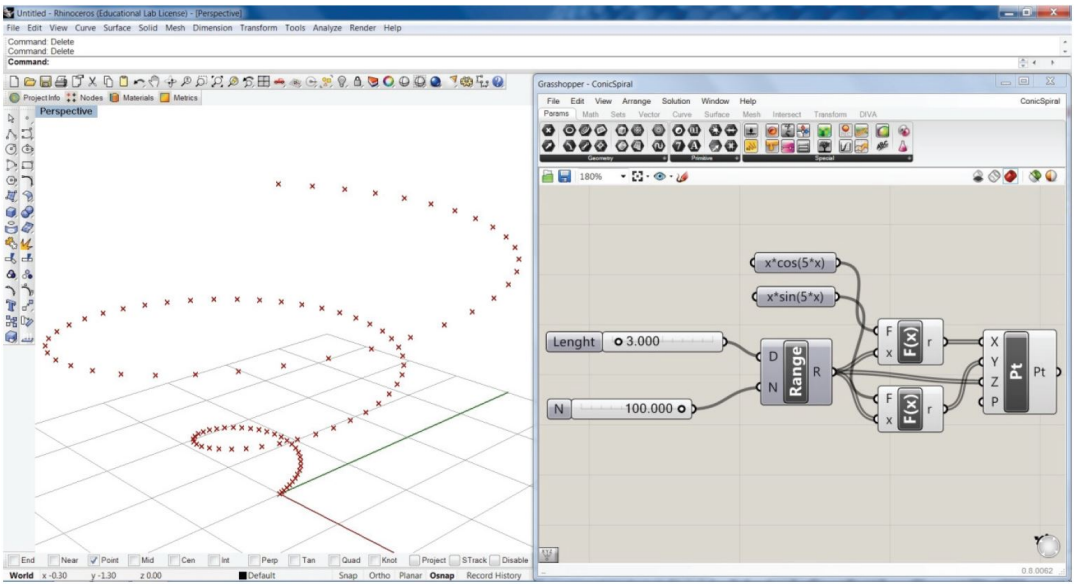

Figure 2.18: An example of visual programming with Grasshopper where the points of a conical spiral are computed (right) with corresponding output in Rhinoceros3D (left) [2]

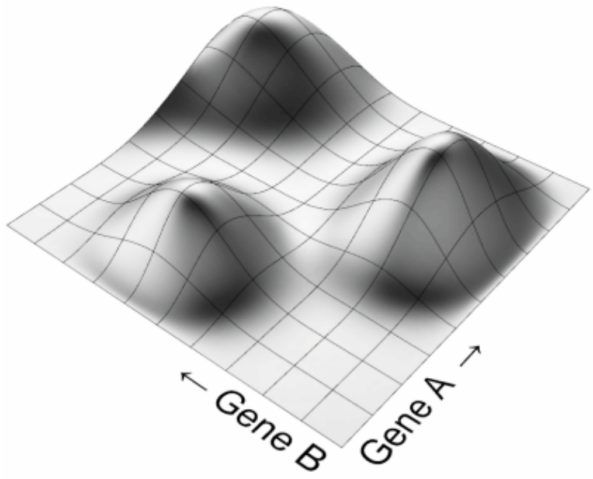

Figure 2.19: Fitness landscape of two genes [18]

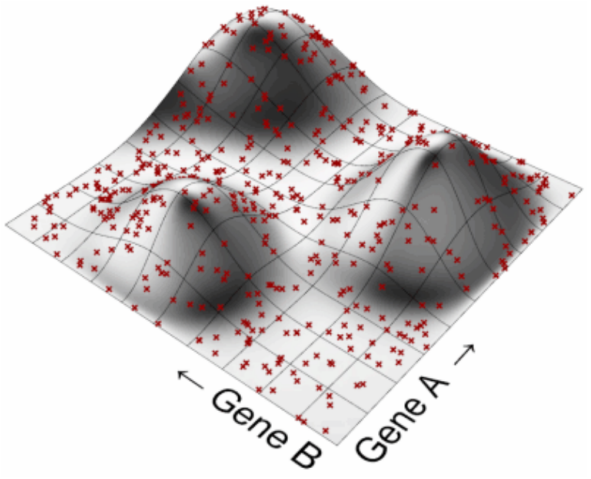

Figure 2.20: Fitness landscape populated with random genomes [18]

2.4.1. Fitness

Evolutionary solvers test the fitness of every solution regarding any combination of input parameters. The fitness can be whatever we want it to be, in the case of this thesis it could be the amount of material used, expressed in the weight of the bridge structure. It is the goal to minimize the weight which is the result of a certain combination of the input parameters defined earlier in the process.

In evolutionary computation input parameters are described as genes and the fitness of the solution, which is the result of a combination of genes, can be depicted in a fitness landscape. This landscape will have n+1 dimensions, n being the number of genes. The matter will therefore be explained using 2 genes. Figure 2.19 shows the fitness landscape of Gene A and B, where every combination of A and B results in a certain fitness of the solution. The evolutionary solvers' job is to find the highest point in this landscape. In case of a minimization this landscape will be inverted and then the objective will be to find the lowest point.

At the start of optimization the shape of this landscape is yet unknown, therefore the solver starts by populating this landscape with random individuals. These individuals are called genomes, which are specific values for each gene. In the example this could be $\{A = 3, B = 6\}$ [18]. The solver then assesses the fitness of every generated genome, which gives Figure 2.20.

Since the solver is looking for the highest grounds, it kills off the worst performing genomes and focusses

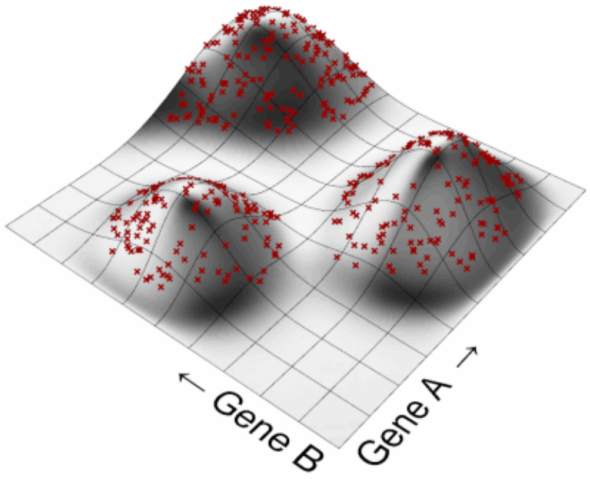

Figure 2.21: Fitness landscape with best performing genomes [18]

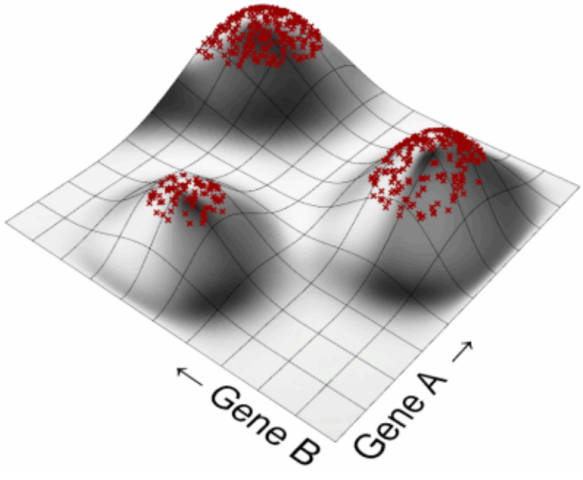

Figure 2.22: Fitness landscape where the highest peak is reached [18]

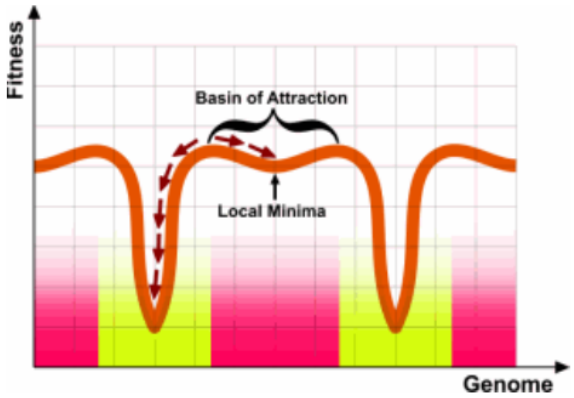

Figure 2.23: Fitness landscape with global and local minima [18]

Figure 2.24: Chance of mating for isotropic selection [18]

on the remainder, Figure 2.21 shows this remainder. Since the first generation of genomes was picked at random, it is unlikely that the best solution is already amongst them. Therefore, the solver breeds the best performing genomes of generation 0 to create generation 1. When breeding, the offspring will end up somewhere in the intermediate model-space, exploring fresh ground [18]. The new population is no longer completely random and will be clustering around the three peaks in the fitness landscape. These steps are then repeated, killing the worst performing and breeding the best performing offspring, until the highest peak is reached, as can be seen in Figure 2.22 [18].

Since high fitness is rewarded by the solver, each individual will try to maximize its own fitness. It will therefore climb the steepest way uphill, in the same way as water flows the steepest path downhill. This means that every peak in the landscape has its own basin of attraction. This basin says nothing about the quality of the peak, since a large basin can have a low peak. These low peaks are called local optima, see Figure 2.23, and if there are lots of them, it makes it hard for the solver to find the global optimum, since many genomes get stuck at these local peaks.

2.4.2. Selection

The evolutionary solver has to select which genomes get to mate to produce offspring and which ones don't. There are many selection algorithms available, the most basic ones will be described.

Isotropic selection is a selection algorithm where every genome gets to mate. In fact, one could say there is no selection. The function of this algorithm is to damp the speed of running uphill, and therefore preventing the solver to get stuck at a local optima. Exclusive selection is an algorithm where only the top X% gets to mate. The third algorithm is biased selection, where the chance to mate increases with higher fitness. This

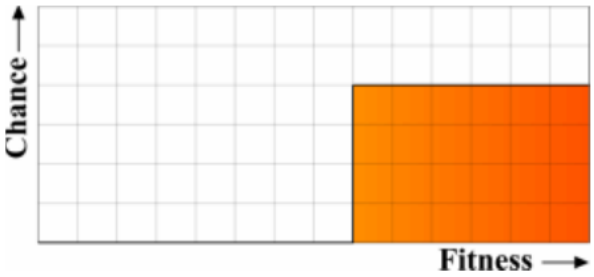

Figure 2.25: Chance of mating for exclusive selection [18]

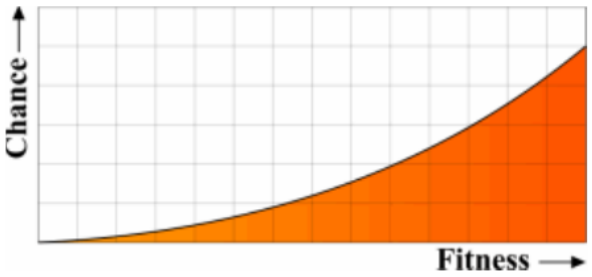

Figure 2.26: Chance of mating for biased selection [18]

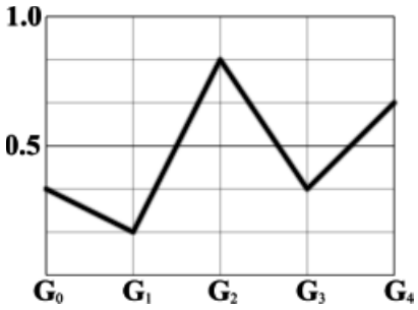

Figure 2.27: Genome graph of a genome with five genes [18]

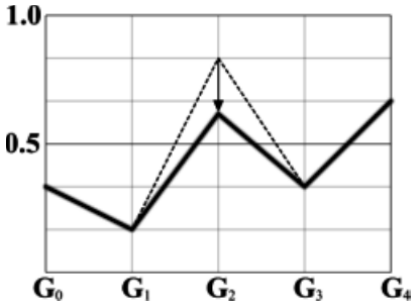

Figure 2.28: Point mutation of one gene in the genome graph [18]

algorithm can be amplified by using power functions, damping or exaggerating the curve [18]. Figures 2.24, 2.25, and 2.26 show the chances of mating for the fitness of the genome of these different algorithms.

2.4.3. Coupling and merging

Once the selection of genomes which are allowed to breed is made, these genomes have to be coupled. Finding a mate for a selected genome is based on distance in gene-space. As explained earlier, genomes consist of a number of genes, or input parameters, and the distance in gene-space is described by the similarity of genes. The less similar the genes, the further apart are the genomes.

The possible mate should not be too close. If two genomes are very similar and their fitness is high, this could lead to fit offspring. But if only genomes which are very similar breed, the genetic diversity will decline, which could be called incest, increasing the risk of getting stuck at a local optimum and decreasing the chance of finding another basin. On the other hand, excluding all genomes in close proximity will increase the chance that the offspring will end up between two peaks in the fitness landscape, in a valley. It seems best to balance the distance between the genomes to maintain diversity and to prevent incompatibility.

When a mate is selected, offspring has to be produced. Two basic options to create offspring are crossover coalescence and blend coalescence [18]. With crossover coalescence, the offspring inherits a random number of genes from one parent, and the rest from the other. The gene value is maintained with this method. Blend coalescence combines the genes from both parents, essentially averaging their values. Preference can be assigned relative to the fitness of the parent, where the gene values of the fitter parent are more prominent.

2.4.4. Mutation

Mutation of genes is a way to introduce diversity. All previous steps of selecting, coupling and breeding are intended to increase the fitness of the genomes, but they also decrease the genetic diversity. By mutating some genes diversity is introduced and this decreases the chance for the solver to get stuck at local optima. It therefore enables the solver to keep exploring the fitness landscape.

Figure 2.27 shows a genome graph. In this graph one genome consisting of five genes is shown. The genes are set along the horizontal axis, while the range of each gene, from 0% to 100%, is set along the vertical axis. Each genome has its own genome graph, which makes this a suitable representation to find sub-species or lone individuals [18]. Figure 2.28 shows a point mutation of one of the genes, therefore also changing the genome graph.

3

Bridge Design

Before the optimization of the different bridge typologies can start, it should be clear which parameters are of importance in the structural behaviour of each type of bridge. For each typology one or more basic designs are made, based on a couple of requirements and suitable for the Dutch environment. The designs will be basic to eliminate any parameter that is only influenced by aesthetics or other choices not related to the structural behaviour. Based on the basic designs the most important parameters can be defined.

3.1. Requirements

To be able to compare the different typologies, all bridges will have to satisfy the same set of requirements. These requirements should be defined in such a way that for every typology a feasible design is possible. Otherwise it could occur that one typology will never yield an acceptable solution and then the comparison will not be fair. Girder- and truss beam bridges, as well as arch bridges, are able to span a single distance without intermediate supports. This is not the case with cable stayed bridges. To prevent large bending moments in the pylon, the forces on both sides of the pylon should be balanced. This can be done by means of large anchored backstays or by providing multiple spans.

With this in mind a fictitious case is developed where a road has to cross a river with two adjacent roads. Since girder beam bridges have a maximum range of about eighty to ninety metres, the main span, crossing the river, will be sixty metres long. On both sides of the river there will be a zone of five metres available for supports. Next to this zone, a two-way road with cycle- and footpath is located. For this road a width of fifteen metres is reserved. The clearance of the bridge will be twelve metres, to let the largest inland ships, of class VI, pass, which need a clearance of 11.35 metres [4]. A schematic overview of this case is presented in Figure 3.1, with one design for a cable stayed bridge visible. On the bridge itself, the minimal clearance for road traffic is 4.80 metres, 4.50 metres for the height of trucks plus a safety margin.

The road which crosses this river will be a single carriageway with a cycle-and footpath on one side, this is a common configuration. Figure 3.2 gives an overview of the Dutch single carriageway. It consists of two traffic lanes of 2.75 metres wide, a median of 0.80 metres in between the traffic lanes, road markings and a shoulder of 2.40 metres wide. The total paved width is 7.50 metres. For bridges, the shoulder, and therefore also the obstacle free zone, may be decreased in width as long as the hazardous zone is shielded [19]. For the road design of the bridge, the traffic lane is widened to a width of 3.00 metres. On one outer side there should be room for a parapet, an inspection walkway and a fence. The standard width for this part is 1.40 metres. The footpath on the other side should be 2 metres wide [12], and the cycle path should be 3 metres wide [21]. For the hard shoulder a width of 0.80 metres is chosen, so that the total width of the bridge deck is 16 metres. A schematic cross section of the road on the bridge is depicted in Figure 3.3.

To define the traffic loads acting on the bridge, Eurocode 1 (EC1) is used. For bridges, EC1 gives four load models (LM). Load model 1 (LM1) gives point loads and uniformly distributed loads (UDL) which cover most of the normal and heavy traffic and is used for standard calculations. Load model 2 is a single axle load and is used for shorter members. Load model 3 is a series of axle loads representing special vehicles with exceptional loads. Load model 4 represents a crowd of people [3]. In case of the two-lane bridge, LM1 will be sufficient. Loads from cyclists and pedestrians are low compared to traffic loads, they will not be taken into account in this study.

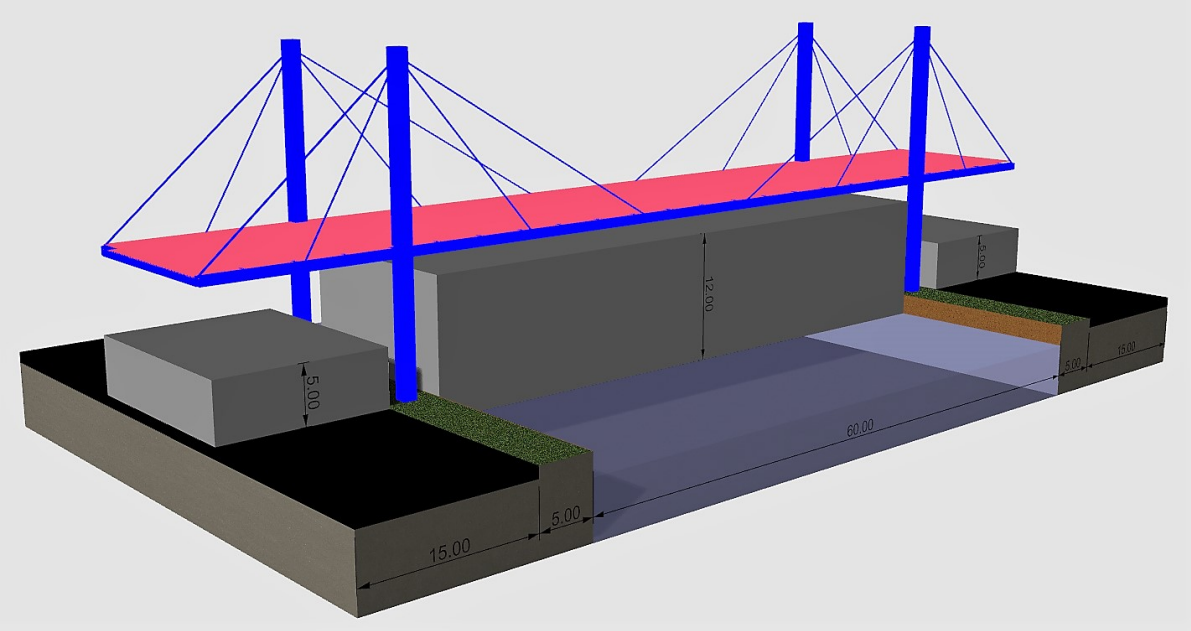

Figure 3.1: Schematic three-dimensional overview of the boundaries for the bridge posed by the river and the roads in the fictitious case [m]

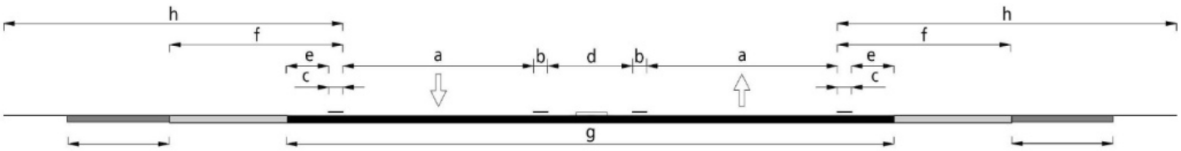

Designelement	[m]
a. traffic lane	2,75
b. road marking	0,15
c. road marking	0,15
d. median	0,80
e. correction lane	0,30
f. shoulder	2,40
g. road surface	7,50
h. obstacle free zone	6,00

Pavement
Unsealed shoulder
Verge

Figure 3.2: Cross section of a Dutch single carriageway [19]

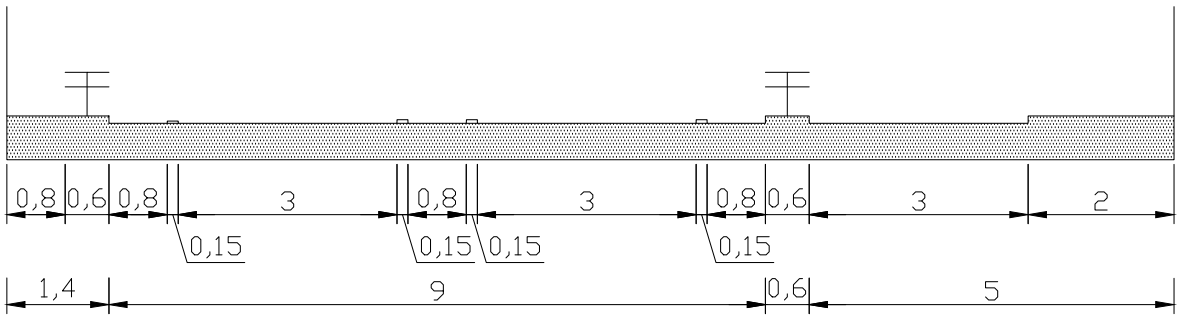

Figure 3.3: Schematic cross section of the road on the bridge with cycle- and footpath [m]

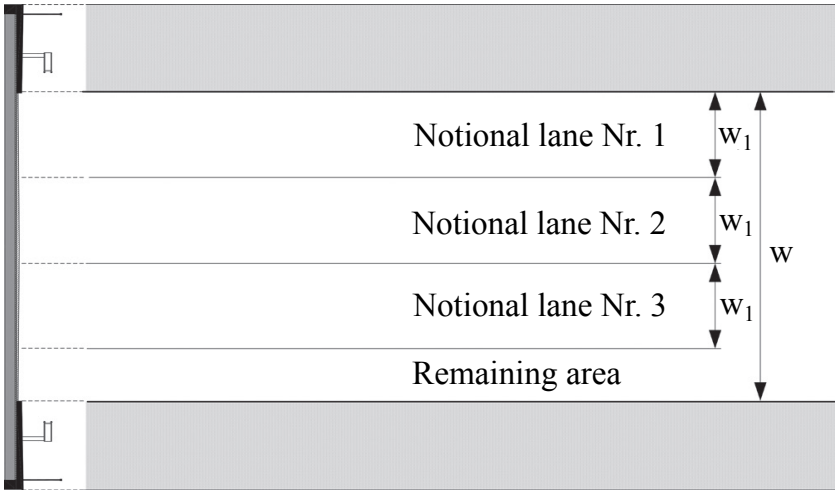

Figure 3.4: An example of lane numbering with notional lanes [20]

Table 3.1: Characteristic load values for LM1

Location	*Axle loads* $Q_{ik}[kN]$	*UDL system* $q_{ik}[kN/m]$
Lane number 1	300	9
Lane number 2	200	2.5
Lane number 3	100	2.5
Other lanes	0	2.5
Remaining area	0	2.5

To place the loads from LM1, the carriageway will be divided into notional lanes of three metres wide. Taking the loads according to Table 3.1 into account, the notional lanes are then placed on the carriageway in the most unfavourable way, of which Figure 3.4 gives an example. In the case discussed, the width of the carriageway is nine metres, which gives exactly three notional lanes of three metres wide. The most unfavourable way to load the bridge would be to place the highest loads on the most outer side of the carriageway and the lowest loads on the other side, resulting in maximal asymmetric loading. The axle loads should be placed at such a position along the span that they have the most unfavourable effect. The bridge deck will be loaded as in Figure 3.5, without the remaining area.

3.2. Girder Beam Bridges

There are two types of girder beam bridges, the I-girder bridge and the box-girder bridge. For the steel I-girder bridge typology two designs will be made. One design with six girders, the multi-girder bridge, and one with two large girders, the double-girder bridge. The advantage of a double-girder bridge is that there are fewer girders to erect and therefore less supports necessary. However, when one girder is damaged, there is no redundancy to redistribute internal forces. This problem is overcome by the use of more girders, like the multi-girder bridge. Additionally, the girders carry a smaller part of the load and can therefore be more slender, decreasing the structural height of the bridge. For the box-girder bridge one design is investigated.

The girder beam bridges can either be statically determinate or indeterminate. While being statically determinate, there are no bending moments at the internal supports, but the midspan bending moment is larger compared to the indeterminate beam. This means that the height of the cross section of the indeterminate beam can be reduced, but it should also be designed to carry negative bending moments at the intermediate supports.

3.2.1. Multi-girder Bridge

The main bearing structure of the multi-girder bridge will be formed by six I-girders and a concrete slab, connected by shear studs. By using an even number of girders, bracing is possible without connecting more than two girders. If more than two girders are connected, the bracing will take part in the transverse spreading of loads in the final stage and should be designed accordingly [7]. Preferably, the girders should be spaced

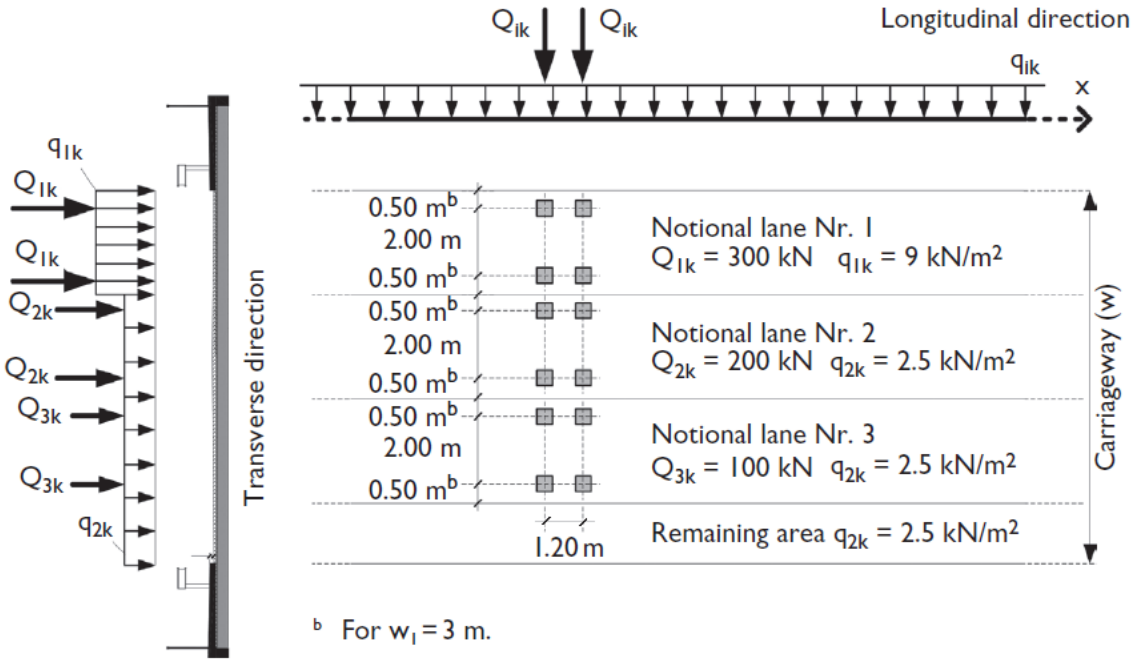

Figure 3.5: Loads of LM1 on the carriageway [20]

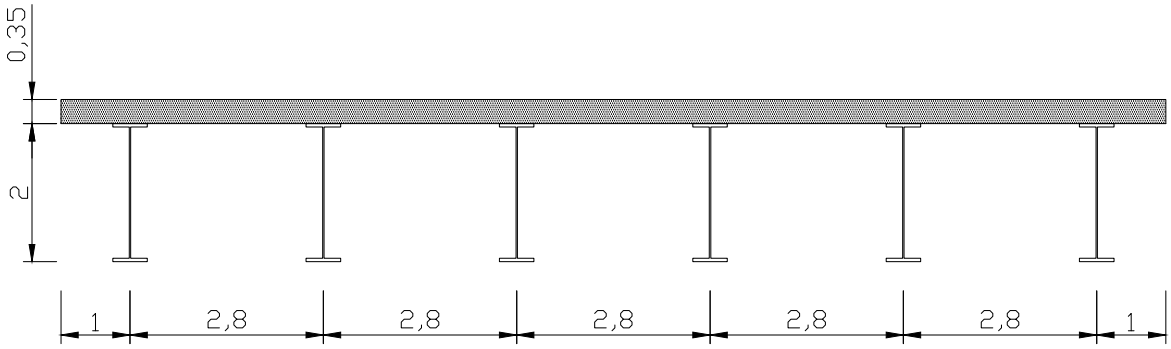

Figure 3.6: Schematic cross section of the multi-girder beam bridge [m]

between 2 and 4 metres, and the cantilever of the deck at the sides of the bridge should be smaller than 1.5 metres. Bracing should be spaced at 6 metres and the depth to span ratio h/L of the girders will be around 1/30 [20]. The thickness of the concrete deck will be around 1/10 of the distance it spans, with a minimum of 35 cm to accommodate reinforcement.

With these design rules the first design for the multi-girder bridge can be made. For the main span of 65 metres, the girders will be around 2 metres high. The girders are spaced at 2.8 metres, letting the concrete slab cantilever over a distance of 1 metre. This design is depicted in Figure 3.6.

For the structural optimization with the parametric model, some parameters have to be defined. These parameters should be of large influence on the behaviour of the structure. The main bearing elements are the girders, where the web carries the shear forces and the flanges carry the bending moments. The concrete slab carries bending moments in compression and acts as plan bracing. Its thickness should be kept to a minimum to limit its contribution to the deadweight. The cross bracing increases buckling resistance of the girders.

The upper flanges of the girders have no real structural contribution, since the concrete slab will take up the compression forces. They are only necessary for the connection between the girders and the deck and its dimensions are therefore kept constant with a thickness of 20 mm and a width of 200 mm. Especially the dimensions of the lower flange are varied to resist the loads, with the thickness of this flange ranging between 30 and 80 mm and the width being lower than fifteen times its thickness. When these limits are

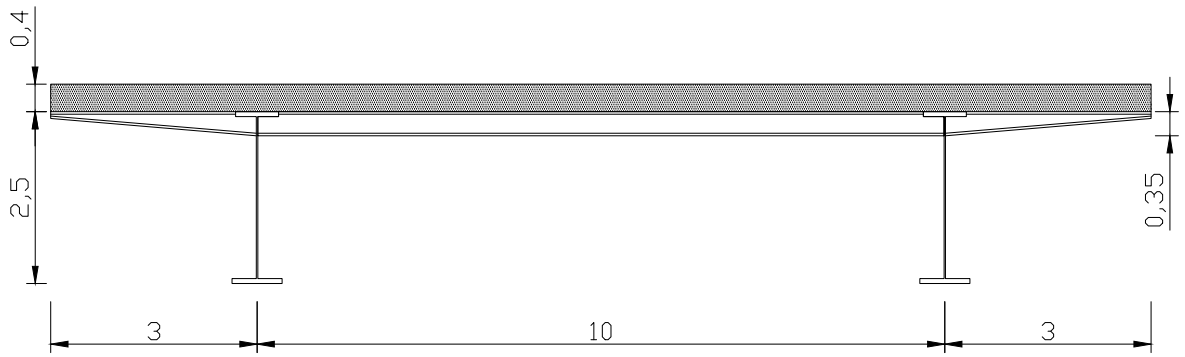

Figure 3.7: Schematic cross section of the statically determinate double-girder beam bridge [m]

reached, the height of the web can be adjusted. The thickness of the web will be set to 15 mm. The thickness of the concrete deck will be around 1/10 of its span, in this case that would be 280 mm. This is lower than the minimum thickness, so the deck will be 350 mm thick. For the bracing, which is spaced at 6 metres, a deadweight of 50 kg/m² deck surface is assumed. For this bridge design, the dimensions of the lower flange and the height of the web of the I-girders will be parameters.

3.2.2. Double-girder Bridge

The double-girder bridge consists of two I-girders, a concrete slab and cross girders. If the main girders are spaced more than 8 metres apart, the cross girder can be placed directly under the concrete slab to support it. In this way the slab thickness can be kept to a minimum, the cross girders should then be spaced at around 4 metres. To prevent torsional overloading, the cross girders should be bolted to the main I-girders, making them simply supported. To support the cantilevering slab, the cross girders can also cantilever towards the ends of the slab. The depth to span ratio of the girder is about 1/24. The web thickness of the girders rarely exceeds 20 mm, but the flanges can be more than 600 mm wide and 60 mm thick [20]. It should be kept in mind that the strength of the steel plates could reduce with increasing thickness. As is the case with the multi-girder bridge, the thickness of the concrete slab should be around 1/10 of its span. The height of the cross girders is about 1/30 of their span.

According to these design rules and estimations, the design of Figure 3.7 for the double-girder bridge is made. The girders have a height of 2.5 metres for the main span and are spaced at 10 metres. The cross girder is placed directly under the concrete slab, spaced at 4 metres, and cantilevers 3 metres towards the end of the slab to minimize its thickness. The cross girder is 350 mm high and the concrete slab is 400 mm thick.

As is the case with the multi-girder bridge, the important parameters for the double-girder bridge are the dimensions of the lower flange and the height of the web of the I-girders. The same rules as for the multi-girder bridge apply to the dimensions of the I-girders, the upper flange being 20 mm thick and 200 mm wide, the web being 15 mm thick and the lower flange having a thickness between 30 and 80 mm and a width which is lower than fifteen times its thickness.

3.2.3. Box-girder Bridge

To increase the economy of the bridge, it is beneficial to decrease the amount of box-girders and to increase their spacing. The support the box-girder provides for the concrete slab could be seen as fixed, increasing its lateral bending stiffness. The slab can therefore span larger transversal distances. With this in mind the bridge should be designed with two box-girders, a concrete slab, internal diaphragms and cross-bracing at the supports. The boxes will be narrow and will have a trapezoidal shape. Narrow boxes have a higher resistance to torsion and distortion due to their larger height than width. With the trapezoidal shape the width of the bottom flange is further reduced, increasing its buckling resistance and reducing the shear lag effect. The top of the steel box will be open to minimize steel consumption, the concrete slab closes the box.

The box-girder bridge could be seen as an optimization of the multi-girder bridge by providing higher torsional resistance by connecting the lower flanges to form a box. Especially for bridges with high torsional loading this is beneficial, but in the case considered in this research there are no such high torsional loads. The extra steel used to connect the lower flanges will result in a higher material usage. This consumption of steel could be reduced by making the boxes more narrow. This will however increase the distance the concrete

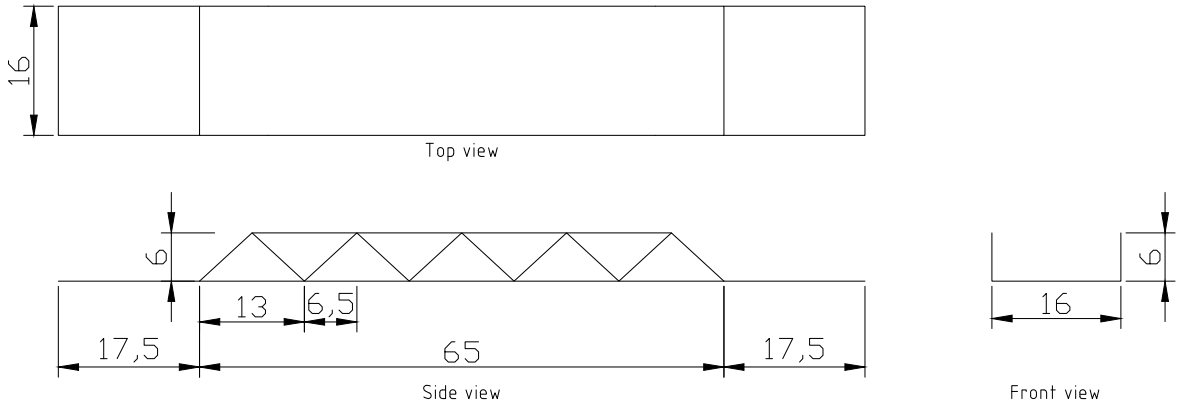

Figure 3.8: Schematic cross sections in grid lines of the truss beam bridge with girder bridges for the side spans [m]

slab will have to span, increasing the height of the slab and, following, increase the concrete consumption and its deadweight, which will in turn also lead to an increase of steel needed for the box-girders to carry this extra deadweight. Due to these considerations it is decided to eliminate the box-girder bridge from further investigation and optimization, since it is predicted that, for the fictitious case considered in this research, this type of bridge will always have a higher material consumption than the multi-girder bridge.

3.3. Truss Beam Bridge

From the many types of truss bridges, the warren truss without verticals is chosen for the design. In this way the structure is kept simple and by removing the verticals there are less elements and joints, making the design more economic. Since the Netherlands is a flat country, the deck of the bridge should be as low as possible to prevent large approach ramps. These ramps have a very large impact on the total costs of the bridge. The truss will therefore be a through truss. The truss members can be open or closed sections. For compression forces the closed box-section usually has a lower slenderness ratio about the weak axis and wind induced vibrations are lower. The complete deck will pass through the truss, this means that the truss elements are connected to the outsides of the deck structure.

As a rule of thumb, the distance between the bottom and top chord of the truss can be estimated on 1/10 of the length. Lateral bracing of the trusses is not necessarily needed, therefore they will initially be designed without. The dimensions of the truss itself might become somewhat larger compared to the design with braces, the amount of elements and connections is however reduced, decreasing the amount of material used and therefore increasing its economy. If bracing would be necessary, the minimal clearance of 4.80 metres should be taken into account.

All truss-members will be rectangular hollow sections for the reasons mentioned earlier and to reduce the dirt- and water accumulation compared to open cross sections. The side spans of this case can be either crossed by trusses or by simple girder beam bridges. Since a truss for such a short span will probably not be efficient, only the option with a girder bridge for the side spans will be investigated. Figure 3.8 shows the design for the truss bridge with the girder beam bridge for the side spans. Which type of girder beam bridge this will be, will depend on the optimization results for the girder bridges. For the main span the height of the truss will be 6 metres.

The multi-girder beam bridge can be used for the design of the deck, with the girders spanning in transversal direction between the two trusses. As starting point, I-girders of 550 millimetres high are used, spaced at a distance between 2 and 4 metres, being a multiple of the bay-width of the truss. The height corresponds with the rule of thumb for the height to span ratio of 1/30. The thickness of the concrete slab will be 1/10 of its span. The focus of the design optimization is on the truss itself, the deck will therefore not be optimized.

The parameters for the optimization will be the outer dimensions and thickness of the members of the trusses and the height of the truss. All diagonals will have the same angle to keep the design simple. To reduce the material consumption, members with lower compression- or tension forces should have a smaller cross-sectional area. This will be achieved by reducing the elements' wall thickness, while keeping the outer dimensions the same as other members, assuring good connectivity between members and keeping the outer appearance the same for the whole truss. As a starting point, all elements will have outer dimensions of 1 by

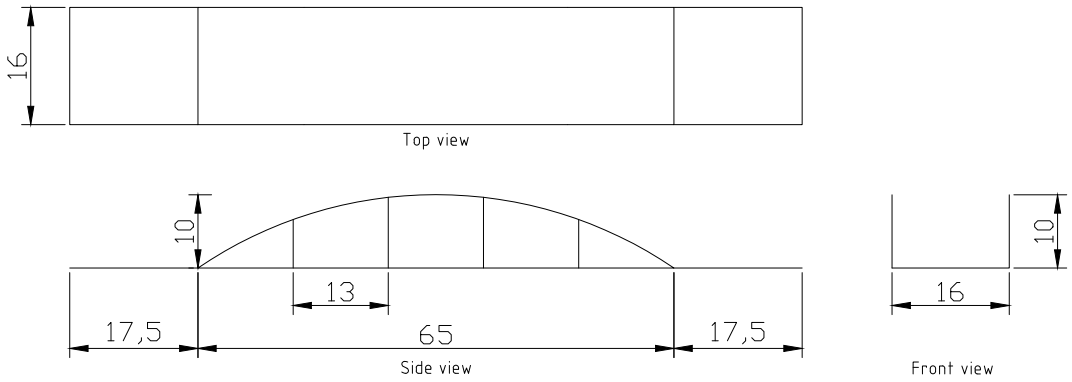

Figure 3.9: Schematic cross sections in grid lines of the arch bridge with vertical hangers [m]

1 metre. The top- and bottom chords, as well as the portal diagonals, will have a thickness of 30 mm and the other diagonals will have a thickness of 20 mm.

3.4. Arch Bridge

For the same reason as for the truss bridge, the arch bridge will be of the through type. The stiffness of the bridge will mainly come from the arch, and not from the deck, to investigate the influence of the arch. This means that the dimensions of the arch will be larger to take up the compression forces and bending moments. In this way the deck can be thinner, reducing the height of the bridge needed for the desired clearance. To take up the horizontal thrust forces from the arch, the deck will act as a tie. To investigate the arrangement of the hangers, a design for both straight and diagonal hangers will be made.

The arch will consist of two parallel steel ribs and steel hanger rods. For the same reason as with the truss bridge, transversal bracing will not be applied. As a rule of thumb the height of the arch will be 1/6 of the span, making it around 10 metres high. The ribs will be rectangular hollow sections, their height being about 1/70 to 1/80 of the span [6]. The deck of the arch bridge will have two longitudinal girders, which are acting as ties, cross girders supporting the deck, and a concrete deck slab. As is the case with the truss bridge, the deck will not be of major importance in the optimization. The longitudinal girders should however be designed to take op the horizontal thrust forces from the arch. The ties will be steel hollow box-girders, spanning the distance between the supports and are supported by the hangers. Since the deck will pass through the two arches, the ties will be attached to the outsides of the deck structure and are situated underneath the arch ribs. The cross girders will be spaced at around 4 metres, dividing the hanger spacing into equal parts, and span a distance of 16 metres, making them 550 mm high. The concrete slab will be 400 mm thick for the span of 4 metres. Again, for the side spans the most optimal girder beam bridge will be used.

The best shape for an arch structure would be the shape of the thrustline resulting from external loading. Since the external loads constantly change and cannot be predicted exactly, there will be no single thrustline. The best shape for the arch to approximate the thrustline will be a parabolic one. The outer dimensions of the ribs and ties will be 1 by 1 metre and their initial thickness will be 30 mm. The hangers will be joined to the deck structure at locations of the cross girders. Figure 3.9 shows an example for the design of the arch with vertical hangers and Figure 3.10 provides one with diagonal hangers.

The parameters for the arch bridge are the height and thickness of the arch ribs, the dimensions of the ties and the diameter of the hangers.

3.5. Cable Stayed Bridge

As is the case with the other bridge typologies, there are numerous options for the design of the cable stayed bridge. In longitudinal direction a design with one pylon and a design with two pylons will be investigated. In the first case the cable stayed bridge will carry the main span and one side span, the other side span will be carried by the most optimal girder beam bridge. With two pylons, both pylons will carry the main span together and both have one side span as back span.

The pylon itself will be designed as a concrete H-frame. With the H-frame there are two planes of cable stays which are anchored at the outer sides of the bridge deck, providing torsional stability and making the

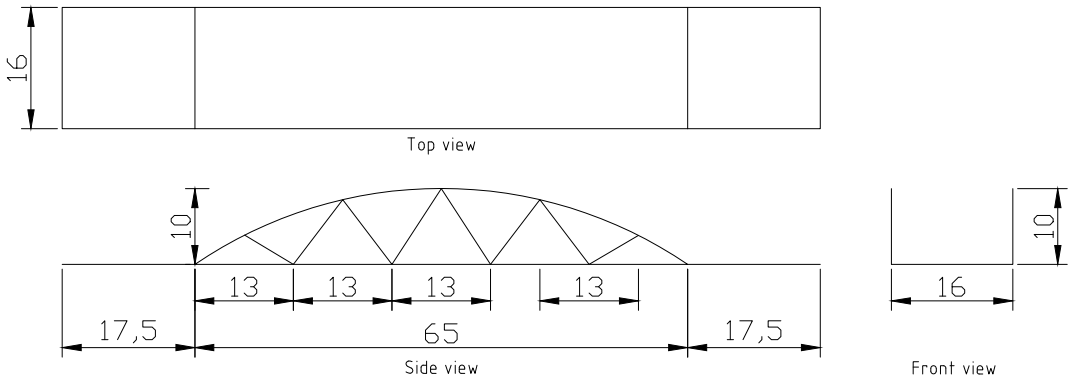

Figure 3.10: Schematic cross sections in grid lines of the arch bridge with diagonal hangers spaced at equal distances [m]

design of the deck more simple. The deck can pass through the two pylons, keeping the load model the same as with the other typologies. By keeping the design of the pylons straight, no additional horizontal forces are introduced to the foundation.

The deck should be designed to carry both the local bending moments introduced by the traffic loads and the horizontal compression component of the stay force. A concrete deck would be efficient to carry the compression forces, but it will also induce larger loads to the stay cables due to its higher self-weight. To reduce the deadload of the deck, but to provide sufficient compression resistance, a composite deck structure is applied. This is composed of steel box-section members as longitudinal girders, steel cross beams supporting the deck slab and a concrete deck slab which is able to carry large parts of the compression forces. The longitudinal girders will have outer dimensions of 0.80 metres and will be 30 mm thick. The cross beams are spaced at around 4 metres, as to divide the spacing between the stays in equal parts, and will span a distance of 16 metres, therefore becoming 550 mm high. The concrete slab spans a distance of 4 metres, making it 400 mm thick.

Of the two different types of cable stayed bridges, the harp type and the fan type, only the fan stay system will be investigated. From a structural point of view the harp system is inefficient; the stays are all under the same low angle, increasing sag of the cable and increasing the compression force in the deck. The anchor points in the pylon of the fan system should be spaced at around one to two metres to provide sufficient space for the anchor system. In the structural model however, it is beneficial to have only one anchor point for all stays. This will simplify the model and reduce costs for calculation, while not deviating a lot from the true situation.

The parameters that are of importance for the cable stayed bridge, and which will be investigated, are the dimensions of the pylon, the stays and the dimensions of the longitudinal girders. The outermost cable stay should have a minimal angle to the horizontal of 30 degrees. This then defines the minimal height of the pylon. The stays should divide the spans in equal numbers, in this case they will therefore be spaced at 13 metres at main span and 8.75 metres at the back span. The pylon will be a concrete hollow box section, its dimensions largely depending on the normal force introduced by the stays.

Figure 3.11 shows the fan type cable stayed bridge with only one pylon, and Figure 3.12 shows the bridge with 2 pylons. In Figure 3.13 the harp type cable stayed bridge with one pylon is depicted, which shows the cable configuration and clarifies why this type will not be investigated.

3.6. Input Parametric Model

Regarding all bridge designs of this chapter, an overview is presented of the input that is needed for the parametric model.

Every bridge carries the same road, of which its input values for the design are presented in Table 3.2. These values correspond to the ones given in Figure 3.3. In Table 3.3 the boundary conditions posed by the bridge surroundings are given. These values define the length of the spans and the minimum height of the structure.

All the parameters which will be changed during optimization are presented in Table 3.4. With all values presented in these tables, together with some bridge-specific values, all bridge typologies can be designed in the parametric model, as will be described in the next chapter.

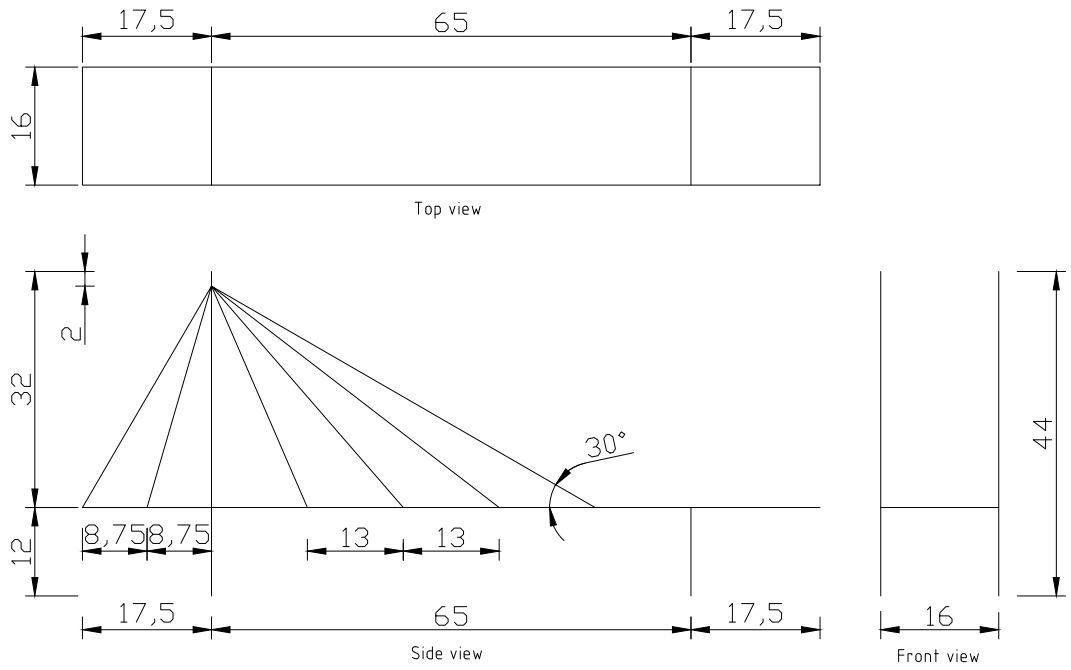

Figure 3.11: Schematic cross sections in grid lines of the fan type cable stayed bridge with one pylon [m]

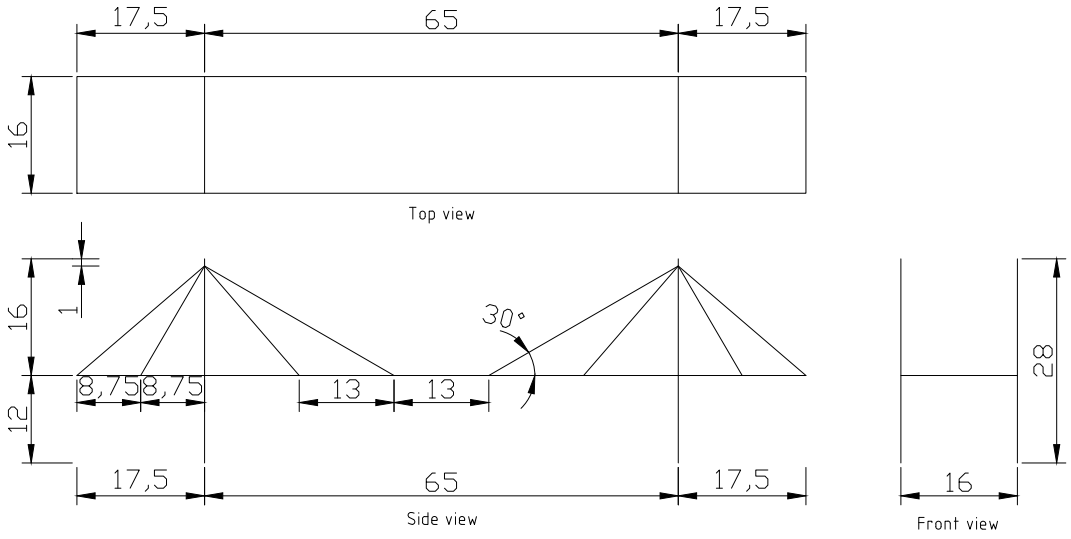

Figure 3.12: Schematic cross sections in grid lines of the fan type cable stayed bridge with two pylons [m]

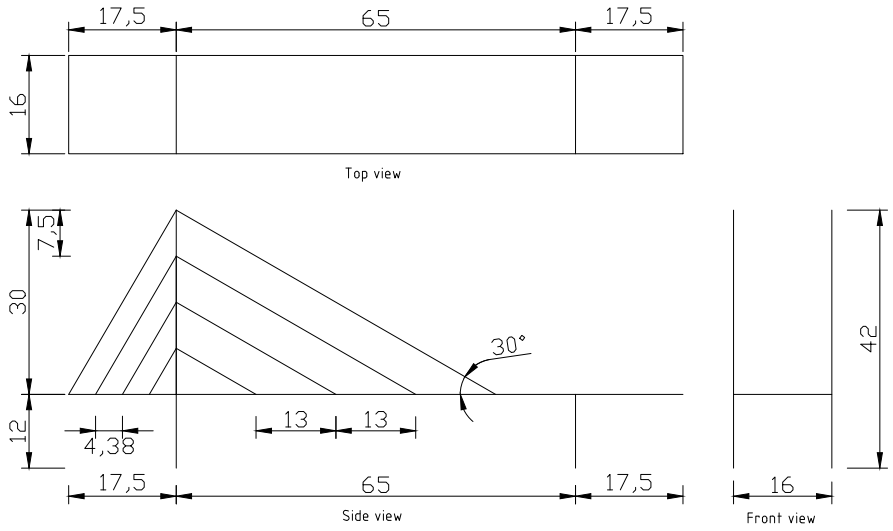

Figure 3.13: Schematic cross sections in grid lines of the harp type cable stayed bridge with one pylon [m]

Table 3.2: Input for elements which make up the design of the road

Road design	[m]
Width carriageway	9
Width cyclepath	3
Width footpath	2
Width parapet	0,6
Width inspection walkway	0,8

Table 3.3: Boundary conditions that apply to all bridges

Boundary Conditions	[m]
Length main span	60
Length side span	15
Space intermediate support	5
Minimal clearance river	12
Minimal clearance road	4,8

Table 3.4: The parameters which will be optimized per bridge typology

Bridge Typology	Parameters
Girder beam bridges	Height web
	Width lower flange
	Thickness lower flange
Truss bridge	Height truss
	Thickness chord and portal members
	Thickness bay diagonals
Arch bridges	Height arch
	Thickness arch ribs
	Outer dimensions arch ties
	Thickness arch ties
	Diameter hangers
Cable stayed bridges	Outer dimensions pylons
	Thickness pylons
	Thickness girders
	Diameter stays

4

Parametric Design and Optimization

This chapter covers the parametric design, analysis, and optimization of the bridge typologies discussed previously. At first, the general parametric model input will be discussed. These are the boundary conditions from the fictitious case and the loads from Load Model 1 and they apply to every bridge. Following, the basic scheme of the parametric model will be explained and afterwards the design, structural analysis and optimization is discussed separately per bridge.

The goal of the optimization is to minimize the overall costs of the bridge structure while complying with regulations concerning maximum allowable deflection and stresses.

4.1. Software

For the parametric design, calculation of the bridge structures and the optimization a combination of integrated software is used. The basis runs on 3D-CAD-modelling software Rhinoceros3D. Within this program all designs are visualised. The actual parametric design is done with Grasshopper, a graphical algorithm editor tightly integrated with Rhino. Finite element modelling and analysis of the bridge structures is performed using Karamba, which is a plug-in for Grasshopper. Finally, the optimization is done by Galapagos, an evolutionary solver that comes with Grasshopper. An overview of their logo's is presented in Figure 4.1.

All of these software programs work within a single environment. This highly improves the workability of the design and optimization process and increases overall speed. Furthermore, every change in design is analysed instantly, giving immediate feedback.

4.2. General Model Input

For every bridge considered the same general boundary conditions apply, coming from the requirements. These are the different spans, the space for the intermediate supports, the minimal clearance under and on the bridge, and the design of the road itself. Also, for each bridge the same loading will be applied, which is Load Model 1 from the Eurocodes. From the design of the road come the width of the bridge and the actual positions of the loads from LM1.

Figure 4.2 shows that the boundary conditions for the design of the bridges are defined as parameters

Figure 4.1: Logo's of the software primarily used for the design, analysis and optimization of the bridge structures

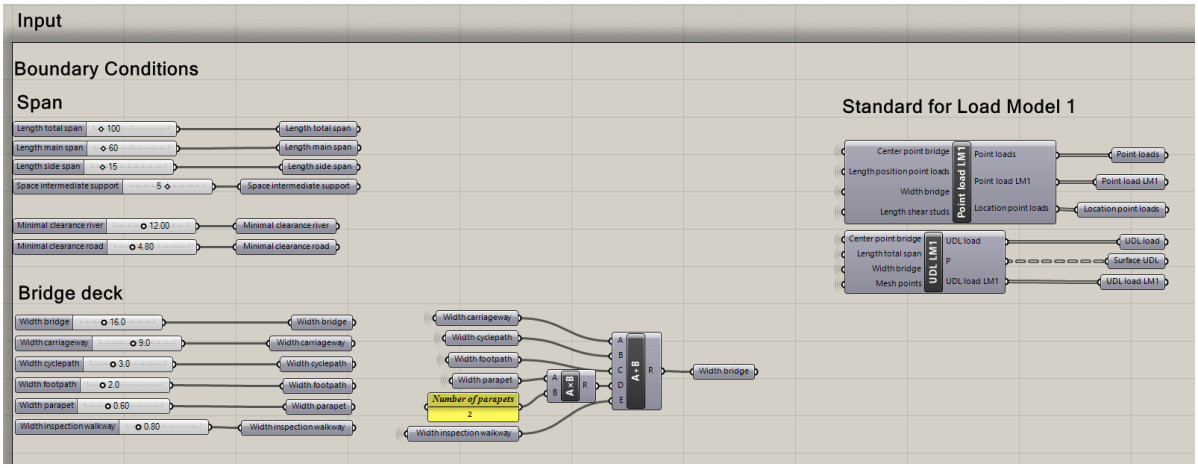

Figure 4.2: General Boundary Conditions applying to every bridge design

and can thus be changed according to the needs of every new project. In this case they are set to the values defined in the fictitious case considered in this research. Since the loads are the same for each bridge, a cluster is made which defines the exact location of the loads. The position of the point loads can be changed in longitudinal direction in order to find their most unfavourable position.

To estimate the total costs of each bridge structure, some unit costs per kilogram of material are defined based on estimations used by Movares during preliminary design stages. These costs include detailing and connections. Structural steel will cost around 5 Euro per kilogram, steel cables around 15 Euro per kilogram and concrete will cost 0,25 Euro per kilogram of material.

4.2.1. Structure Parametric Model

The whole parametric model will consist of seven parts, one for each bridge design. Every bridge model is composed following the same certain flow of data.

It starts with input values such as the boundary conditions, road design, fixed and parametric element dimensions, loads and material unit costs. With these input values the geometry of the bridge is constructed. This geometry consists of nothing more than lines and surfaces. With the finite element analysis plug-in Karamba, all element properties, support conditions, connectivities and loads are defined and assembled into one bridge model. This bridge model is then analysed and also used to calculate the weight and costs of all elements.

The structural response of the bridge is verified with hand calculations and after approval the optimization cycle is started. In this cycle, it is checked whether the behaviour of the bridge fulfills requirements regarding maximum deflection and utilization of elements. When the requirements are not met, the solution should be discarded. When they are met, the total cost of that particular solution is recorded. The parametric element dimensions specified in the input of the model will be changed, until the optimization converges and no cheaper solution is found. The lowest cost solution is then reported as the solution of the optimization.

For every bridge this scheme is repeated, within the same parametric model. A graphic overview of this process is presented in Appendix A in the form of a flowchart.

4.2.2. General Remarks

There are some general remarks about the parametric model which apply to every bridge. There is no reinforcement designed for the concrete elements in the bridges, but the concrete properties are modified in such a way that they include the effects of reinforcement. This means that the Young's Modulus and specific weight of the concrete elements are such as if reinforcement is present. The Young's Modulus defines the stiffness of a material, which is its resistance against deformation. This modification of the concrete properties is already included in the Karamba plug-in [17].

The shear studs connecting the beams with the concrete deck are purely modelled to ensure the whole bridge structure behaves as intended. Without the shear studs the girders and the deck would lie in the same plane and thus be rigidly connected, which does not comply with reality. The shear studs are not designed in detail since they are not of major importance nor influence in the optimization of the structures. Because of

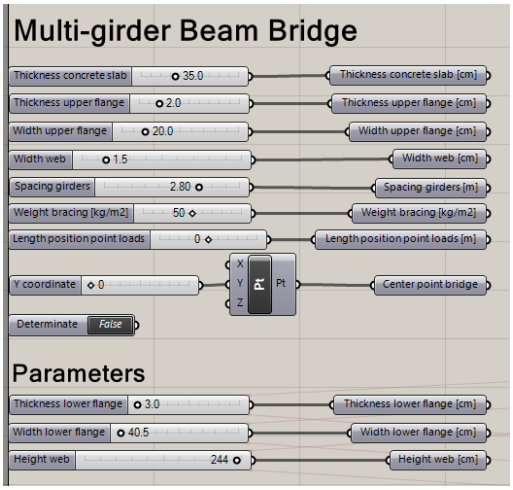

Figure 4.3: Input and parameters for the multi-girder bridge

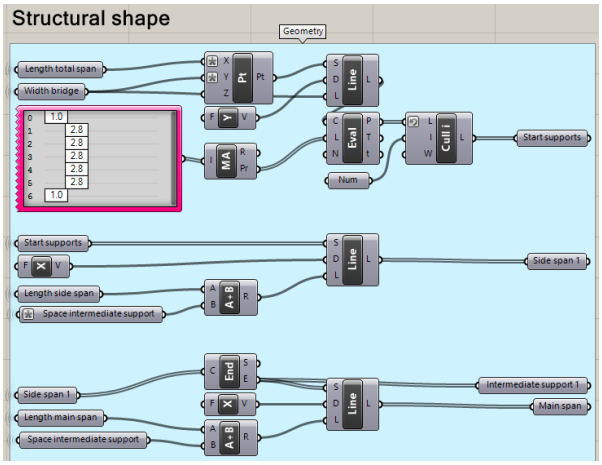

Figure 4.4: Part of the description for the geometry of the multi-girder bridge

this restriction they are also not included in the cost calculation.

The structural analysis of the bridges is done with the first order theory for small deflections. Calculations according to this theory are based upon equilibrium of the undeformed structure. This theory therefore does not take the deformation of the structure into account. Loads acting on the deformed structure will impose different, most of the time larger, forces on the structure. Using the first order theory therefore underestimates the actual sectional forces. This solver comes with the Karamba plug-in.

Whilst optimizing the bridge structures, a criteria is that the Unity Check (UC) of the concrete deck, as well as of important elements in the structure, is below 0.8. This means that the utilization of the elements considered is at 80% of their maximum capacity. The utilization of the different elements is calculated by the Karamba component "Utilization of Elements". For beams this element calculates the ratio between actual stress and yield stress, including buckling. For shells the ratio between yield stress and Von Mises stress in every shell element is considered as the utilization.

Most of the verification of the bridge models is done with the use of a simplified load acting on the bridge deck. A load of 10 kN/m² is placed on the total bridge deck as test load. This loading is used for the simplified hand calculations performed, after which the results are checked with the outcome of the parametric/finite element model of the bridges.

As explained in section 2.4, there are numerous settings for the evolutionary solver. For every optimization run executed during this research, the same settings will be applied. Each generation has a population of 50 genomes, of which a maximum of 5% will be carried over to the next generation. The other 95% is generated by an inbreeding factor of 75%, which means that the solver breeds quite similar genomes. In general this means that 50 variants will be calculated per generation, of which a maximum of 2 to 3 variants may be copied to the next generation. Most of the other variants in the new generation are obtained by combining parametric values of the best performing variants. After 50 generations of not finding a new, better solution, the solver is stopped.

4.3. Multi-girder Bridge

The design of each bridge starts with the predefined dimensions of all elements and whether they are set as constant or as parametric, see Figure 4.3. In case of the multi-girder bridge it is decided to change the dimensions of the lower flange and the height of the web to optimize the design. With these values the structural shape of the bridge is modelled in centre lines and surfaces. A part of this geometric description can be seen in Figure 4.4. The spacing between the girders for example is clearly visible. The resulting geometry is visible in Figure 4.5, where one can see the centre lines for the longitudinal girders and shear studs, the location of the supports and the surface of the deck.

4.3.1. Element Properties

With the geometry defined in Grasshopper, all element-specific properties, as well as the support conditions and the loads, can be assigned with the Karamba plug-in for Grasshopper. For every different type of element

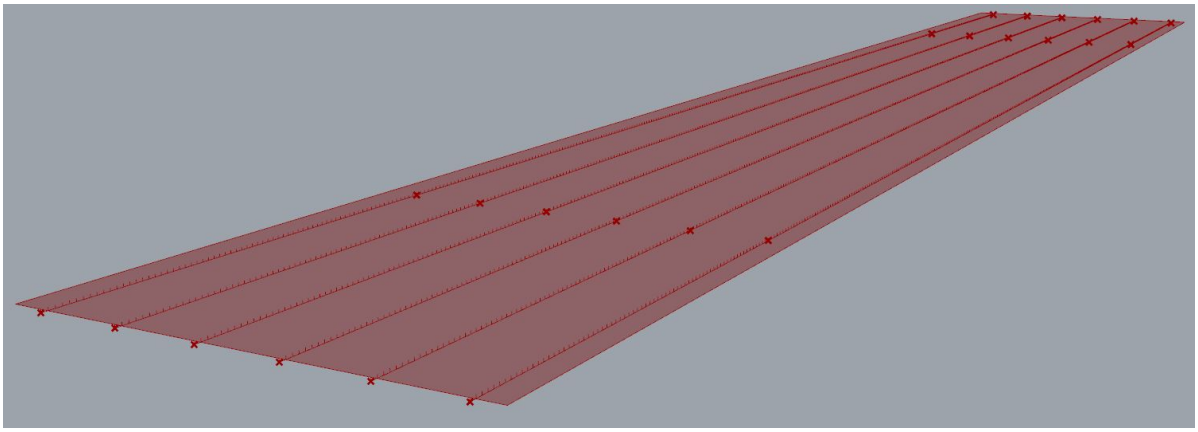

Figure 4.5: Geometry of the multi-girder bridge described in centre lines

of the structure, the element itself, its cross-section and its material is defined and eventually assembled into one bridge model, together with the support conditions and loads. An example of how these properties are modelled for the longitudinal girders can be seen in Figure 4.6. All predefined dimensions of the I-shaped cross-section are given as input, as well as the lines representing the beams. Steel of the strength S355 is chosen as material for the girders. The surface representing the deck is meshed and then modelled as a shell element with reinforced concrete properties of strength class C30/37 with a Young's Modulus of 3300 kN/cm² and specific weight of 2500 kg/m³. One transversal line of supports is pinned, the others are sliding supports. A cross-section of the modelled bridge, as well as a 3D overview, are depicted in Figure 4.7 and Figure 4.8 respectively.

4.3.2. Structural Analysis

The assembled model is then analysed using first order theory for small deflections. For each group of elements, like the girders from Figure 4.6, forces, deflections, deformation energy and utilization are returned. For shell elements also the principal stresses and Von Mises stresses are calculated. The maximum displacement, total mass and internal elastic energy of the total model are also given. Figure 4.9 gives an example of some results for the total bridge model and the girders of the brige. The graphical display of the bending moments in the girders, resulting from the loads of LM1,is depicted in Figure 4.10, together with the maximum values of the positive and negative bending moment. The orange part refers to negative bending moments and the green part to positive ones. Keep in mind that the positive z-direction is upwards.

The bending moment diagrams of the girders clearly show that the bridge is asymmetrically loaded in transverse direction, inducing higher bending moments on one side of the bridge. It is also visible that on some girders point loads are acting, resulting in a dent in the diagram at mid-span.

4.3.3. Verification

The obtained results from Karamba should be verified to be sure that there are no errors in the model. This is done by applying simple load cases on the bridge and comparing the outcomes with hand calculations. When both results do not match, taking into account some margin due to the difference between the real model and simplified calculations, the Grasshopper model should be analysed to find the errors causing this mismatch.

The results from Karamba will also be used to optimize the structure. It is therefore of importance that no mistakes occur which will stop the optimization in a preliminary stage or which will cause wrong end results. One of these errors could be stress singularities, these high peak stresses will result, for example, in a too large utilization of a certain element and thus in discarding the complete bridge design.

A simple example of verification concerns the equilibrium of vertical forces. The sum of the reaction forces in z-direction should be the same as the sum of the external loads in z-direction. This is depicted in Figure 4.12, which shows that there is only a slight difference of somewhat more than one kilo Newton, this is acceptable.

Not only the equilibrium of forces should be checked, but also the deformation of the structure. The

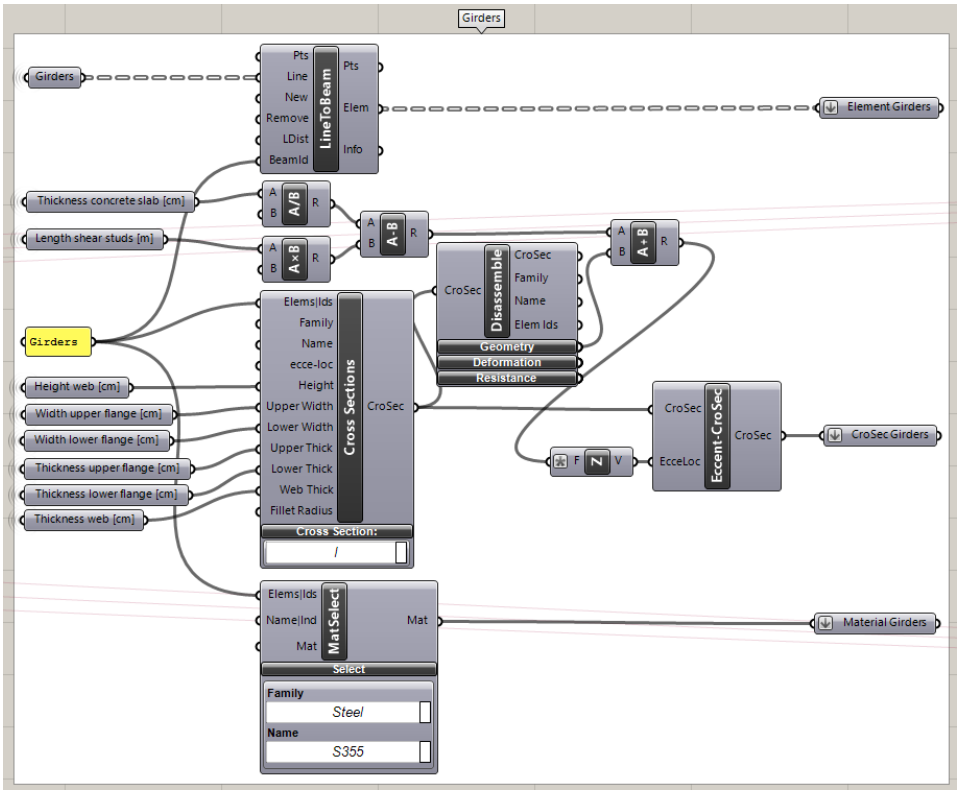

Figure 4.6: Properties of the girder elements as modelled with Karamba in Grasshopper

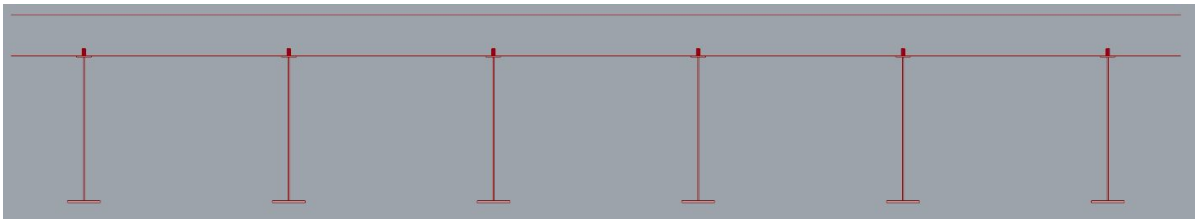

Figure 4.7: Cross-section of the multi-girder bridge as modelled with Karamba in Grasshopper

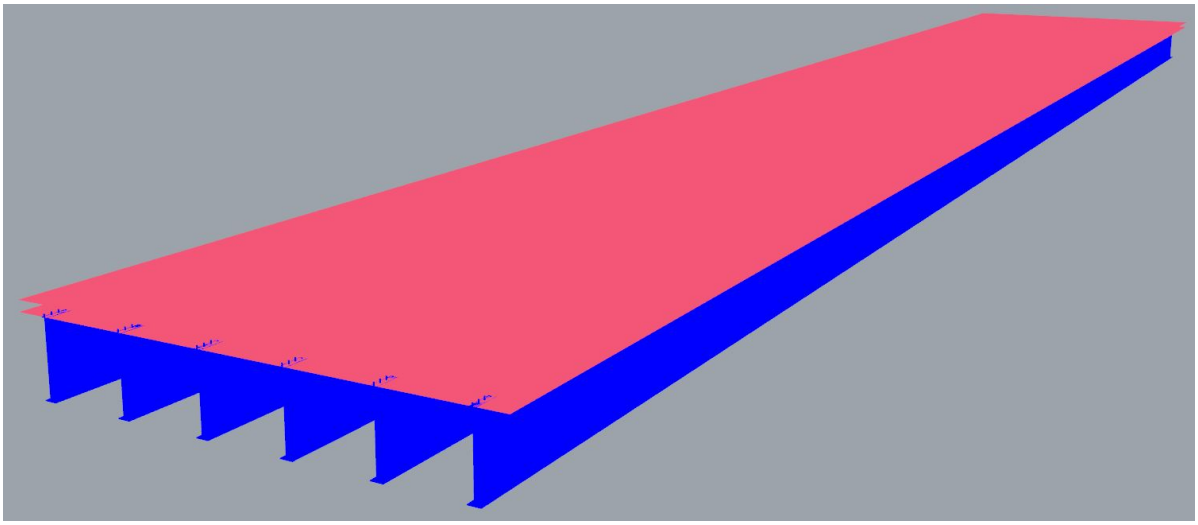

Figure 4.8: Multi-girder bridge as modelled with Karamba in Grasshopper. In blue the girders, in red the concrete deck

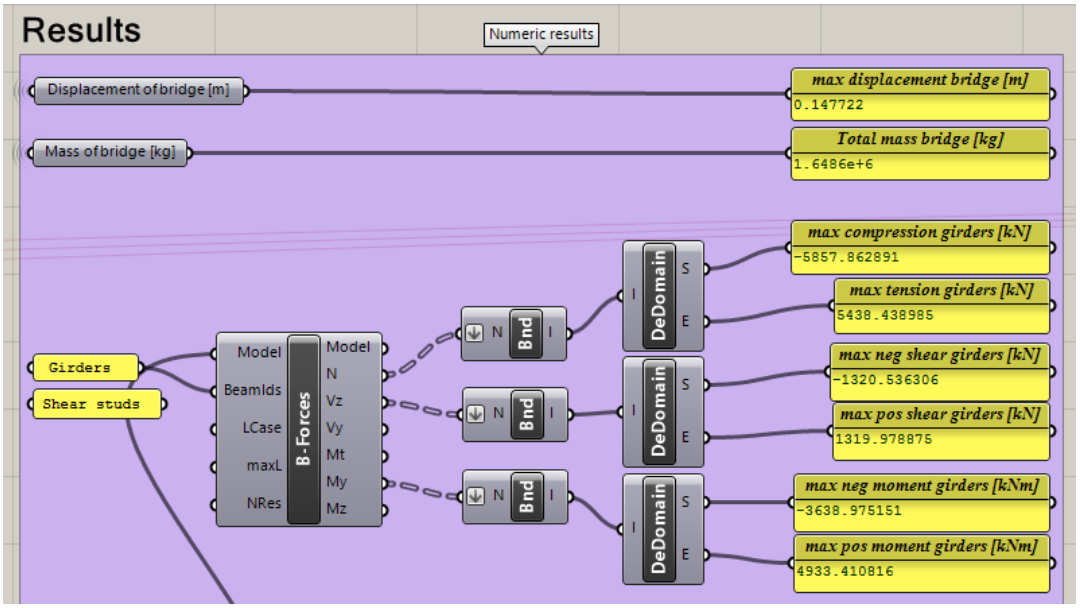

Figure 4.9: Numeric resultant forces in the girder of the multi-girder bridge for LM1 as obtained with Karamba

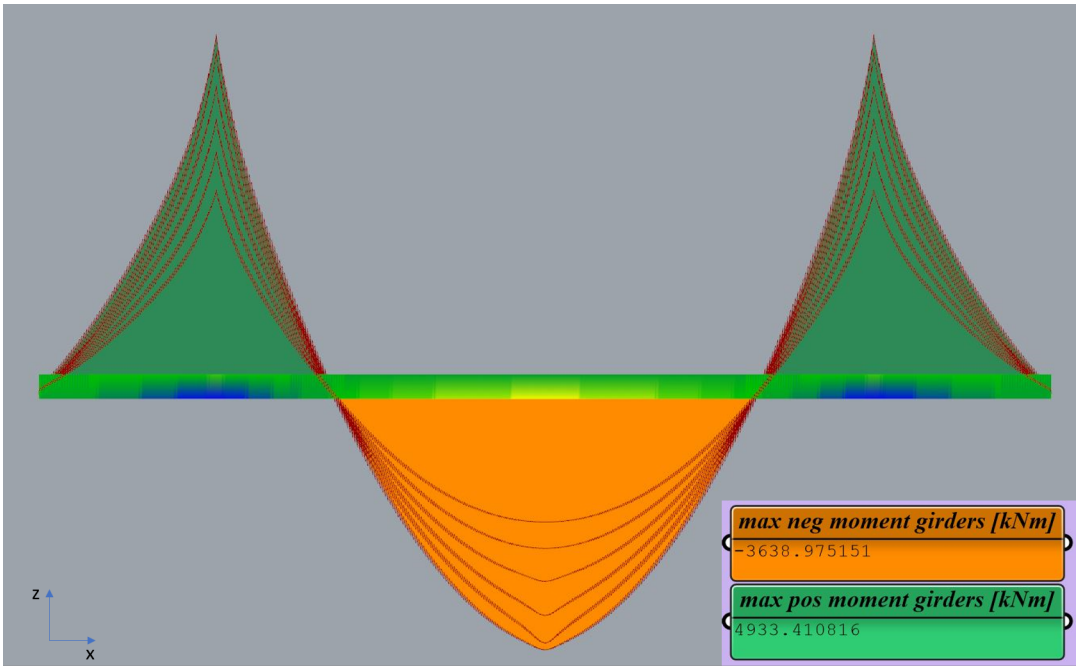

Figure 4.10: Bending moment diagram of the girders for LM1 as obtained with Karamba

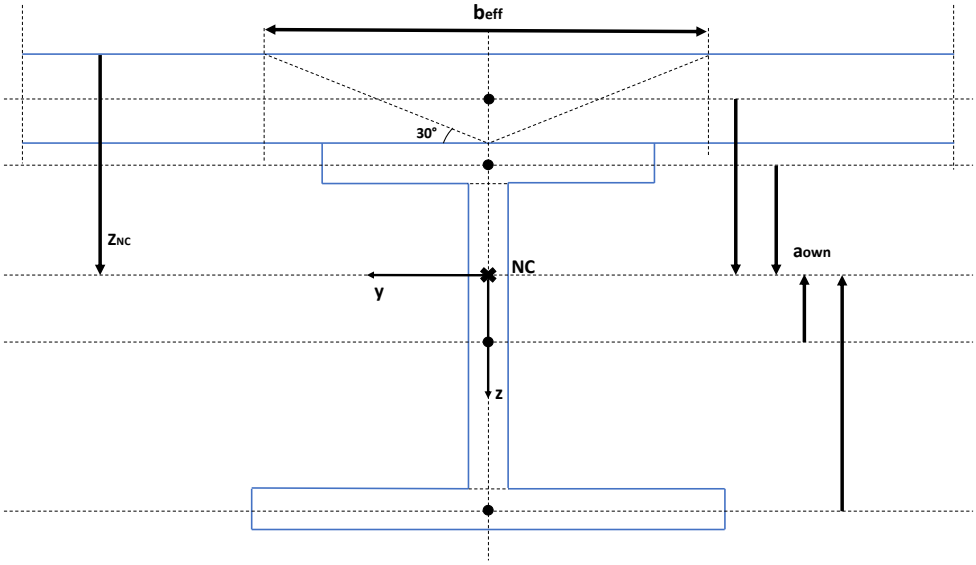

Figure 4.11: Cross-section of the girder bridge showing the normal force centre, the internal lever arms and the effective width of the concrete slab

deformation of one girder is calculated with the engineering formula

$$w = \frac{ql^4}{384EI}$$

for a beam clamped at both ends, which resembles the main span of the bridge. The moment of inertia I has to be calculated for an inhomogeneous cross-section consisting of one girder and a part of the concrete deck. The effective width of the concrete deck that contributes to the bending stiffness of the cross-section can roughly be estimated as $b_{eff} = 2 * h_c / tan(30)$ where b_{eff} is the effective width of the slab and h_c is the height of the deck slab. Any difference between the hand calculation and the result from the FE-model will come from this estimation of the effective width, since the FE-model will calculate the effective width precisely. The cross-section is symmetric in one axis, which runs through the centre of the girder in z-direction. The position of the normal force centre (NC) is on this axis of symmetry, making its y-coordinate zero. To find the position of the normal force centre in z-direction, the formula

$$z_{NC} = \sum \frac{ES_z}{EA}$$

is used, with regard to the top of the deck [11]. A schematic overview of the cross-section with the used values is visible in Figure 4.11. With an effective width of the concrete deck of 1212 mm, an E_s of 210000 N/mm² and an E_c of 33000 N/mm², this forumal yields a z_{NC} of 946.6 mm measured from the top of the cross-section.

With the position of the NC defined, the EI of the cross-section can be calculated. Of every rectangular part of the cross-section, its $I_{zz,own}$ is calculated with $I_{zz} = 1/12bh^3$, as well as its surface A_{own} and the distance of its own NC to the NC of the total cross-section, which is its own lever arm a_{own}. The formula for the EI of an inhomogeneous cross-section is

$$EI_{zz} = \sum E_{own} * (I_{zz,own} + A_{own} * a_{own}^2)$$

For the multi-girder bridge this gives an EI_{zz} of $2.75 * 10^{16}$ Nmm². This value can be used in the engineering formula for the deflection described earlier, where the part of the load carried by the girder equals the width of the spacing of 2.8 m, making $q = 10 * 2.8 = 28$ kN/m and the lenght of the span $l = 65$ m. This gives a deflection of $w = 47.29$ mm.

In the parametric model, the test load of 10 kN/m² is applied on the total bridge structure, and the intermediate supports are set as being clamped, just as assumed with the engineering formula. The maximum deflection at mid-span of the girders in this model is $w_{model} = 46.08$ mm. Our calculated value is 2.64% larger and this is acceptable.

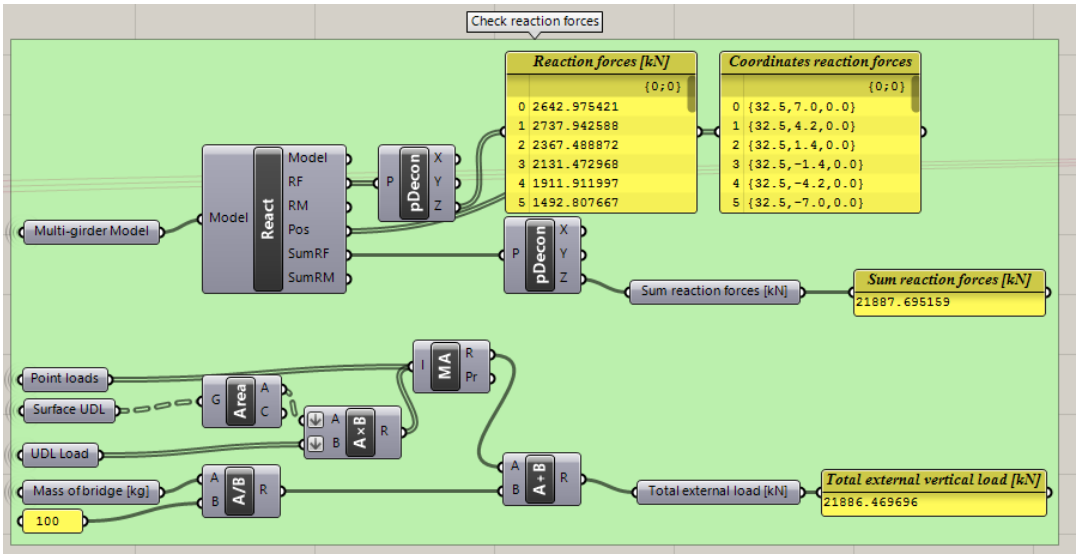

Figure 4.12: Verification of the reaction forces of the multi-girder bridge for LM1 as obtained with Karamba

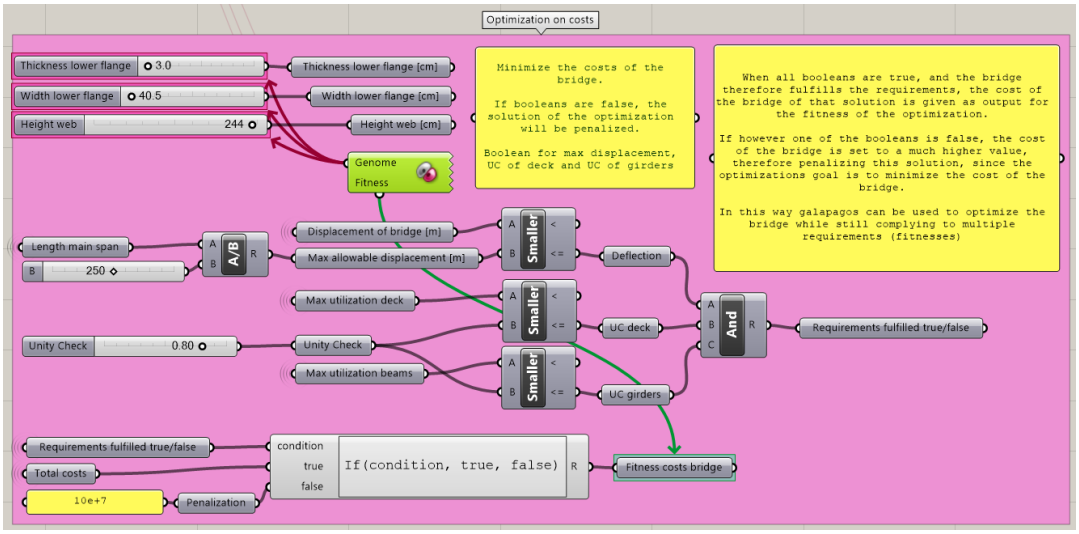

Figure 4.13: Part of the Grasshopper description to optimize the multi-girder bridge towards the lowest costs

4.3.4. Optimization

With the multi-girder bridge model verified, the structure is ready for optimization. The goal of optimization is to minimize the costs of the bridge structure. Since only certain dimensions of the girders are varied during this optimization, and the thickness of the concrete deck is kept constant, the minimization of costs will also lead to a minimization of the total weight of the structure. During the optimization, all solutions still have to comply with the restrictions on maximum deflection and stresses.

For the optimization the evolutionary solver Galapagos is used, which comes with Grasshopper. This solver can test the fitness of one solution by varying multiple parameters. To guide the solver towards a viable solution, an if-statement is used where solutions which exceed the utilization or maximum deflection are penalized. If one of these conditions is not satisfied, or in other words if their boolean turns false, the if-condition returns a very high number as being the total cost of the bridge, see Figure 4.13. In this way the solution is penalized and because the solver is searching for the lowest possible value, it is guided away from this set of combinations of parameters.

Galapagos is then set to minimize the costs of the bridge and the evolutionary solver is started to search for the optimum solution. How this solver works is explained in section 2.4. Galapagos has optimized the bridge twice, and both runs returned the same answer. The result of the optimization is that the dimensions of the

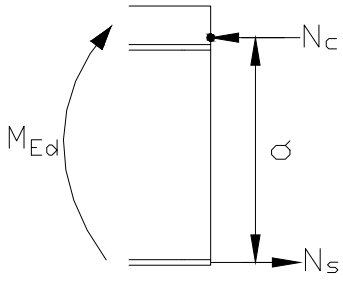

Figure 4.14: Moment equilibrium over the cross-section of the multi-girder bridge

bottom flange are at the lowest range of their parameter, while the height of the web is almost at its maximum. The reason for this is quite simple, the I-profile girder, together with the concrete deck, has to balance the bending moments induced by the external loads. Taking a look at the internal moment equilibrium over the cross-section of the structure, the external bending moment M_{Ed} has to be compensated by the tension force in the girder N_s, which acts mainly in the bottom flange, and the compression force in the concrete deck, N_c. This is shown in Figure 4.14. If moment equilibrium is calculated around the point of application of the compressive force, the moment has to be compensated by the tension force in the bottom flange times the distance between these two forces, a. This internal bending moment, M_{Rd}, is calculated with the formula

$$M_{Rd} = f_y * A_s * a$$

with f_y being the yield stress of the steel, A_s the surface of the bottom flange and a being the internal arm. Since the yield stress is constant, this formula shows us that M_{Ed} can be compensated by increasing the surface of the bottom flange or by increasing the internal arm, which in this case is mainly the height of the web. Since the web has a lower thickness than the minimal thickness of the flange, increasing the height of the web will use less material than increasing the dimensions of the flange, thus having a smaller impact on the increase of the costs of the structure, and this is why the optimization algorithm tends to maximize the height of the web and comes up with the obtained solution.

All variants generated by Galapagos are recorded and outlined in a Parallel Coordinate Plot (PCP), provided by Design Explorer 2 from the CORE Studio from Thornton Tomasetti [1]. With such a PCP different design spaces can be explored quickly. Each parameter has its own vertical axis, having the same range as the parameter in Grasshopper. For each variant the values of its parameters are connected with a line, which ends at the value of the fitness of that solution, which is in this case the cost of the bridge. Figure 4.15a shows the PCP for the multi-girder bridge. The solutions that do not satisfy the requirements, and are therefore penalized with high costs, are clearly visible. Looking at Figure 4.15b its becomes clear that the height of the web should have a minimum of about 200 cm to get solutions which satisfy the requirements. Figure 4.15c shows the solution with the lowest cost, where one can see that the height of the web is around its maximum and the dimensions of the lower flanges are at their minimum, as explained earlier. Figure 4.15d shows the solution which has the lowest height of the web and still satisfies the requirements. This solution might not be the one with the lowest costs according to the calculations within the scope of this research, but looking at a wider picture, a lower web decreases the structural height of the bridge and therefore also decreases the height of the approach structures adjacent to the bridge, therefore decreasing the overall costs of the total project.

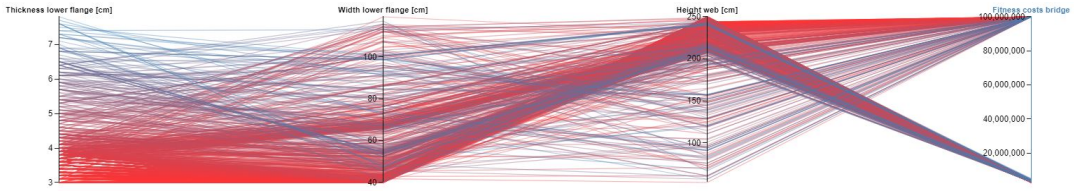

(a) Parallel Coordinate Plot showing all variants produced by Galapagos while optimizing the multi-girder bridge [1]

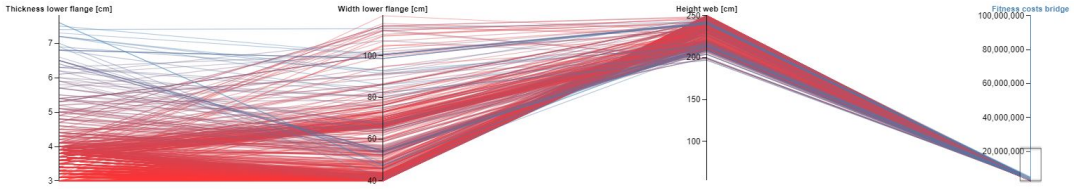

(b) Parallel Coordinate Plot showing the variants which satisfy the requirements, produced by Galapagos while optimizing the multi-girder bridge [1]

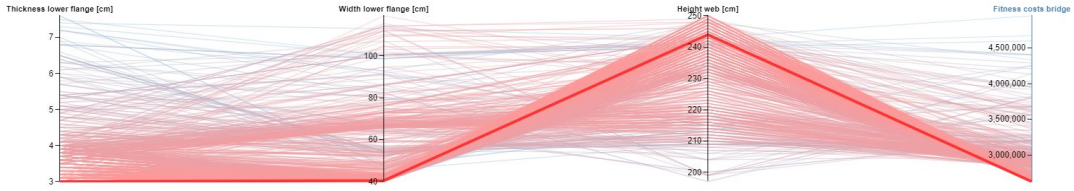

(c) Parallel Coordinate Plot showing the solution with the lowest cost produced by Galapagos while optimizing the multi-girder bridge [1]

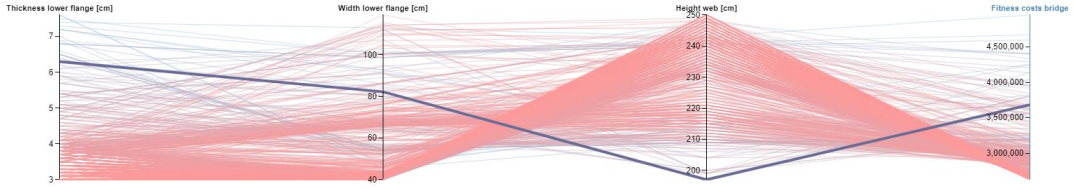

(d) Parallel Coordinate Plot showing the variant which has the lowest height of the web, produced by Galapagos while optimizing the multi-girder bridge [1]

Figure 4.15: Parallel Coordinate Plots showing different selections of solutions produced by Galapagos while optimizing the multi-girder bridge. At (c) and (d) the parameters are rescaled to provide a better overview

4.4. Double-girder Bridge

The double-girder bridge is modelled in the same way as the multi-girder, with the difference that there are only two longitudinal girders. The cross-beams are introduced as well, with a desired spacing of four meters to sufficiently support the concrete deck. The actual spacing is somewhat larger, so that the spans are divided in equal numbers. The spacing of cross-beams at main span is $65/16 = 4.0625m$, and at the side spans is $17.5/4 = 4.375m$. The dimensions of the lower flanges and the height of the web of the girders are set as parameters and the resulting centre-line geometry of the bridge, including the location of supports, can be seen in Figure 4.16.

4.4.1. Element Properties

With Karamba all the element properties are defined. Steel of the strength S355 is used for the girders and cross-beams and the concrete deck is of C30/37 quality. One transversal line of supports is pinned, the rest is sliding, and loads according to LM1 are applied.

The cross-beams are not part of the optimization, so they will be calculated separately. It strongly depends on the construction method applied, but the highest loads that will act on the cross-beams will be present if the concrete deck is cast in situ and is still wet, inducing high self-weight loading on the beams, without having any stiffness, thus providing no support to the beams. To find the right I-profile able to resist this load, the critical bending moment M_{cr} and section modulus W are used. With a UC of 0.8, the M_{cr} should be larger than $M_{Ed}/0.8$. Every available I-profile has its own characteristic W and an I-profile which is able to

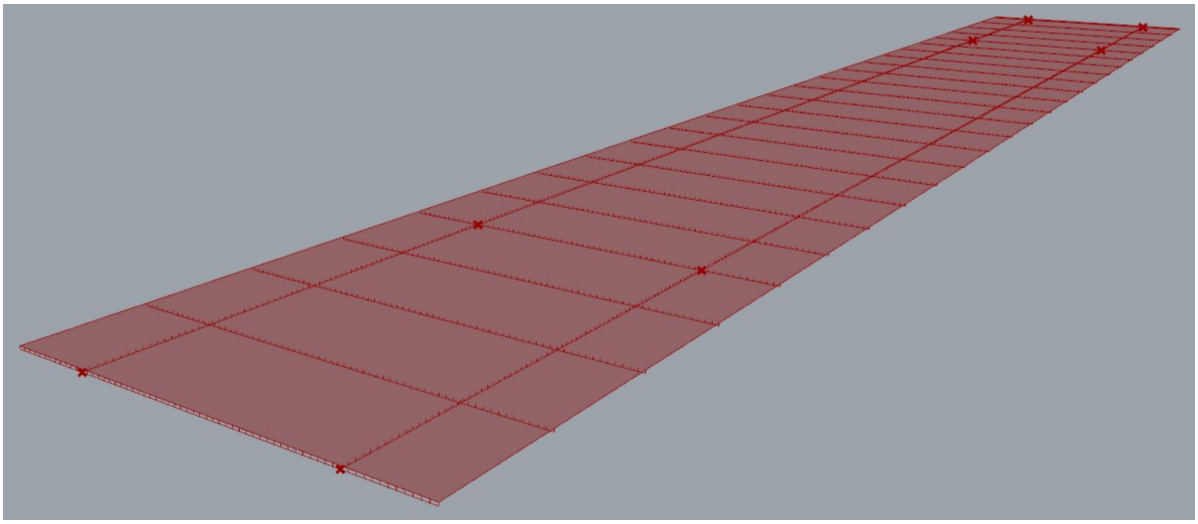

Figure 4.16: Geometry of the double-girder bridge described in centre lines

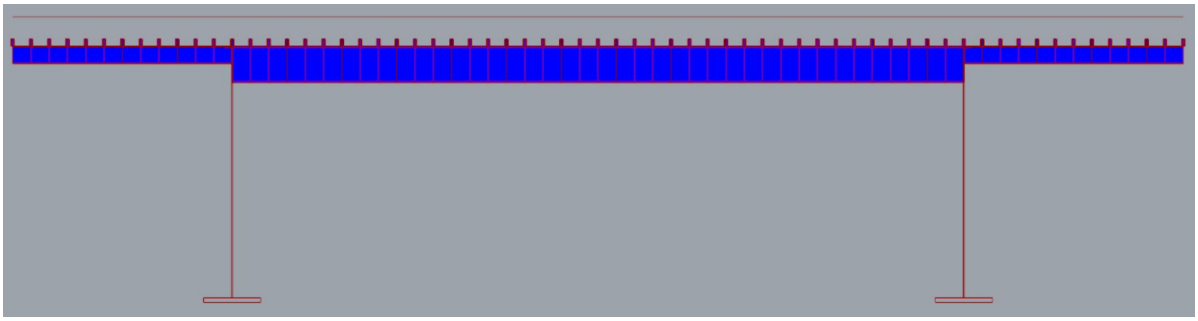

Figure 4.17: Cross-section of the double-girder bridge as modelled with Karamba in Grasshopper

withstand a certain bending moment, should have a W which is larger than M_{cr}/f_y, giving us the formulas

$$W = M_{Ed}/0.8/f_y$$

$$M_{Ed} = 1/8ql^2$$

With the design of a concrete slab of 40 cm thick and a spacing between the beams of 4.375 m, this leads to a load of $0.40 * 25 * 4.375 = 43.75kN/m$. The span between the two longitudinal girders is 10 m, giving a maximal bending moment of $M_{Ed} = 1/8 * 43.75 * 10^2 = 547kNm$. The section modulus should then be greater than $W = 547 * 10^6/0.8/355 = 1.926 * 10^6 mm^3$. From the list of available I-profiles, an IPE500 with a W of $1.928 * 10^6$, will be sufficient to carry the load.

The cantilevering cross-beams were designed to decline in height while approaching the sides of the deck slab. Since it is not possible to model a variable cross-section in Karamba, the cantilevering cross-beams are given half the height of the cross-beams between the girders. The connection between the centre cross-beams and the girders is modelled as being hinged, whilst the cantilevering cross-beams are fixed to the girders.

In the final stage, when the concrete deck is hardened and load-carrying, the cross-beams will be over-dimensioned. To provide stability against buckling of the longitudinal girders, however, the larger dimensions of the cross-girders are beneficial. A cross-section of the modelled bridge, as well as a 3D overview, are depicted in Figure 4.17 and Figure 4.18 respectively.

4.4.2. Structural Analysis

The bridge is analysed with the first order theory for small deflections. The total deflection and weight of the bridge structure are visible in Figure 4.19, as well as the maximum forces in the main girders. What these

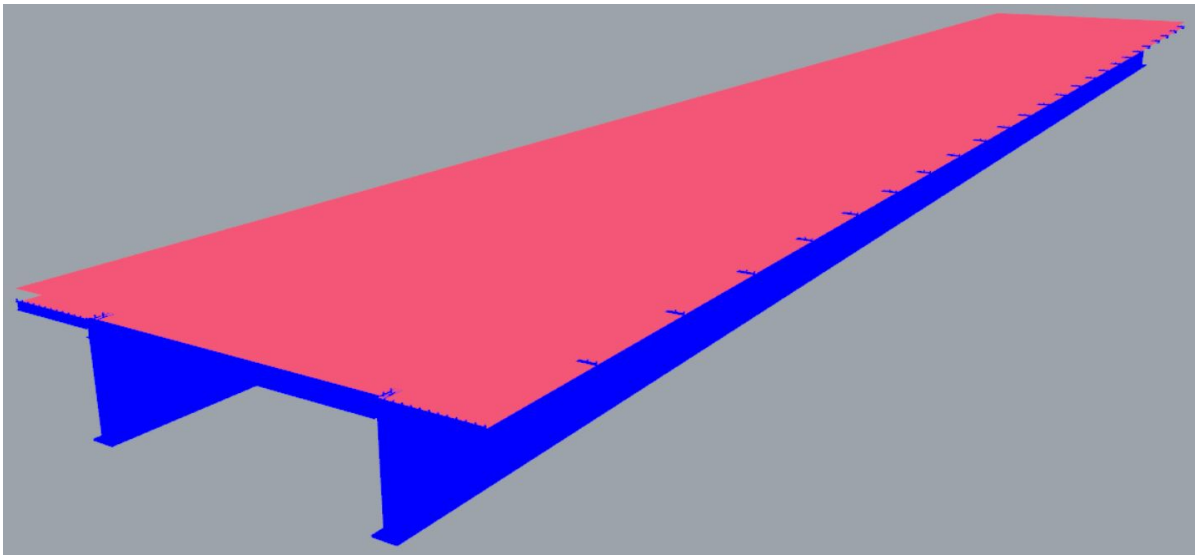

Figure 4.18: Double-girder bridge as modelled with Karamba in Grasshopper, in blue the girders, in red the concrete deck

results show is that the maximum compression force in the girder at the position of the intermediate supports is almost as large as the maximum tensile forces at midspan. Especially at the high compression zones sufficient resistance to buckling should be present.

Figure 4.20 shows the bending moment diagrams of the main girders. As it was the case with the multi-girder bridge, it is clear that the bridge is asymmetrically loaded in transverse direction, resulting in a higher bending moment in one girder. The effects of the point loads are visible in this bending moment diagram as well. The girders themselves are set to display their utilization, where blue refers to high compression and yellow to high tension. The bending moments of the cross-beams are shown in Figure 4.21. There are small hogging moments near the connections with the main girders, but what is more interesting are the relatively higher bending moments in the cross-beams located between the intermediate supports. This is due to the fact that the external forces are transferred towards the supports, leading to an increase in stresses near the supports. It is also visible that the point loads at mid-span not only induce higher bending moments at the cross-beam directly beneath their point of application, but also have some effects on the neighbouring cross-beams due to the load-spreading effect of the deck slab.

4.4.3. Verification

Before the optimization is started, the results obtained with Karamba should be verified. The verification for the design of the cross-beams has already been carried out. Figure 4.22 shows the check for the equilibrium of vertical forces, the external loads and reaction forces in z-direction, which only differ by a small amount.

The deformation of the main span can be approximated with the engineering formula

$$w = \frac{ql^4}{384EI}$$

which is valid for the deflection at mid-span of a beam clamped at both ends. To compare the deformation calculated by the Karamba model with hand calculations using this formula, the bending stiffness EI has to be calculated for an inhomogeneous cross-section consisting of one girder and a part of the concrete deck. Just as with the multi-girder bridge the effective width of the concrete deck slab which contributes to the bending stiffness of this cross-section can be approximated by $b_{eff} = 2 * h_c / tan(30)$ where h_c is the height of the concrete deck. Following the procedure previously used, first the z-coordinate of the normal force centre should be calculated. See Figure 4.11 for an explanation of the used values. The position of the normal force centre in z-direction is calculated with

$$z_{NC} = \sum \frac{ES_z}{EA}$$

With an effective width of the deck of 1386 mm, an E_s of 210000 N/mm² and and E_c of 33000 N/mm², this formula yields a z_{NC} of 1646.4 mm.

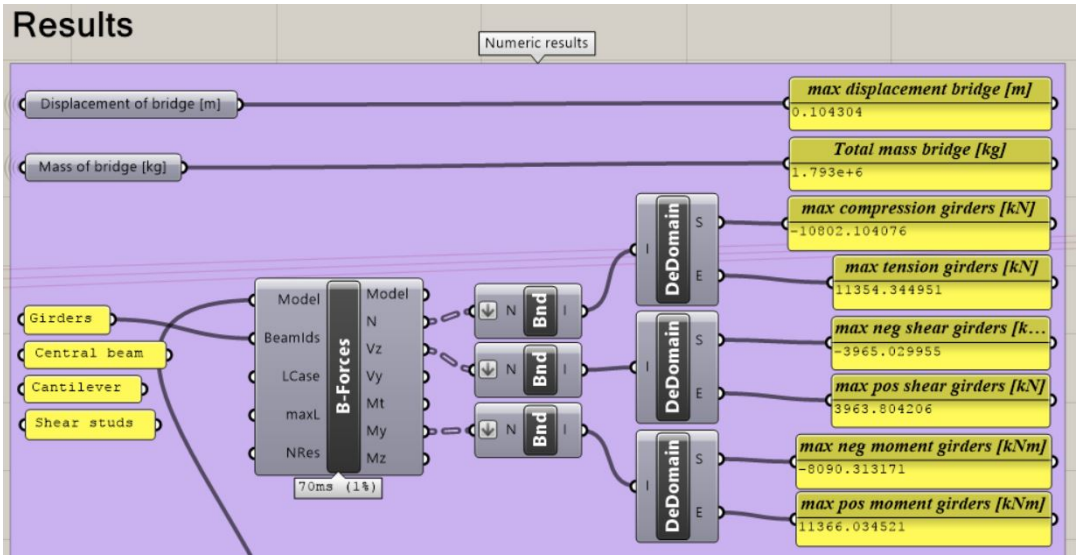

Figure 4.19: Overview of the maximum displacement and total weight of the bridge, including maximum beam forces in the main girders due to LM1

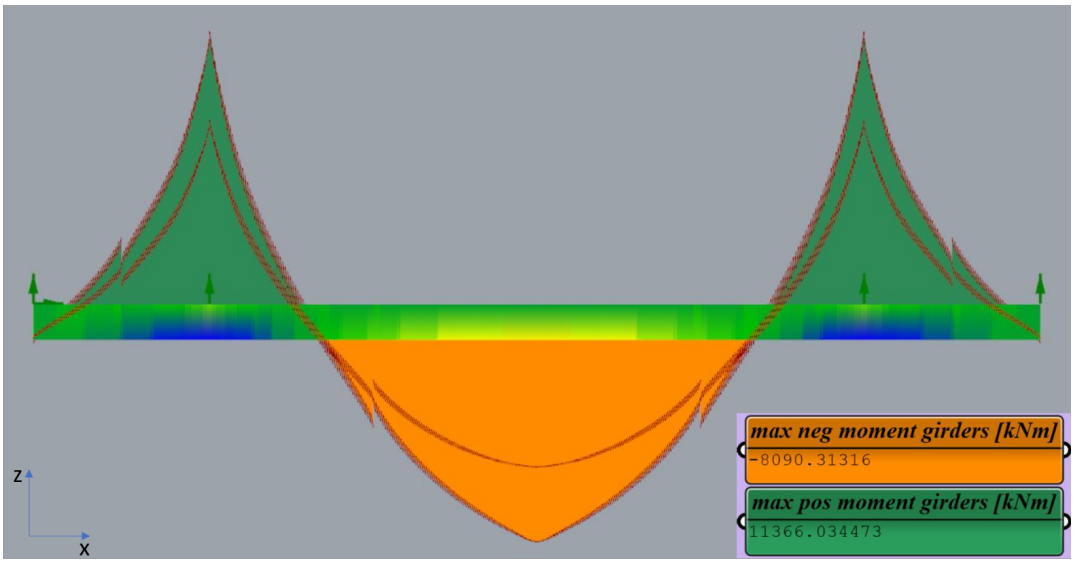

Figure 4.20: Bending moment diagram of the main girders including utilization of the girders due to LM1

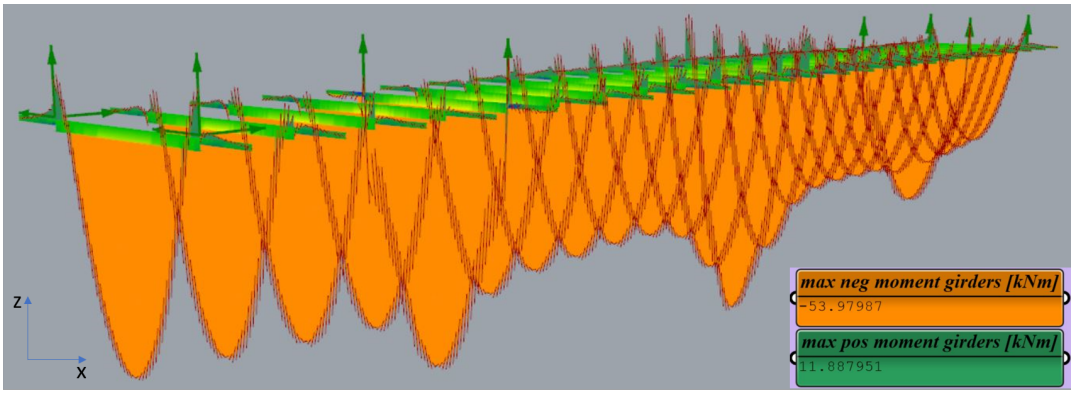

Figure 4.21: Bending moment diagrams of the cross-beams including utilization of the beams due to LM1

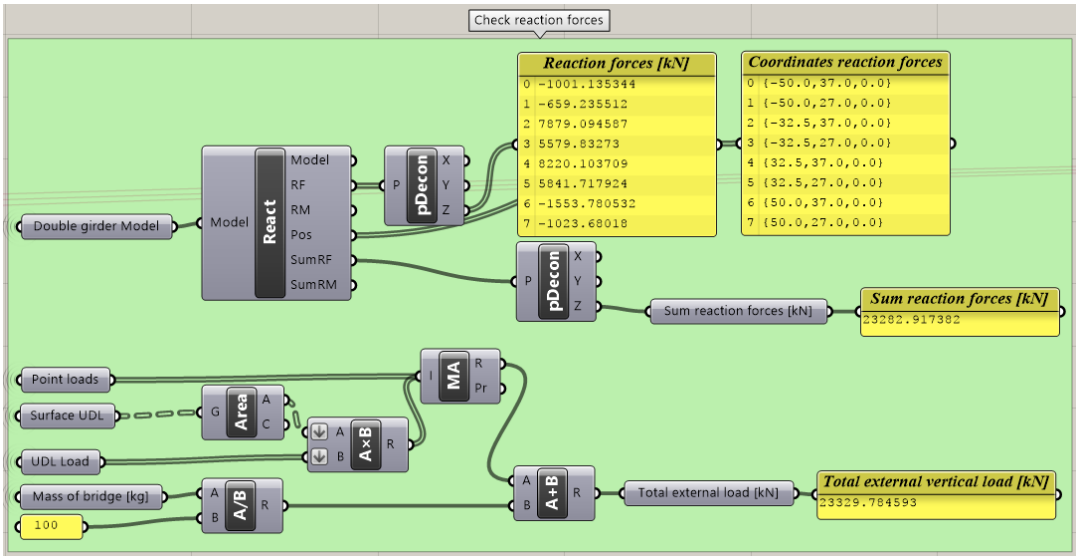

Figure 4.22: Verification of force equilibrium in z-direction between external loads and reaction forces for LM1

Of every rectangular part of the cross-section, the $I_{zz,own}$ is calculated with $I_{zz} = 1/12bh^3$, as well as its surface A_{own} and its own lever arm a_{own}. The formula for the EI of an inhomogeneous cross-section is

$$EI_{zz} = \sum E_{own} * (I_{zz,own} + A_{own} * a_{own}^2)$$

For the double-girder bridge this gives an EI_{zz} of $10.24 * 10^{16}$ Nmm². This value can be used in the engineering formula to calculate the deflection, where the surface load q of 10 kN/m² acts on half the width of the bridge, which is 8 metres, making $q = 10 * 8 = 80$ kN/m and the length of the span $l = 65$ m. This gives a deflection of $w = 36.32$ mm.

In the parametric model the test load of 10 kN/m² is applied on the total deck surface. The intermediate supports are set as clamped, just as assumed with the engineering formula. The maximum deflection at mid-span calculated by the model is $w_{model} = 37.01$ mm. This is 1.86% larger than calculated with the engineering formula. This difference will come from the fact that Karamba will calculate the effective width of the concrete slab precisely. Additionally, the largest deflection at mid-span in the model will be in between the two girders, where the deck will also deflect in transversal direction. This clarifies the difference and thus the model can be approved.

4.4.4. Optimization

For the optimization of the bridge structure Galapagos is used in the same setting as with the multi-girder bridge. This means that the height of the web and the dimensions of the lower flange are variable parameters and whenever a solution does not meet its requirements, the solution will be penalized with a very high number. The costs of the bridge are calculated by calculating the weight of all elements and multiplying these with their unit-costs. Galapagos is set to find the lowest costs and will therefore tend to move away from the penalized solutions.

The solution obtained with Galapagos is that the height of the web is at the maximum of its predefined range, while the dimensions of the lower flange are somewhat above 50% of their range. The principle of Figure 4.14 also holds for this bridge. This means that the external bending moment M_{Ed} has to be compensated by the internal bending moment $M_{Rd} = f_y * A_s * a$. In this case it is clear that the maximum height of the web, a, is not sufficient and also the dimensions of the bottom flange, A_s, need to be increased to resist M_{Ed}. Since increasing the height of the web will use less material than increasing the dimensions of the flanges, and therefore would have a lower impact on the overall costs, it would seem logical to increase the range of the parameter for the web. But, this would lead to implications for transport and as discussed at the multi-girder bridge, this would also lead to a large increase in the costs for the adjacent bridge structures.

The optimization procedure of Galapagos is recorded and all solutions produced are plotted in a parallel coordinate plot. Figure 4.23a shows all these solutions, while in Figure 4.23b the selection is reduced to the solutions which satisfy the boundary conditions. It is clearly visible that only a small part of the upper range

of the height of the web produces viable solutions, while the ranges of the dimensions of the lower flange have to be above 50% to produce a high enough bending moment resistance. The solution with the lowest costs is highlighted in Figure 4.23c, where the height of the web is at its maximum and the dimensions of the lower flange are at the lowest range of the viable solutions. As explained earlier, this is a logical solution since increasing the height of the web has a lower impact on the costs than increasing the dimensions of the lower flange. For comparison, the solution with the lowest height of the web is highlighted in Figure 4.23d, which shows that for a small reduction in height, the width of the flange has to be at is maximum.

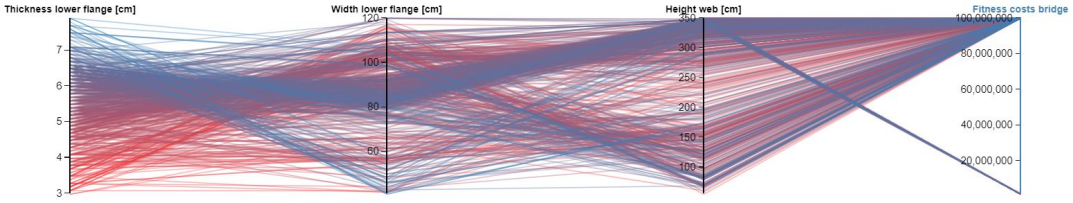

(a) Parallel Coordinate Plot showing all variants produced by Galapagos while optimizing the double-girder bridge [1]

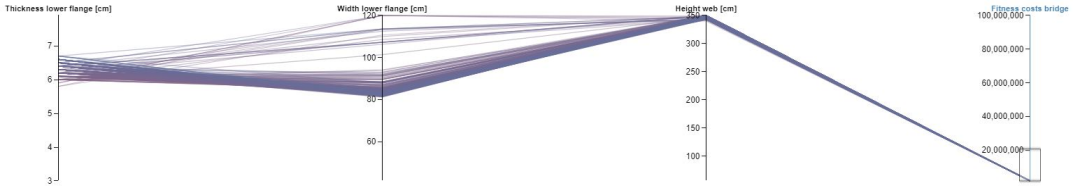

(b) Parallel Coordinate Plot showing the variants which satisfy the requirements, produced by Galapagos while optimizing the double-girder bridge [1]

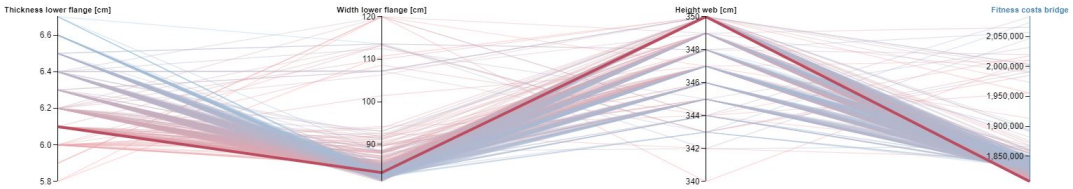

(c) Parallel Coordinate Plot highlighting the solution with the lowest cost produced by Galapagos while optimizing the double-girder bridge [1]

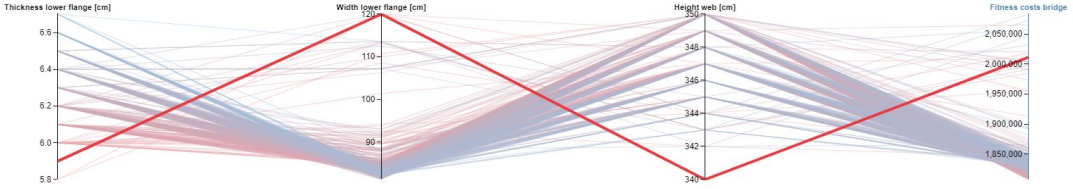

(d) Parallel Coordinate Plot highlighting the variant which has the lowest height of the web, produced by Galapagos while optimizing the double-girder bridge [1]

Figure 4.23: Parallel Coordinate Plots showing different selections of solutions produced by Galapagos while optimizing the double-girder bridge [1]. At (c) and (d) the parameters are rescaled to provide a better overview

4.5. Truss Beam Bridge

The truss bridge is modelled as a warren without verticals. All input parameters and values are visible in Figure 4.24. The outer dimensions of the truss members are kept constant while the height of the truss and the thickness of the box-shaped cross-sections walls are variable. With these values the geometry of the truss bridge is modelled, of which a part of its description is visible in Figure 4.25. The resulting geometry in centre lines and surfaces including the location of supports is visible in Figure 4.26. The desired spacing of the cross-beams is 4 meters to sufficiently support the concrete deck so that its thickness can be kept to a minimum. For structural efficiency and simplicity, however, it is desirable to divide the bays in an equal number of cross-beams. To accomplish this, the bay width of the truss is divided by the desired spacing, the result is then rounded to the nearest whole number and eventually the bay width is divided by this rounded number, resulting in the exact spacing of the cross-beams. In this case the truss of 65 m has 5 bays of 13 m which lead

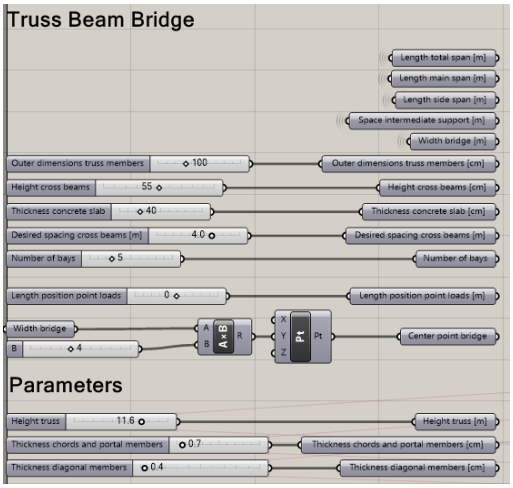

Figure 4.24: Input values and parameters for the truss bridge

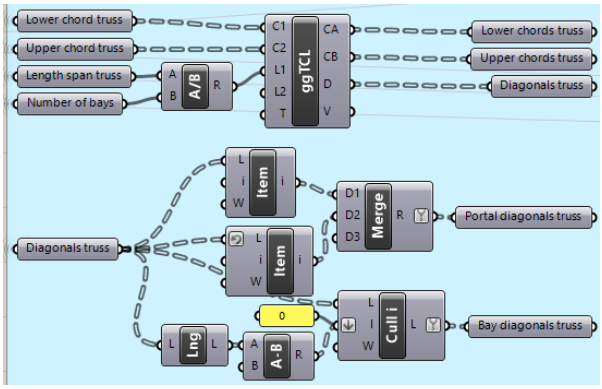

Figure 4.25: Geometric description for the truss shape and the separation into portal and bay diagonals

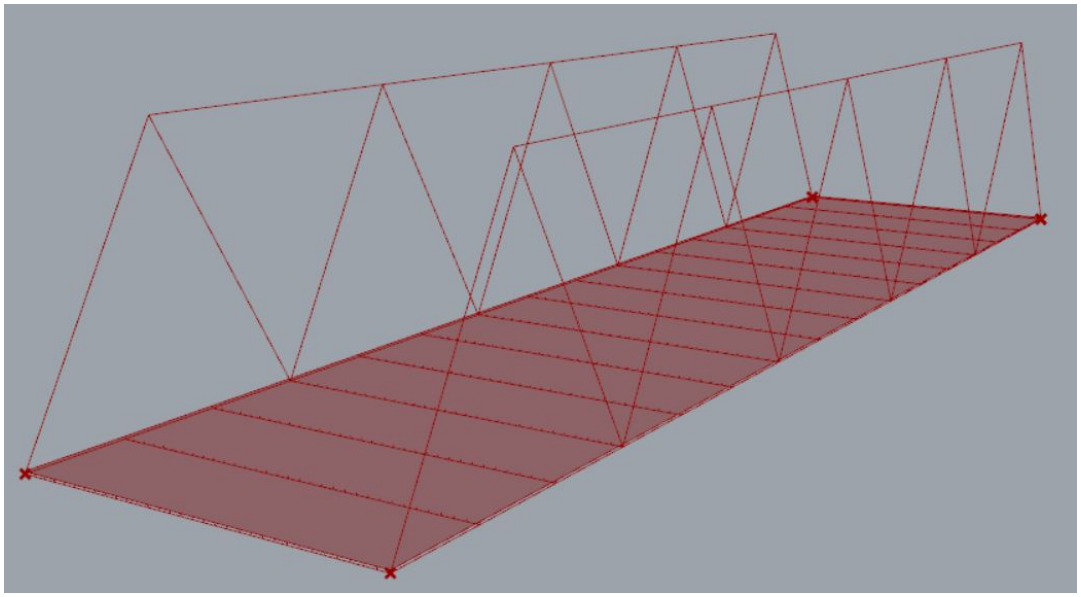

Figure 4.26: Geometry of the truss bridge modelled in centre-lines and surfaces

to a cross-beam spacing of 4.33 m.

4.5.1. Element Properties

All element specific properties, support conditions and loads are modelled with Karamba. All truss members consist of box-shaped members with the same outer dimensions, the cross-beams are I-profiles and the deck is a concrete shell. Since the truss elements all have the same cross-sectional shape, they can be modelled with one Karamba module, as can be seen in Figure 4.27. The different elements are separated by using different names, so that they can be singled out at a later stage more easily for structural analysis. One transversal line of supports is pinned and the other line is sliding, making the truss statically determinate. The standard loads according to LM1 are placed on the bridge, with the point loads at mid-span, where they have the most unfavourable effect for deflection. Steel of strength class S355 and concrete of class C35/45 is used. All properties are assembled into one bridge model and analysed. Figure 4.28 shows a cross-section of the bridge and in Figure 4.29 a 3D overview is presented.

The design of the cross-beams follows the same approach as with the double-girder bridge. The section modulus should be large enough in order to resist the external bending moment. With a span of 16 m, spacing of 4.33 m, and deck thickness of 40 cm, the section modulus is $W = 4.879 * 10^6 mm^3$. HEA650 beams with a

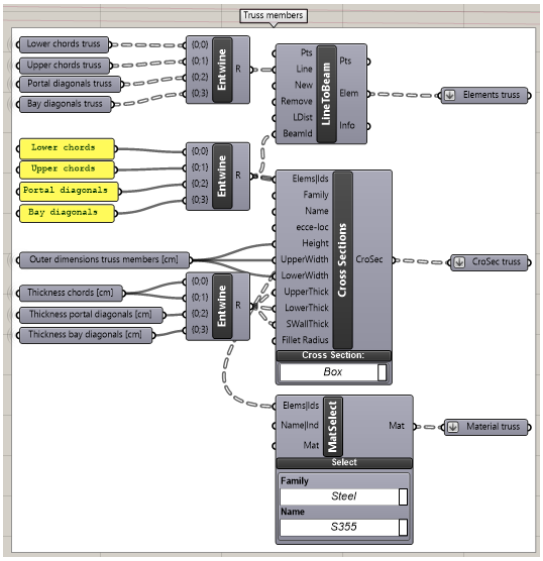

Figure 4.27: Modelling the section properties of all truss members with Karamba, keeping different types of members separated by name

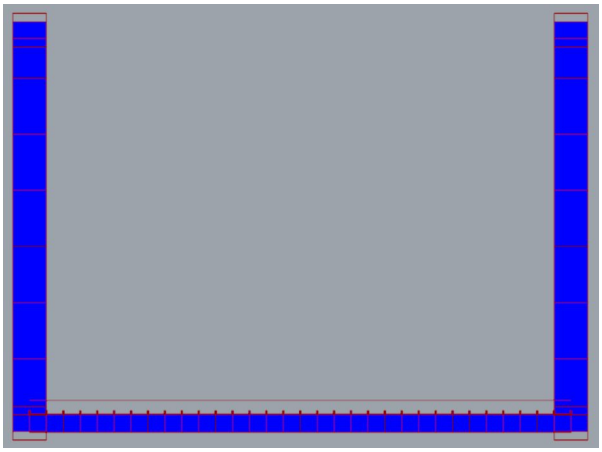

Figure 4.28: Cross-section of the truss bridge as modelled with Karamba

section modulus of $5.474 * 10^6 mm^3$ will be able to carry the load. In the model cross beams of IPE550 are used, this will have a slight influence on the structural behaviour, mostly due to the reduced weight of the IPE beams.

4.5.2. Structural Analysis

With the bridge model assembled and calculated, the results can be analysed. The connections between truss elements are not modelled as being hinged, which in practice would also be the case, and therefore some bending moments in the truss members occur. The truss still transfers the external loading mainly by compressive and tensile forces in its members towards the supports. If a beam is loaded in bending, the top part will be under compression while the bottom part of the beam will be in tension. Figure 4.30 shows all normal forces in the outer truss elements. Figures 4.30a and 4.30b clearly show that the bottom chord is in tension and the top chord is under compression, with the exception that in two parts of the lower chord compression forces are present. This is due to the fact the the outermost bay diagonals are under high tension forces and therefore introduce compression into the bottom chord. From mid-span toward the supports the diagonals are alternating in compression and tension respectively, as can be seen in Figures 4.30c and 4.31. This is also predicted in Figure 2.9.

4.5.3. Verification

Verification of the results of the truss bridge is done by checking the vertical force equilibrium, the normal force in the portal diagonals and the bending moment resistance of the truss.

Verification of the normal force in the portal diagonals is based on the fact that the vertical support reaction must be equalized by the vertical component of the normal force in this diagonal. This is to ensure equilibrium of forces at the supports. Each truss is simply supported and statically determinate, therefore the vertical force component of the support must be equal to

$$R_V = 1/2ql$$

The normal force in the portal diagonal should then be

$$N = R_V / sin(\alpha)$$

with α the angle between the diagonal and the horizontal. In this case the test load of $10kN/m^2$ is applied on the deck surface. Figure 4.32 shows this check of the normal force inside Grasshopper. It is clear that the actual forces acting in the portal diagonals are 1.2% lower than calculated by hand and it can therefore be concluded that this part is correct.

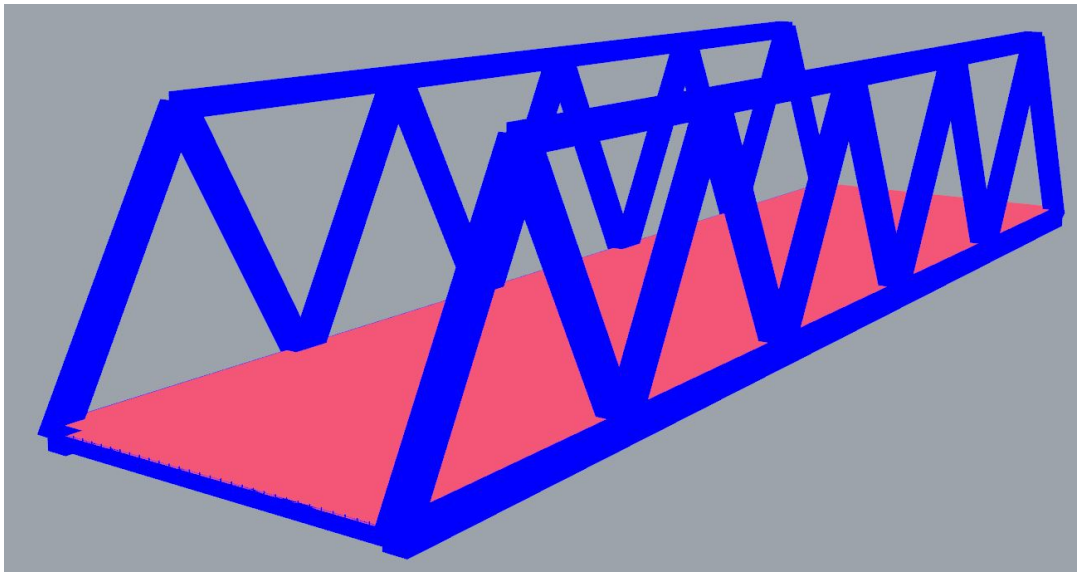

Figure 4.29: Geometry of the truss bridge with section properties as modelled with Karamba

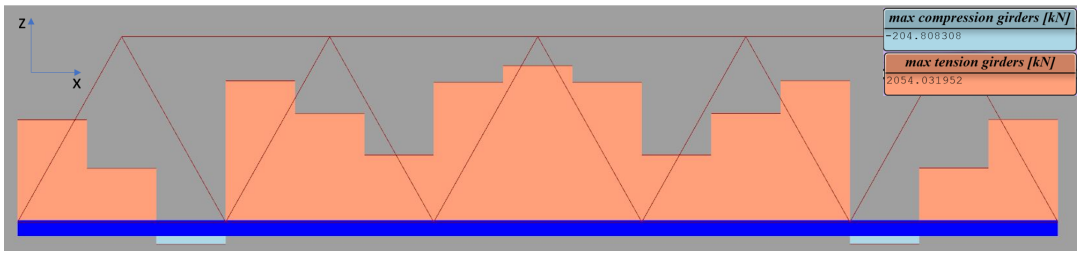

(a) Normal force in the lower chord of the truss

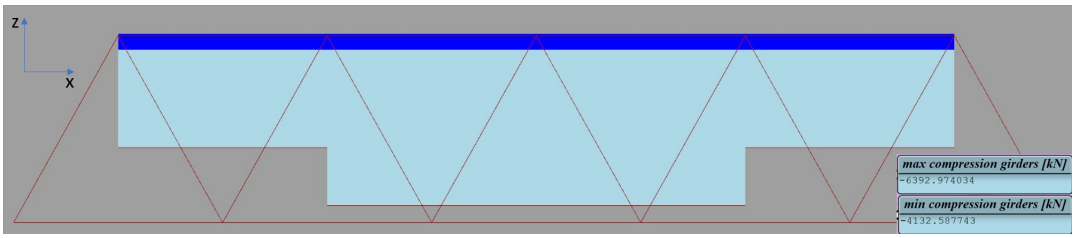

(b) Normal force in the upper chord of the truss

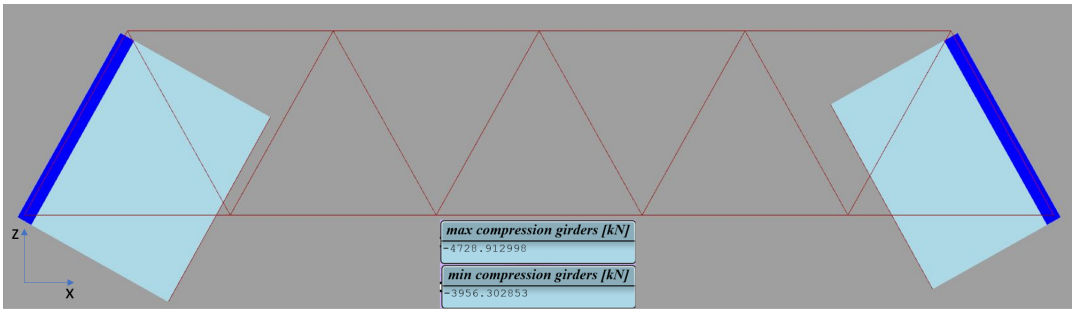

(c) Normal force in the portal diagonals of the truss

Figure 4.30: Normal forces of the outer truss members which are closest to the point of application of the point loads from LM1, red is tension and blue is compression

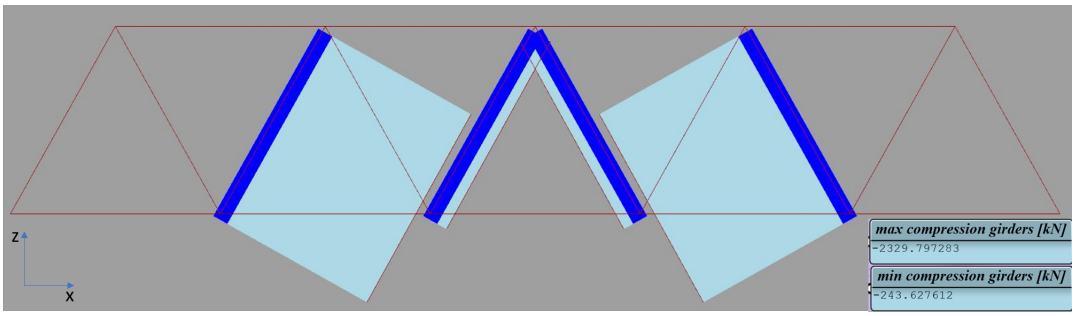

(a) Normal force in the compression bay diagonals of the truss

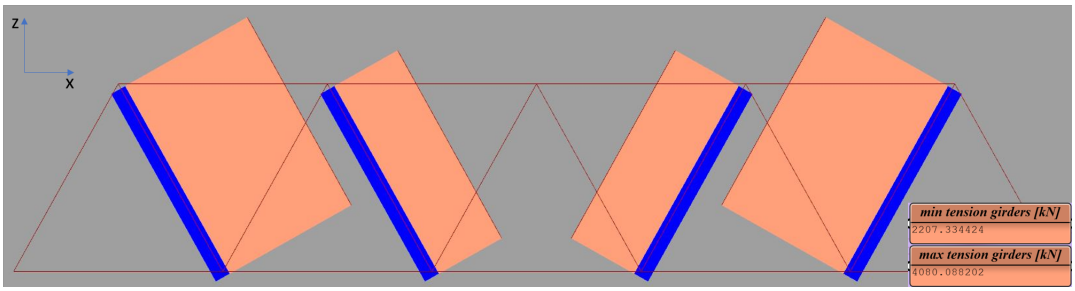

(b) Normal force in the tensile bay diagonals of the truss

Figure 4.31: Normal forces of the bay diagonal truss members which are closest to the point of application of the point loads from LM1, red is tension and blue is compression

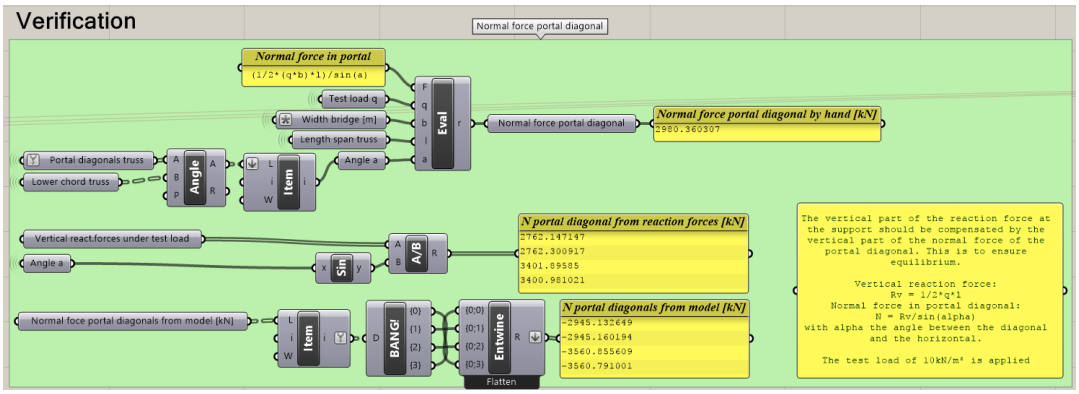

Figure 4.32: Verification of the normal forces in the portal diagonals of the truss bridge

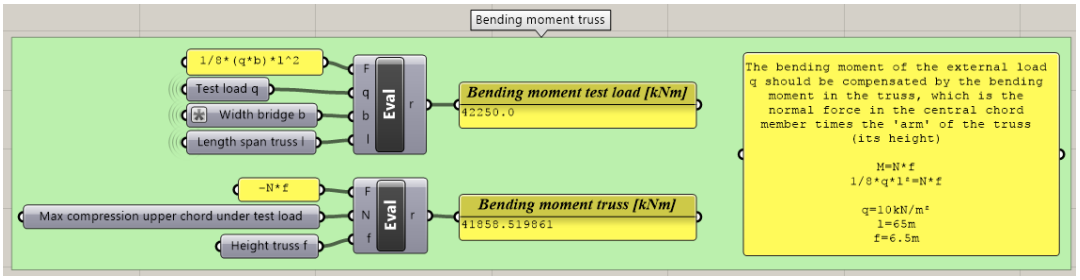

Figure 4.33: Verification of the bending moment resistance of the truss bridge

In the same way that a beam resists bending moments, with tensile forces at the bottom and compression forces near the top which form a couple, the truss resist bending with tension in the bottom chord and compression in the top chord. The external bending moment M_{Ed} should be resisted by the normal force in either the top chord or the bottom chord times the height of the truss, which is the arm f. In other words

$$1/8ql^2 = N * f$$

Figure 4.33 shows that the external bending moment M_{Ed} is only 0.9% larger than the internal bending resistance of the truss. It can therefore be concluded that the truss bridge model behaves as intended.

4.5.4. Optimization

With the structure ready, the weight of the different structural elements is calculated by multiplying the cross-sections with the length of the elements and the unit weight of the material. The different materials are then multiplied with their unit costs to obtain the costs of the structure. In the same set-up as with the girder bridges, Galapagos is set to find the lowest cost for the bridge while still complying with the requirements. This is done by changing the height of the truss, the thickness of the chords and portal members and the thickness of the bay diagonals.

All results are recorded and plotted in a PCP, which is visible in 4.34a. The plot shows that a large variety of values for the different parameters give viable solutions. It is also visible that Galapagos concentrated around solutions with a large truss height and a low thickness of the truss members. Figure 4.34b shows this tendency, where a lot of different combinations of parameters give solutions which meet the requirements. They also produce a large spread in total costs, ranging from 1.2 million to over 11 million Euro.

Figure 4.34c shows the solution with the lowest costs. This solution has a large truss height with thin member walls. Since only steel members are involved in the optimization, minimizing costs is the same as minimizing weight, or volume, in this optimization procedure. The volume of a hollow box member equals the surface A times the lenght l. With the surface being $A = 4ht - 4t^2$, with h the outer box dimension and t the wall thickness, the volume of a member can be described with

$$V = 4hlt - 4lt^2$$

Since the truss members have a much larger h and l compared to the wall thickness t, this function behaves like a linear one, as can be seen in Figure 4.35. The difference between the change of volume over the change of thickness and the change of length, depicted in 4.35a and 4.35b, is equal to the factor of difference between the thickness and the length of the hollow box member. With truss members where the length is a factor 10^2 larger than the thickness, it is evident that for the same decrease in volume, a much smaller decrease in thickness t is needed compared to a decrease in length l. This explains why Galapagos tends to minimize the wall thickness of the truss members.

To minimize the wall thickness, the stresses in the truss members should be as low as possible. This is accomplished by increasing the height of the truss. As discussed during the verification of this bridge, the external bending moment has to be compensated by the internal moment, $M_{Ed} = N * f$. While M_{Ed} is constant, the normal force in the chord members can be decreased by increasing the height of the truss f. In every node of the truss, there must be equilibrium of forces, a lower force in the chords therefore leads to lower forces in the diagonals. The force equilibrium is also affected by the angle between the horizontal and diagonal members. Increasing the height of the truss increases the angle, and therefore also increases the forces in the diagonals. This increase is however smaller than the decrease caused by the larger height

of the truss. With lower normal forces in the truss members, the stresses will be lower and therefore the wall thickness can be reduced. The extra volume due to an increase in height of the truss is compensated by a larger reduction in volume due to a decrease in wall thickness and this explains the solution obtained with Galapagos.

For comparison, the solution with the lowest height of the truss is highlighted in Figure 4.34d. The truss is almost seven metres lower in height, but due to the chords and portal diagonals being nine centimetres thicker and the bay diagonals being almost two centimetres thicker, this solution is four times more expensive.

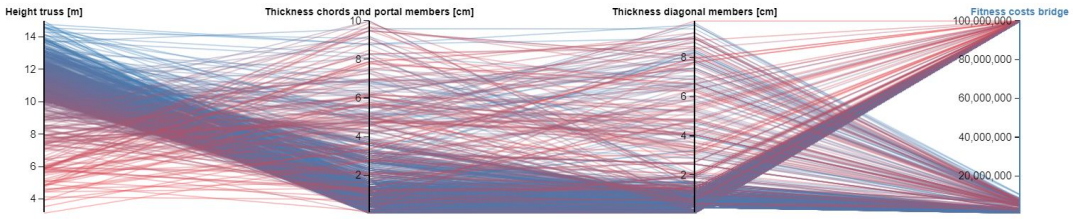

(a) Parallel Coordinate Plot of all solutions produced by Galapagos while optimizing the truss beam bridge

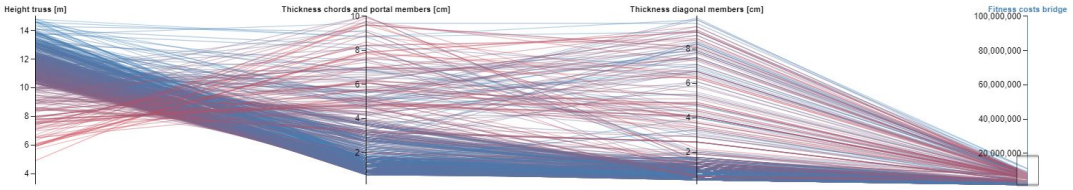

(b) Parallel Coordinate Plot of all solutions meeting the requirements produced by Galapagos while optimizing the truss beam bridge

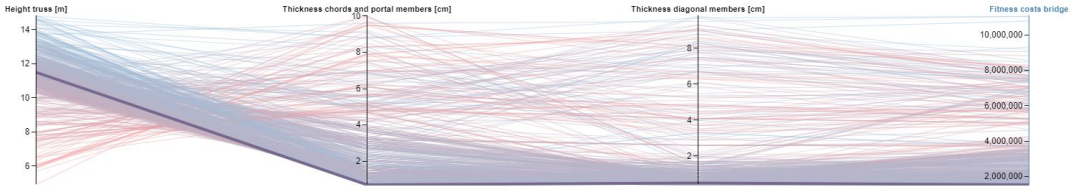

(c) Parallel Coordinate Plot highlighting the lowest cost solution produced by Galapagos while optimizing the truss beam bridge

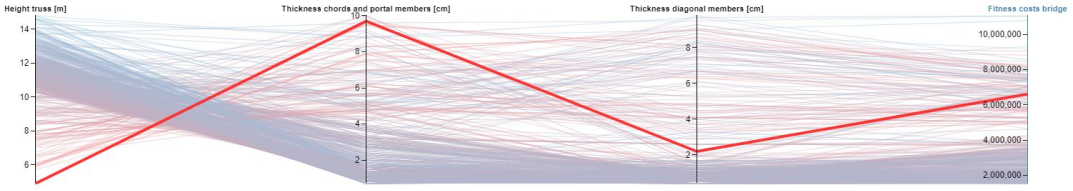

(d) Parallel Coordinate Plot highlighting the solution with the lowest height of the truss produced by Galapagos while optimizing the truss beam bridge

Figure 4.34: Parallel Coordinate Plots showing different selections of solutions produced by Galapagos while optimizing the truss beam bridge [1]. At (c) and (d) the parameters are rescaled to provide a better overview

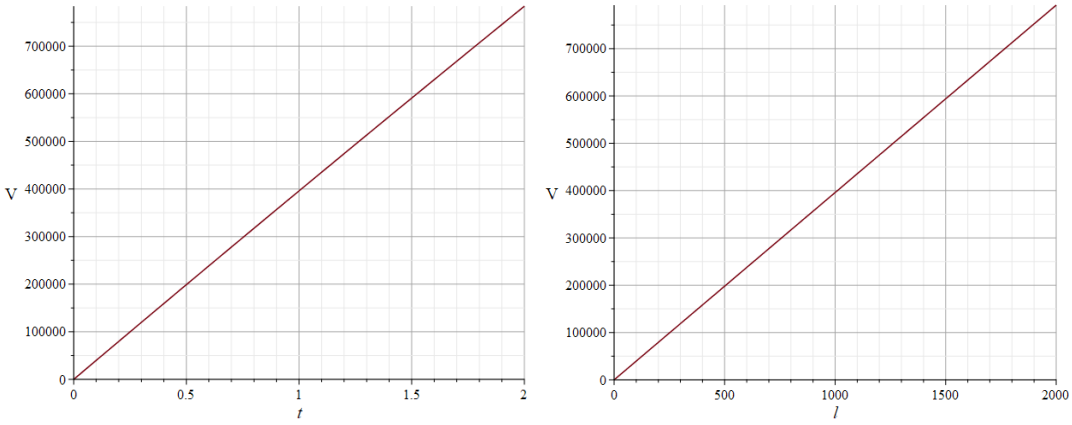

(a) Change of volume over the change of wall thickness, $h = 100$ and $l = 1000$

(b) Change of volume over the change of length, $h = 100$ and $t = 1$

Figure 4.35: Graphs showing the change of volume of a hollow box member for the change of either the wall thickness t or the length l

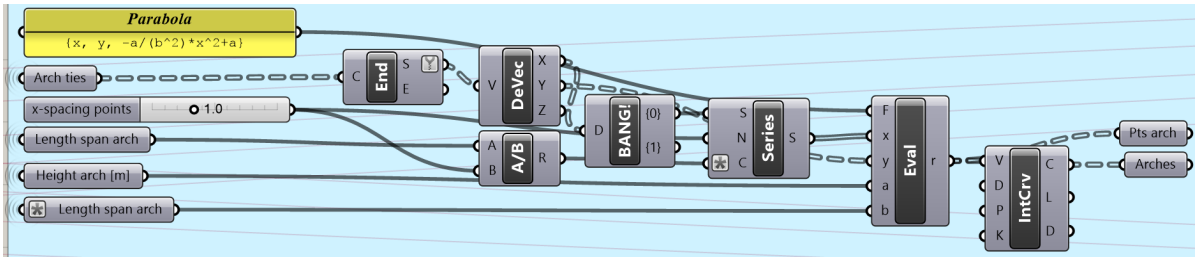

Figure 4.36: Part of the geometric description showing the parabolic function used to model the arch

4.6. Arch Bridge with Vertical Hangers

The shape of the arch is described by a parabolic function, $z = (-a/b^2) * x^2 + a$ in the x,z-coordinate system, where a is the height and b is the span of the arch. The arches are pinned at one side and sliding at the other side, since the soil conditions usually are bad in the Netherlands. Two longitudinal hollow box-shaped girders act as ties to take up the horizontal thrust forces from the arches. They are supported by vertical hangers suspended from the arch. The concrete deck is supported by cross-beams spanning the transversal distance between the ties and spaced at preferably four metres. For simplicity and structural efficiency, it is desirable that the cross-beams are spaced at such distances, as to divide the bay width between the hangers in equal numbers. This is also visible in Figure 4.39, where the 3D geometric model of the arch bridge is visualized.

As explained in the previous chapter, the arch bridge was originally designed without lateral bracing between the arches. In this case however, the arches would tend to topple inwards, causing large and unwanted deformations. In order to maintain their shape, the base of the arches would need to be very wide and stiff. It is therefore decided to add lateral bracing between the arches at the locations of the joints of the hangers. The minimal clearance for traffic of 4.80 metres is taken into account as a constraint for the minimal height of the bracing. The bracing elements between the arches are not designed in detail, but purely modelled to provide transversal stability for the arches.

Figure 4.37 shows all the input values and parameters used for this model. The outer dimensions of the arch ribs are kept constant, as well as the deck thickness and design for the cross-beams. The height of the arch and the thickness of the ribs, as well as the dimensions of the ties and the diameter of the hangers are parametric and input for the optimization. In Figure 4.36 a part of the geometric description for this arch bridge is visible which shows the parabolic function used to model the arch.

4.6.1. Element Properties

With Karamba all properties are assigned to the different elements. The arch ribs, as well as the longitudinal ties are hollow box sections. The vertical hangers are modelled as being steel rods which can't take any bending, making the connections hinged. This part can be seen in Figure 4.38, where bending of the element is

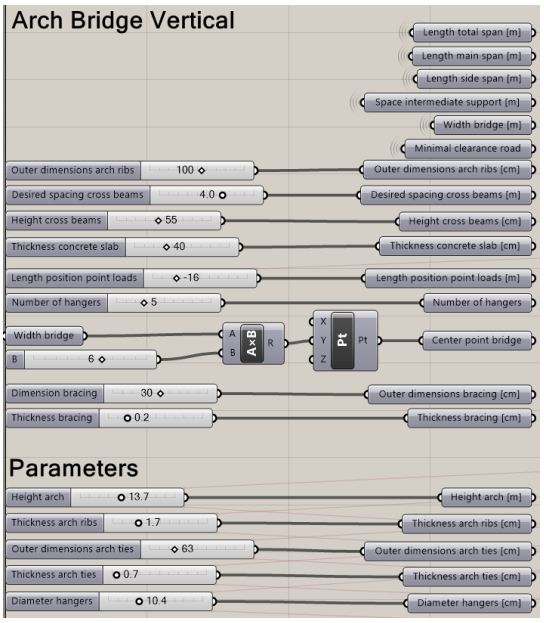

Figure 4.37: Input values and parameters used to model the arch bridge with vertical hangers

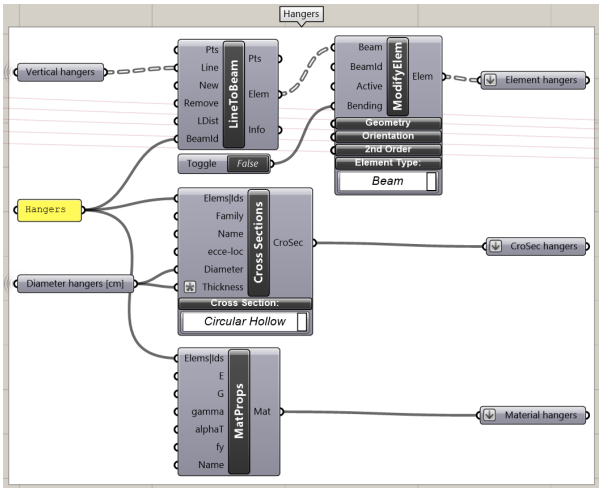

Figure 4.38: Description of the hanger properties with Karamba, showing that the elements can't take bending so that they are modelled as being hinged

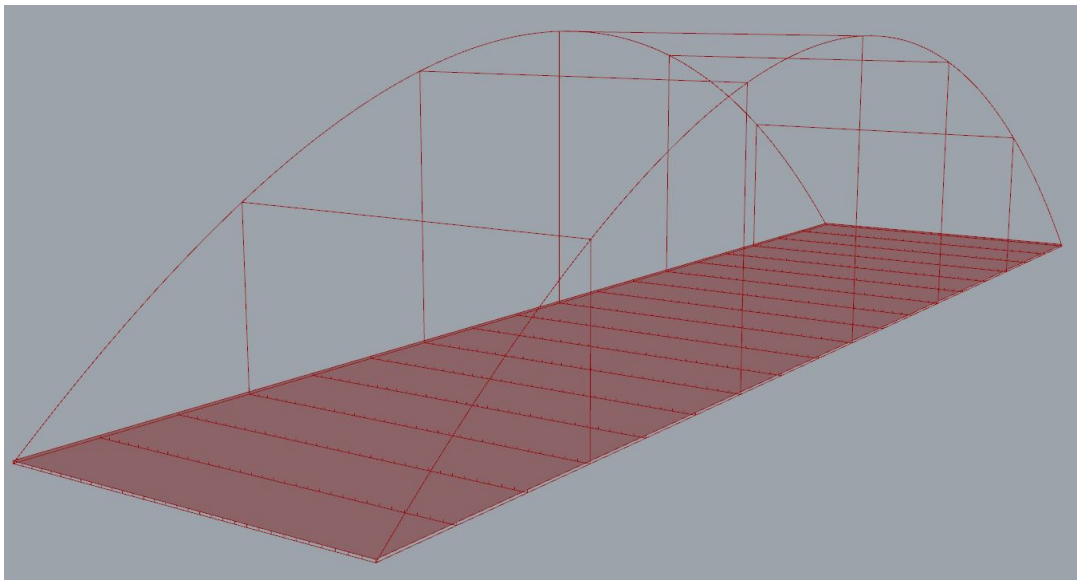

Figure 4.39: Geometric model of the arch bridge with vertical hangers in centre lines and surfaces

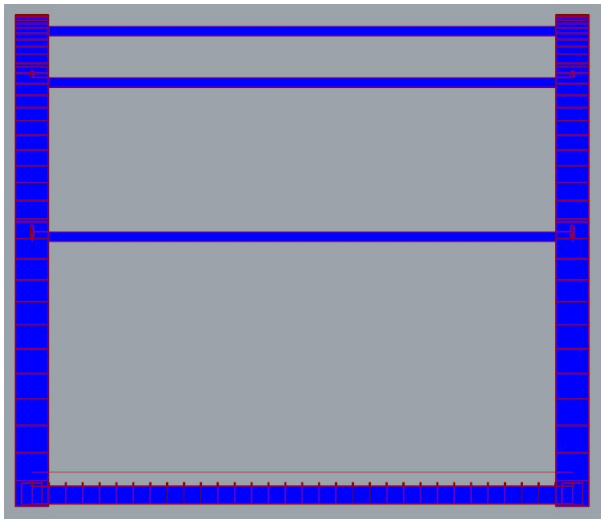

Figure 4.40: Cross section of the arch bridge with vertical hangers

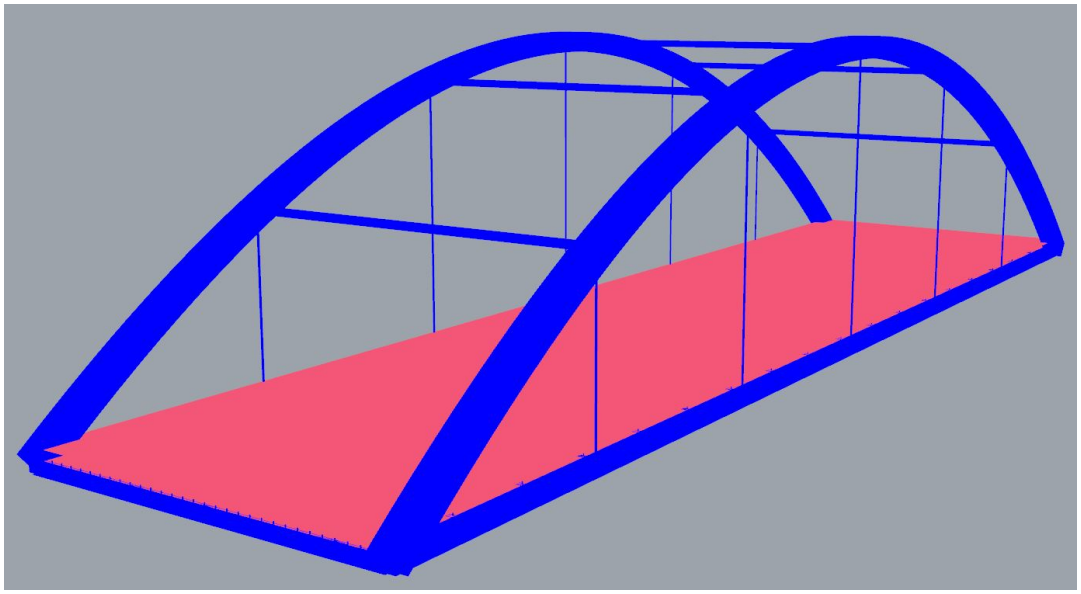

Figure 4.41: 3D model of the arch bridge with vertical hangers, in red the concrete deck and in blue all steel elements

set to false. The concrete deck is 40 cm thick and supported by cross-beams of IPE550, which are in turn supported by the ties with hinged connections, making the cross-beams simply supported. If the cross-beams were to be calculated to carry the full wet concrete weight, a section modulus of $4.068 * 10^6 mm^3$ would be needed, resulting in an HEA550 beam. The spacing of the cross-beams is again desired to be four metres, but changed to the closest number which divides the hanger spacing equally. The transversal bracing between the arches are rectangular hollow section beams which are purely modelled to stabilize the arch ribs and therefore are not calculated separately. Rectangular hollow sections are chosen as to have no weak axis for buckling. A cross section and 3D overview of the arch bridge with all section properties is visible in Figures 4.40 and 4.41.

4.6.2. Structural Analysis

In a parabolic tied arch, the horizontal force H is constant and the bending moment consists of two parts and can be described with the formula

$$M = M^a + M^H$$

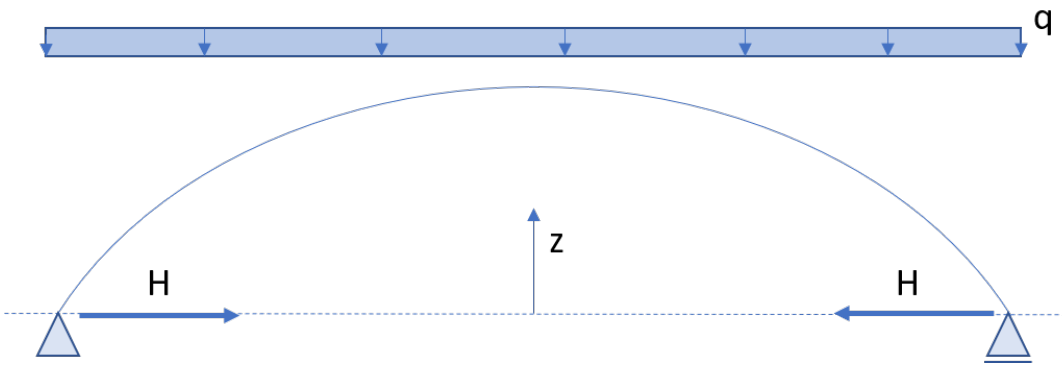

Figure 4.42: Parabolic tied arch with a uniformly distributed constant load q

where M^a is the bending moment equal to a simply supported straight beam under uniform loading and M^H is the bending moment due to the horizontal forces at the supports. In case of the tied arch, the horizontal forces are taken up by the ties, and the resulting bending moment in the arch is $M^H(x) = H * z(x)$ where $z(x)$ is the shape of the arch. In case of a uniformly distributed load, as is depicted in Figure 4.42, the bending moment of a straight beam has a parabolic shape in the form of $M^a(x) = 1/2 * qx(l-x)$. Since the arch has a parabolic shape, $z(x)$ is a parabolic function and therefore M^H will also be parabolic, but in the opposite direction of M^a. As a matter of fact, M^a and M^H will cancel each other making M zero when the arch is loaded by a uniformly distributed constant load.

The worst loading condition for arches is asymmetric loading, since this induces large bending moments in the arch. The largest moment occurs when the arch is loaded by a UDL over only one half of the span of the arch, or equivalently by a point load acting at one quarter of the span. When an arch structure is asymmetrically loaded, the load can be split-up in a symmetric constant load, and a contra-symmetric load, as is depicted in Figure 4.43. In case of a parabolic arch shape, the symmetric load will cause no bending moments. The contra-symmetric load will cause bending moments, and the arch will deform in an S-like shape.

Since EC1 describes that the point loads of LM1 should be positioned at the most unfavourable position in length-direction of the bridge, it is expected that this is at a quarter of the span. To be sure, Galapagos is used to find the location of the load which yields the largest deflection of the bridge. The outcome of this optimization run is that the point load should indeed be located at a quarter of the span. A magnified deflected shape of the arch can be seen in Figure 4.44, where the predicted S-like shape is clearly visible.

With the load positioned, the structural behaviour of the bridge can be analysed. The normal force in the arch rib consists of only compression, which is to be expected. Figure 4.45 shows the normal force diagram of one of the arch ribs. It shows that the normal force gradually increases from the top towards the supports. Earlier it was stated that the horizontal force component H is constant over the arch. With the inclination of the arch increasing from the top towards the support, and with a constant horizontal force component, it is to be expected that the normal force will gradually increase towards the supports. The vertical hangers introduce additional normal forces as can be noticed by the peaks. Since the point loads from LM1 are at the left quarter of the arch, the normal force at this side is slightly larger.

Since the bridge is asymmetrically loaded, and the shape of the thrustline of this load does not coincide with the parabolic shape of the arch, bending moments are present in the ribs. Figure 4.46 shows the bending moment diagram of one arch rib. The negative moment on the left and the positive moment on the right are due to the asymmetric point loads of LM1, due to which the left part of the arch tends to bend downwards and the right part of the beam tends to bend upwards, resulting in an s-like shape of the arch, see Figure 4.44 for an impression. The vertical hanger forces introduced in the arch tend to locally bend the arch downwards, hence the peaks in the diagram towards the negative spectrum. Since the arch is loaded by point loads from the hangers, one would expect straight lines in the bending moment diagram. However, as explained earlier, the horizontal forces also cause bending moments in the arch, M^H, which has a parabolic shape.

This bending moment diagram does not look like the conventional diagrams known from a single point load or distributed loads. Therefore it is wise to check if the model produces a more recognizable diagram. The number of hangers is increased to 30, as to distribute the loads from the deck more evenly on the arch and only the point loads from LM1 are considered. Self-weight and the distributed load from LM1 are turned

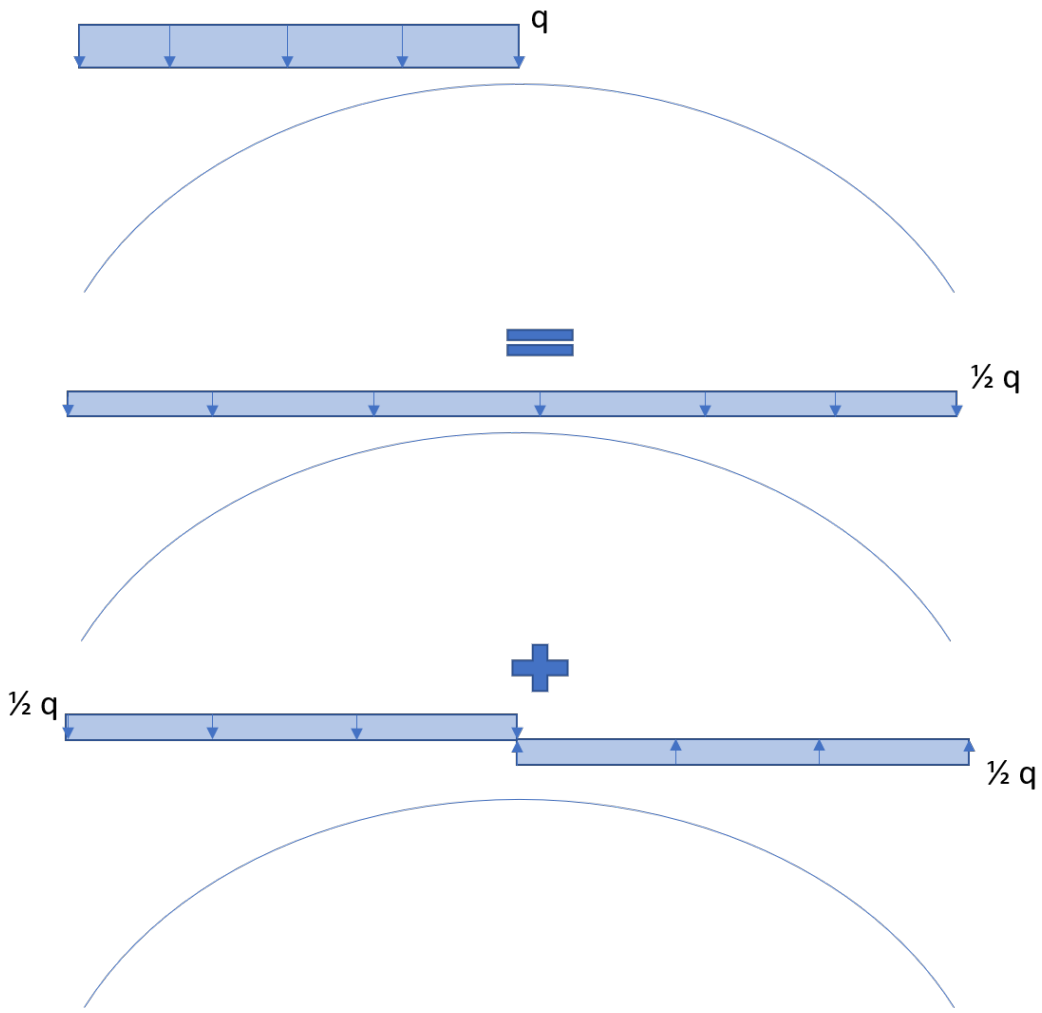

Figure 4.43: Parabolic arch with an asymmetric uniformly distributed constant load q

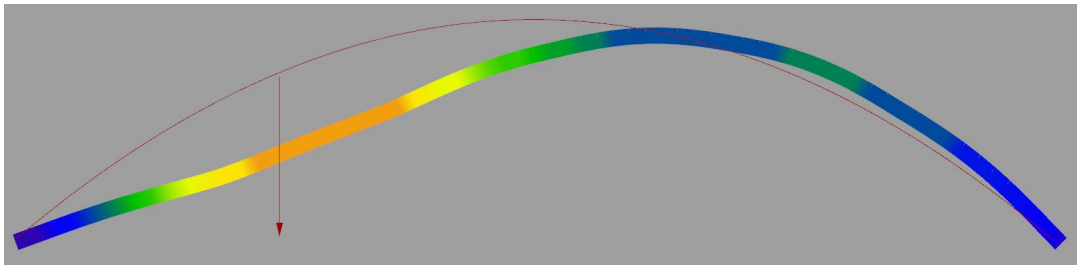

Figure 4.44: Deformation of one arch rib of the vertical hanger arch rib, with the point of application of the point loads and the original arch shape visible, scaled by a factor 40

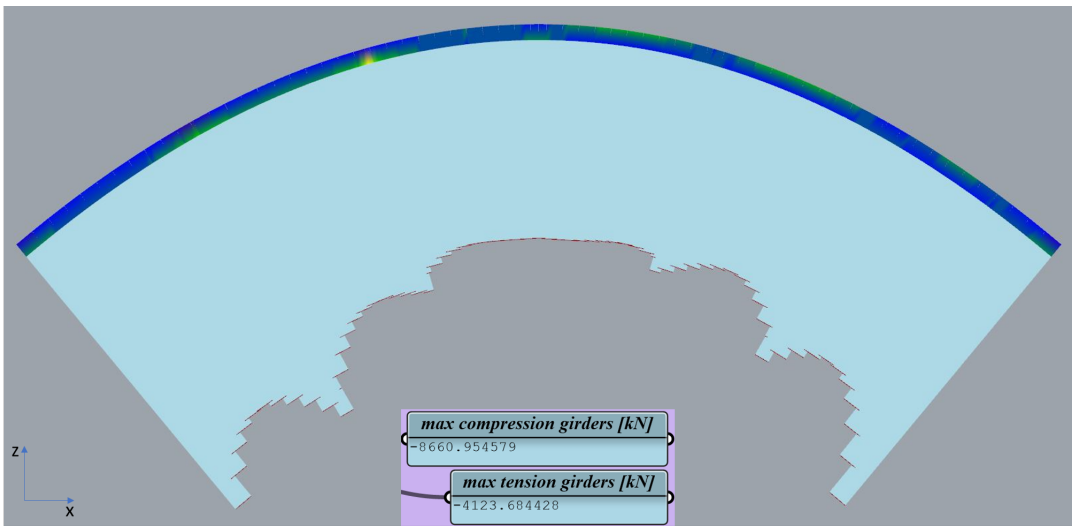

Figure 4.45: Normal force diagram of one arch rib, as obtained with Karamba

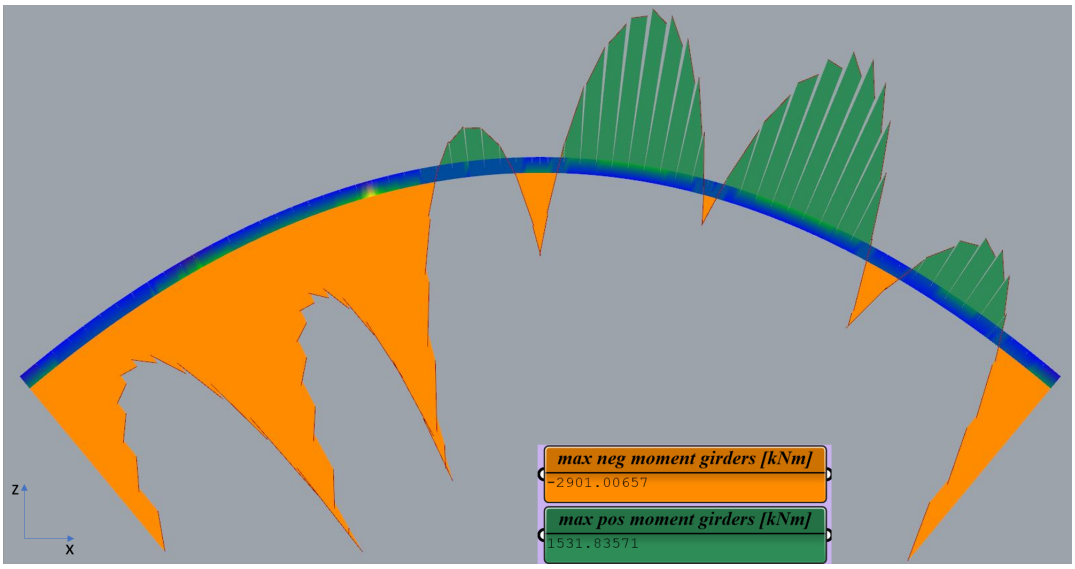

Figure 4.46: Bending moment diagram of one arch rib, as obtained with Karamba

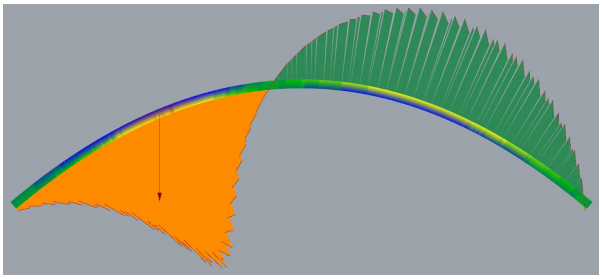

Figure 4.47: Bending moment diagram for arch with increased number of hangers and point load at 1/4 span as obtained with Karamba

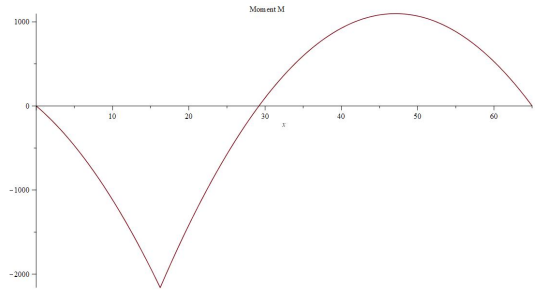

Figure 4.48: Bending moment diagram for an arch with pointload at 1/4 span as obtained by solving the ODE with Maple

off. The resulting bending moment diagram is visible in Figure 4.47. To check this diagram, the bending moment is calculated with the ordinary differential equation (ODE) for an arch by using Maple. The shape of the arch is described with the formula $z = -4fx(l-x)/l^2$, where f is the height of the arch and l the span. The differential equation is

$$ODE = EI\frac{d^4w}{dx^4} + H\frac{d^2z}{dx^2} - q = 0$$

where w is the deflection and H is the horizontal force. The distributed load q is zero in this case and the point load is applied at 1/4 of the span. With the boundary conditions of zero displacement and zero bending moment at the supports, the differential equation is solved and the resulting bending moment diagram is plotted and visualised in Figure 4.48. It is clear that the shapes of these two diagrams are very similar and therefore it can be concluded that the bending moment diagram produced by Karamba is correct. In Appendix B the Maple code to calculate the bending moment is presented.

In this model, lateral bracing between the arches is placed at every connection of the hangers above the minimal clearance of 4.80 metres. It should be noted however that the forces in the bracing elements are low, and only at the top range of the arch bracing would be needed. The maximum compression force in the bracing is 12.6 kN, whereas the buckling force is $F_B = \frac{\pi^2 EI}{l_b^2} = 282.6$ kN. The buckling length is taken as the length of the bracing element, since the connections will be in-between hinged and clamped and hinged connections have a more unfavourable effect on buckling.

4.6.3. Verification

Verification of the arch bridge is done by checking vertical force equilibrium, the normal force in the hangers and the bending moment resistance of the arch. Vertical force equilibrium is checked by calculating the total vertical external load and comparing this to the sum of all vertical reaction forces.

The bending moment resistance M_{Rd} of the arch is calculated by multiplying the normal force in the top of the arch, times the height of the arch $M_{Rd} = N * f$. The bending moment resistance should be equal to the external bending moment, $M_{Rd} = M_{Ed}$. The test load of $q = 10kN/m^2$ is applied and one arch carries half of the width of the bridge. The check to be performed becomes $N * f = 1/8ql^2$. From this formula one can calculate the normal force to be expected in the top of the arch. Figure 4.49 shows that the calculated normal force is only 2% lower than obtained from the model.

The normal force in the hangers should be the same as the sum of the vertical component of the load acting on that part of the bridge which is supported by that hanger. This area supported by one hanger is equivalent to the spacing of the hangers s times half the width of the bridge b. The normal force in the hanger is calculated by multiplying the test load q acting on the bridge times this surface, $N_{hanger} = q * s * b$. Figure 4.50 shows that the calculated normal force in the hangers is within the range of normal forces obtained from the model.

4.6.4. Optimization

The optimization with Galapagos has the same setting as previously used. The weight of all elements is calculated and multiplied with their specific unit cost. New in this case are the cables, which have a higher cost than the steel elements. This could lead to solutions where cable lengths or diameters are reduced by increasing material consumption at other elements. Again, solutions which do not meet requirements are penalized with very high costs.

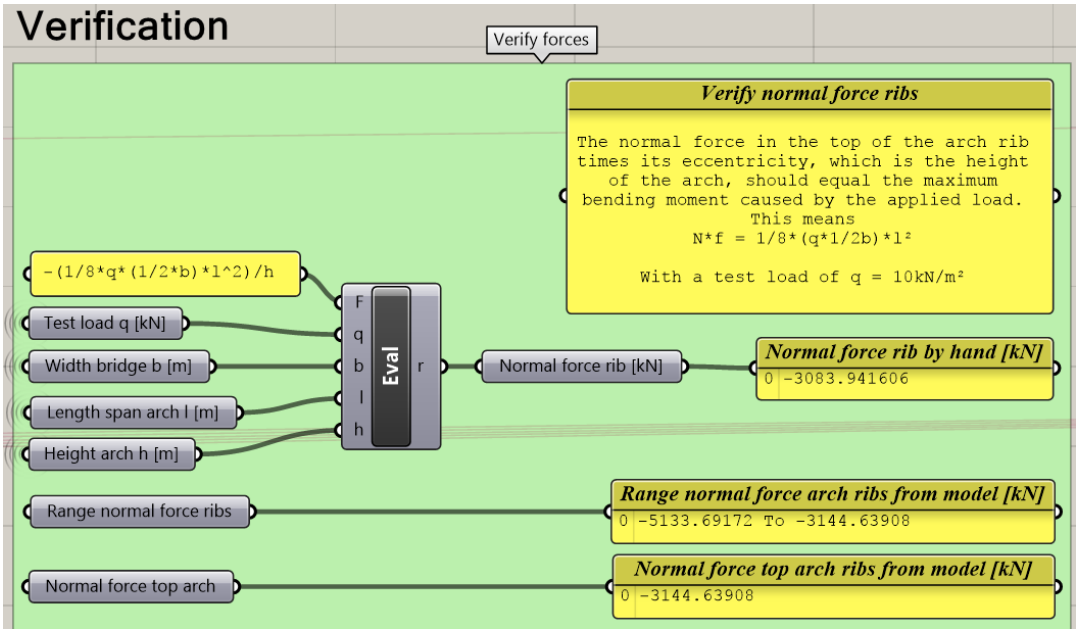

Figure 4.49: Verification of the normal force in the top of the arch ribs

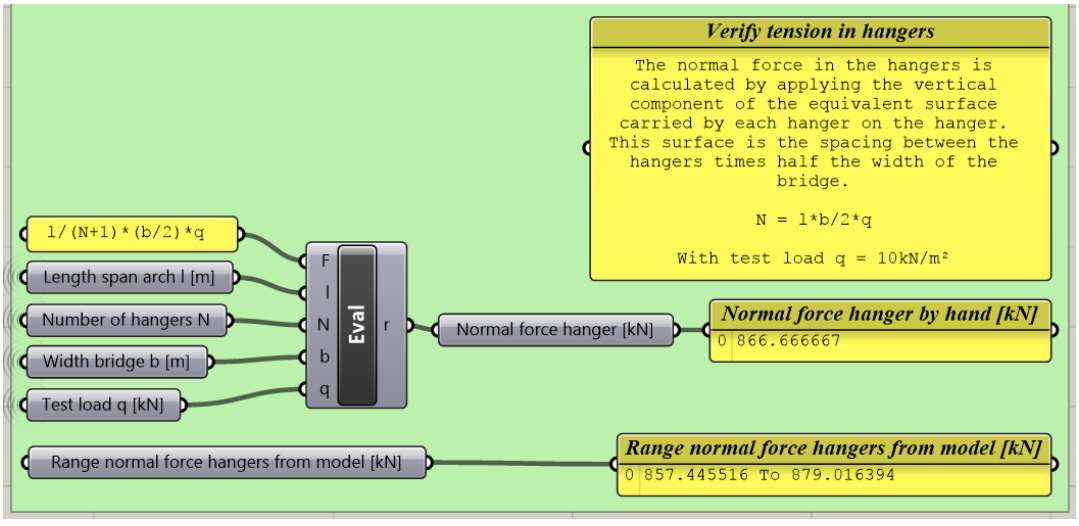

Figure 4.50: Verification of the normal force in the hangers of the vertical arch bridge

All combinations investigated by Galapagos are visible in the PCP in Figure 4.51a. The trend is visible that Galapagos is focussing on solutions with a mid-range height of the arch, low-range dimensions of the arch and tie members and mid-range diameters of the hangers. Looking at all combinations which yield viable solutions in Figure 4.51b, it is clear that there is a minimum diameter for the hangers of about 10 cm as well as for the thickness of the arch ribs of about 1.5 cm. The solution with the lowest cost is highlighted in Figure 4.51c. The prediction that the diameter of the cable would be minimized is true. What is also visible is that the thickness of the arch rib and tie members are at their lower bound. This can be clarified by the fact that decreasing the wall thickness of hollow box sections results in a more efficient way to reduce the volume of the member, and therefore its costs. This is explained in more detail in section 4.5.4. The height of the arch is somewhat increased to reduce the stresses in the arch ribs so that the wall thickness can be reduced. As explained earlier, by increasing the height of the arch the normal force in the top of the arch becomes smaller, since f in the formula $M_{Ed} = N * f$ is increased and M_{Ed} does not change. By increasing the height of the arch, the ratio between normal force and bending moment as a way to carry the load changes. A higher arch will transfer the external loads more by compression than by bending, provided it does not deviate too far from the thrust-line.

Taking a look at the highlighted solution with the lowest height of the arch in Figure 4.51d, one can observe that the arch ties are heavily dimensioned, which implies that the bridge structure relies on the ties to carry substantial parts of the loads.

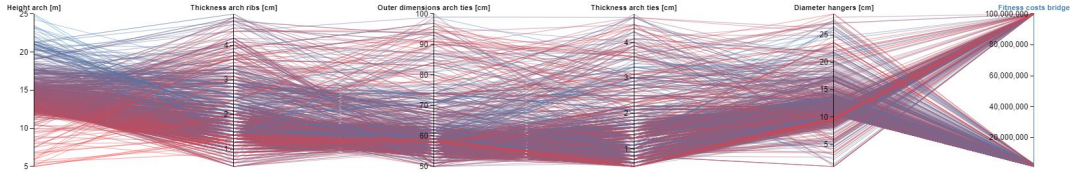

(a) Parallel Coordinate Plot of all solutions produced by Galapagos while optimizing the arch bridge with vertical hangers

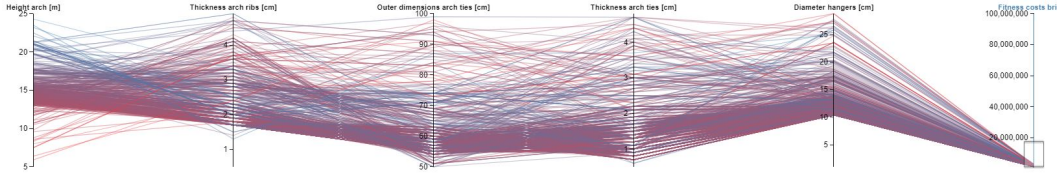

(b) Parallel Coordinate Plot of all solutions meeting the requirements produced by Galapagos while optimizing the arch bridge with vertical hangers

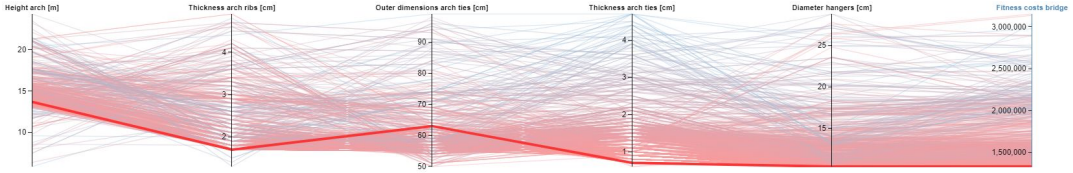

(c) Parallel Coordinate Plot highlighting the lowest cost solution produced by Galapagos while optimizing the arch bridge with vertical hangers

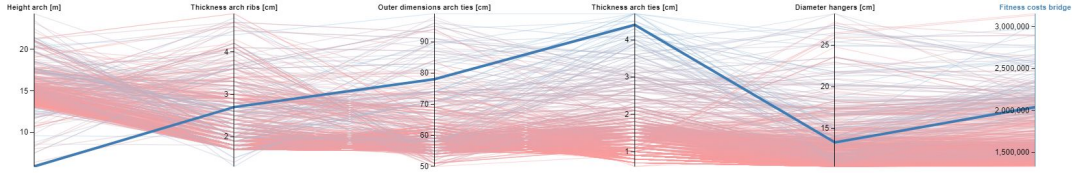

(d) Parallel Coordinate Plot highlighting the solution with the lowest height of the arch produced by Galapagos while optimizing the arch bridge with vertical hangers

Figure 4.51: Parallel Coordinate Plots showing different selections of solutions produced by Galapagos while optimizing the arch bridge with vertical hangers [1]. At (c) and (d) the parameters are rescaled to provide a better overview

4.7. Arch Bridge with Diagonal Hangers

The design of the arch bridge with diagonal hangers is exactly the same as the one with vertical hangers, the only difference being the hanger arrangement. The hangers are modelled as if they were the diagonals of a

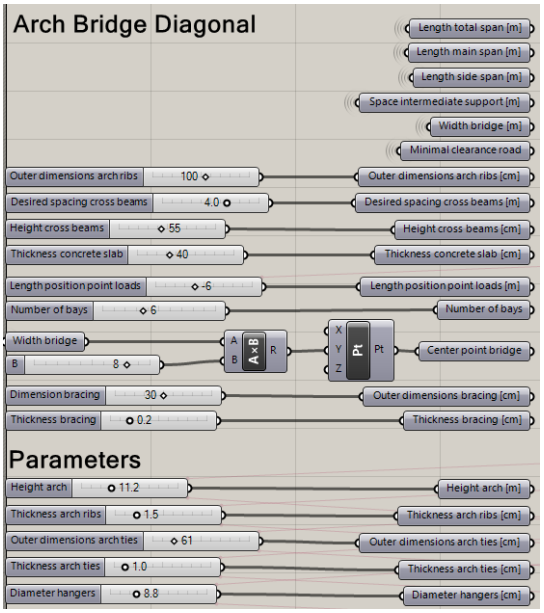

Figure 4.52: Input values and parameters used to model the arch bridge with diagonal hangers

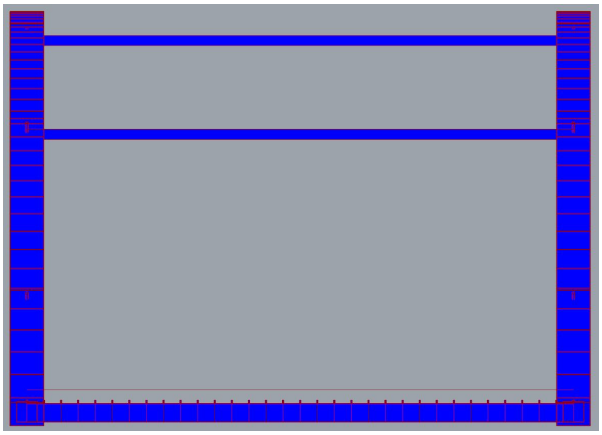

Figure 4.53: Cross-section of the arch bridge with diagonal hangers as modelled with Karamba

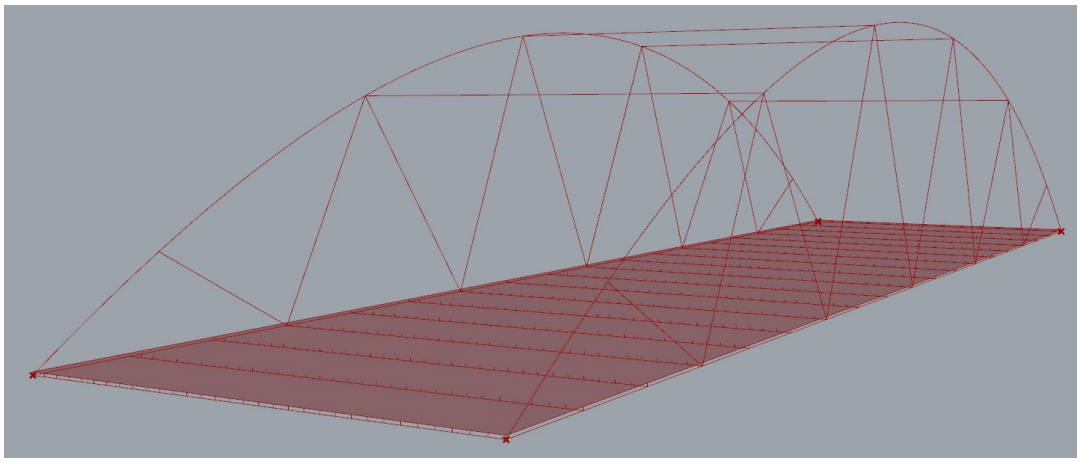

Figure 4.54: 3D model of the arch bridge with diagonal hangers in centre lines and surfaces including location of the supports

warren truss, where the arch ribs and ties are divided into parts of equal length. The cross-beams supporting the deck are spaced at such a distance that they divide the bays in equal numbers and have a spacing close to 4 metres. The arch is described by the same parabolic function, $z = (-a/b^2) * x^2 + a$ in the x,z-coordinate system, where a is the height of the arch and b is its span. Loads of LM1 apply and the arch is pinned at one side and sliding at the other, so that the arch tie takes up the horizontal forces, in stead of the support. The lateral bracing between the arches is not designed in detail, but only modelled to prevent the arches from toppling over. The minimal clearance for traffic of 4.80 metres is taken into account so that there are only cross-bracing beams above this height. The input values and parameters used to model this bridge and the resulting geometry are visible in Figures 4.52 and 4.54 respectively.

4.7.1. Element Properties

The arch ribs and ties are modelled with a steel hollow box cross-section of strength class S355. The arch ribs have a fixed outer dimension of 1 metre, while the dimensions of the ties are parametric. The hangers are modelled as steel rods of strength class S235 and to be unable to take any bending moments, making them loaded only in tension and hinged at the connections. The concrete deck is a 40cm thick shell of class C30/37 and connected to the cross-beams by means of shear studs. The cross-beams support the deck and

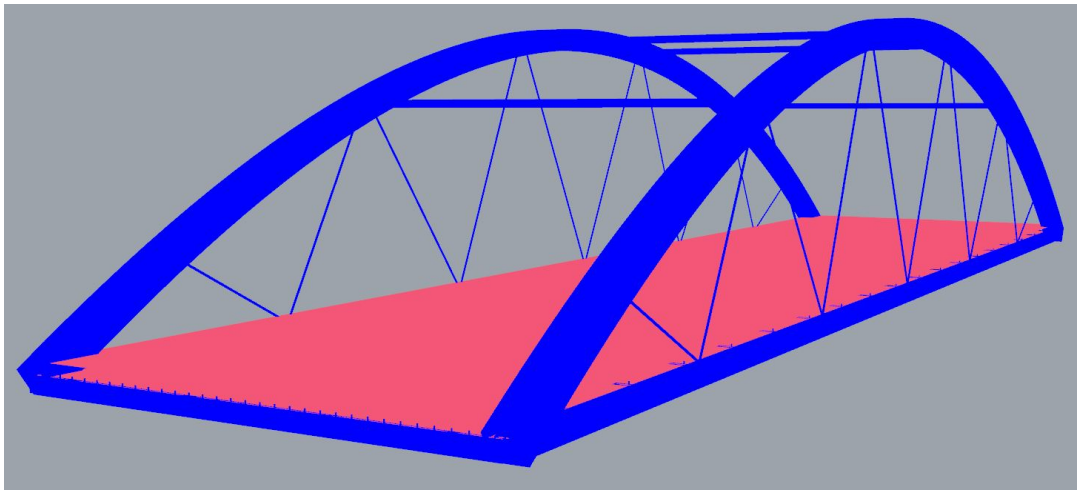

Figure 4.55: 3D model of the arch bridge with diagonal hangers as modelled with Karamba

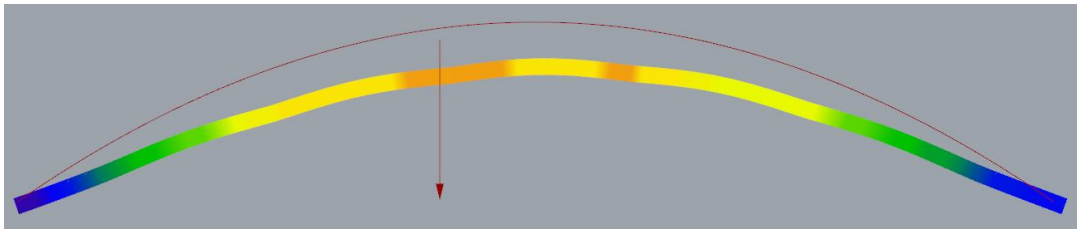

Figure 4.56: Deformation of one arch rib of the diagonal hanger arch rib, with the point of application of the point loads and the original arch shape visible, scaled by a factor 40

span the transversal distance between the arch ties. They are modelled with IPE550 profiles of class S355. The transversal bracing between the arches is not designed in detail, but modelled as square hollow box sections with an outer dimension of 30 cm. One side of the arches is supported by pins while the other side is sliding and LM1 is applied. The resulting bridge model is visible in Figure 4.55 and Figure 4.53 shows the cross-section of this bridge.

4.7.2. Structural Analysis

Before the structure is analysed, the most unfavourable position of the point loads in length direction is searched for. This is done with Galapagos. Just as with the vertical hanger arch bridge, it is suspected that this will be around a quarter of the span of the arch. It turns out that with the diagonal hangers, the location of the point loads which yield the largest deflection of the bridge is at 40% of the span. Looking at a scaled deformation of the arch rib which is at that side of the bridge where the traffic lane is nearest, see Figure 4.56, it is noticeable that the arch deflects more or less as if it were symmetrically loaded, instead of asymmetrically. The diagonal arrangement of the hangers distributes the loads more evenly over the length of the arch, and it provides additional stability against in-plane buckling of the arch, which would result in the s-like shape obtained at the vertical hanger arch bridge.

This behaviour is also visible when looking at the internal forces of the arch rib. The normal forces are distributed more evenly with smaller peaks than at the vertical hanger arch bridge, as can be seen in Figure 4.57. Also the bending moment diagram, visible in Figure 4.58, shows that the forces are more evenly distributed along the arch. The bending moment diagram is almost symmetrical, with slightly larger values at the side of the point loads.

Again, this bending moment diagram does not look like anything standard, and therefore the same procedure as with the vertical hanger arch bridge is followed. The number of bays in between the hangers is increased to 30, distributing the loads more evenly over the arch. Self weight of the structure is turned off, as well as the UDL from LM1, only the point loads from LM1 are applied. The resulting bending moment diagram is visible in Figure 4.59. This diagram is checked by solving the same ODE for arches as with the vertical hanger arch bridge. The difference is that the point load acts at $2/5^{th}$ of the span, since this was found to

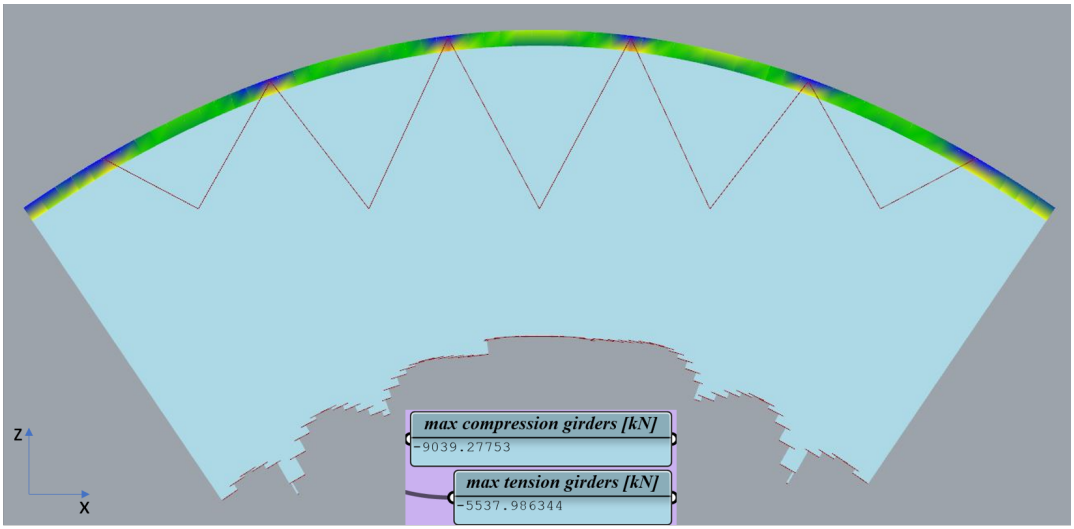

Figure 4.57: Normal force diagram of one rib of the diagonal hanger arch bridge, also showing the location of the diagonals and the utilization of the rib

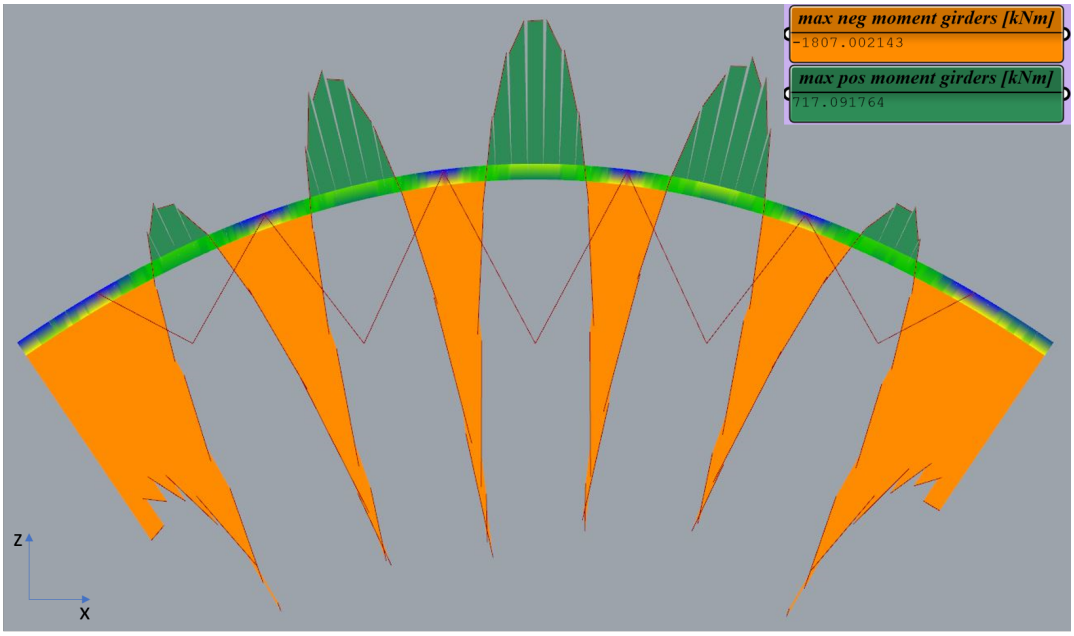

Figure 4.58: Bending moment diagram one rib of the diagonal hanger arch bridge, also showing the location of the diagonals and the utilization of the rib

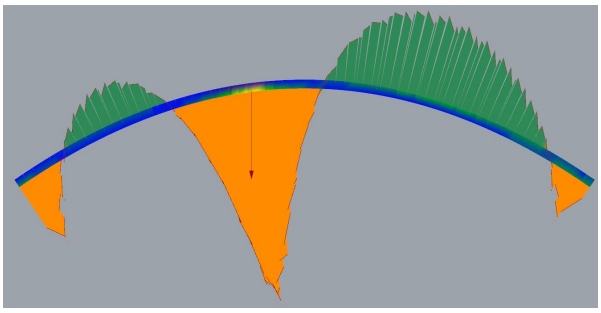

Figure 4.59: Bending moment diagram for arch with increased number of hangers and point load at 2/5 span as obtained with Karamba

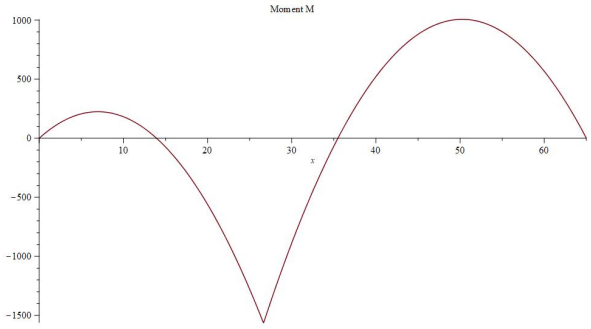

Figure 4.60: Bending moment diagram for an arch with pointload at 2/5 span as obtained by solving the ODE with Maple

be the most unfavourable location for this arch bridge. With the boundary conditions of zero displacement and zero bending moment at the supports, the differential equation is solved with Maple and the resulting bending moment diagram is plotted and visualised in Figure 4.60. In Appendix B the maple sheet used to calculate this bending moment is provided. The shapes of both diagrams are very similar and therefore it can be concluded that the bending moment diagrams for the arch produced by Karamba are correct. The difference near the support, where a bending moment is present in the Karamba model, is due to the fact that the arch is connected to the longitudinal girder in this model.

From structural analysis it follows that the forces in the lateral bracing between the arches are low, therefore only at the top range of the arch bracing would be needed. The maximum compression force in the bracing is 13.6 kN, whereas the buckling force $F_B = \frac{\pi^2 EI}{l_b^2} = 282.6$ kN.

The angles of the diagonal hangers should preferably be between 30 and 60 degrees. This is to ensure that the forces are evenly distributed between the hangers and not become too large or small. In this case, the angle of the outermost hangers is 27.8 degrees. This is still acceptable and the forces in these hangers do not differ too much from the rest, but it should be monitored and changed as soon as these hangers seem to lose their function.

4.7.3. Verification

To verify the behaviour of the bridge model, the internal bending moment resistance and the normal forces in the hangers are checked. With a test load of $10kN/m^2$ the external bending moment is $M_{Ed} = 1/8ql^2$ with q over half the width of the bridge to check one arch. This should be resisted by the internal bending moment M_{Rd} which is the normal force at the top of the arch times the height of the arch, $N * f$. From this equilibrium one can calculate the normal force at the top of the arch. Figure 4.61 shows this verification and that the calculated normal force is only 6% lower than the one from the model.

To calculate the normal force in the diagonal hangers, first the total vertical part is calculated by multiplying the surface load with the equivalent surface carried by the application point of two hangers at the tie. This equivalent surface is the bay width between the hangers times half the width of the bridge. This vertical force is acting downwards and should be compensated by the vertical part of the normal forces of the two hangers in that point. This is visualized in Figures 4.62 and 4.63. The normal forces in the hangers can be calculated with the following formulas:

$$F_\alpha = F_v * sin(0.5\pi - \beta)/sin(\alpha + \beta)$$

and

$$F_\beta = F_v * sin(0.5\pi - \alpha)/sin(\alpha + \beta)$$

The results of these calculations and the normal forces obtained with the model are depicted in Figure 4.64, showing that the calculated values are close to the ones from the model.

4.7.4. Optimization

For the optimization procedure with Galapagos the height of the arch, the thickness of the arch rib members, the outer dimensions and thickness of the tie members and the diameter of the hangers are variable. At the same time, the outer dimensions of the arch ribs, the design of the deck with cross-beams and the cross-bracing is kept constant. Galapagos is set to search for the lowest costs of the bridge structure, while still

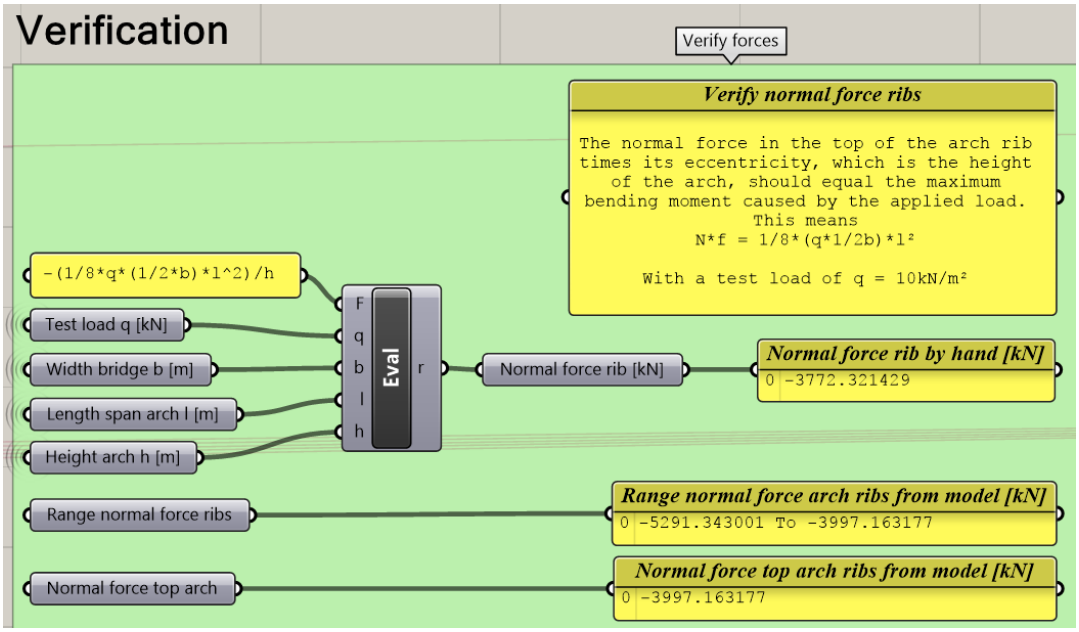

Figure 4.61: Verification of the normal force at the top of the arch, needed to resist the external bending moment

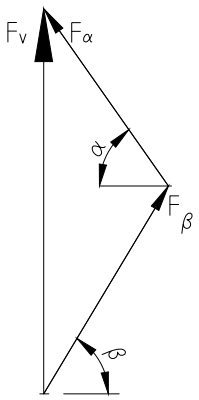

Figure 4.62: Force polygon for equilibrium of equivalent vertical load and hanger forces

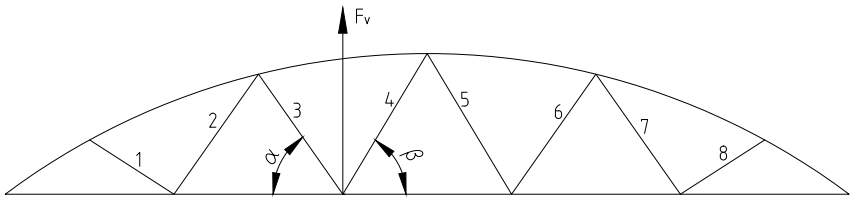

Figure 4.63: Schematization of the diagonal hanger arch bridge with specified angles

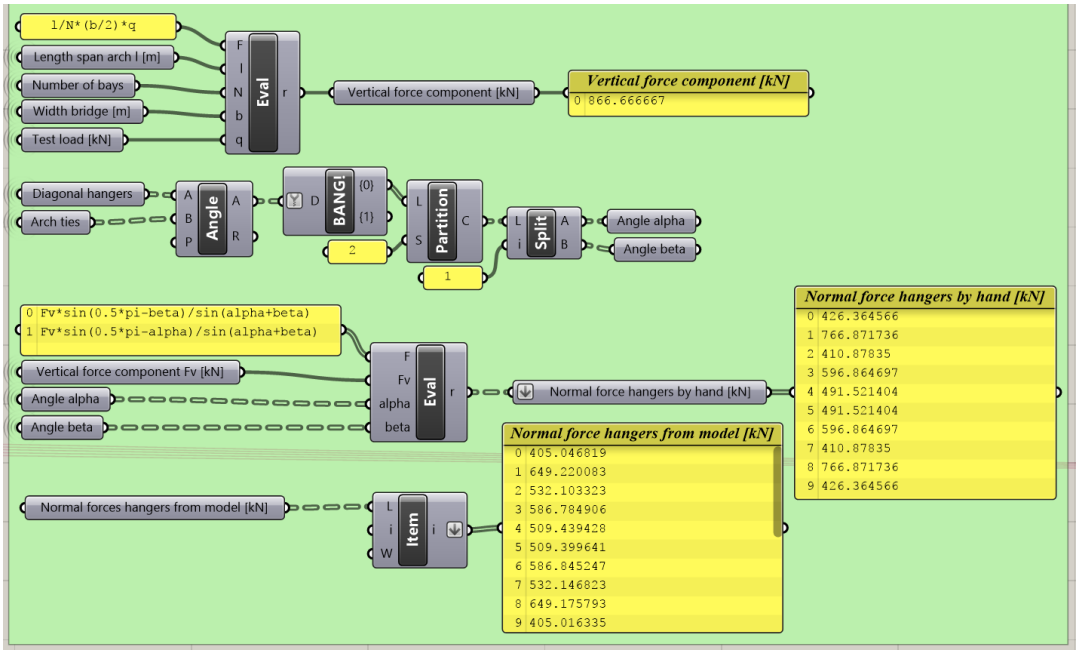

Figure 4.64: Verification of the normal force in the diagonal hangers of the arch bridge

complying with all requirements. Costs are calculated by calculating all element volumes and multiplying with their unit cost.

Figure 4.65a provides an overview of all combinations in a PCP which are explored by Galapagos while optimizing the diagonal hanger arch bridge. As is the case with the vertical hanger arch bridge, the trend is visible that the values of the parameters are at the lower- to mid-range of their spectrum. Again there is a lower bound for the diameter of the hangers, visible in Figure 4.65b. This time it is slightly lower than the vertical hangers, which is logical since there are more cables to carry the same load. Looking at the solution with the lowest cost in Figure 4.65c, it is clear that most of the parameters are at the lowest possible value which still yield viable solutions. Only the outer dimensions of the ties are increased. Increasing the outer dimensions of a hollow box member will have a lower impact on the increase of volume of that member, compared to increasing the thickness of the walls of the hollow box member. Therefore it is logical that the outer dimensions of the tie are increased while the thickness of the walls are kept to a minimum. Because of the more even spread of loads on the arch by the diagonal hanger configuration, the height of the arch can be relatively low, reducing the length of the arch, and therefore also its material consumption. Reducing the height of the arch also decreases the cable length of the hangers, which are the most expensive part per unit volume.

Figure 4.65d displays the solution with the lowest height of the arch. Lowering the height of the arch will induce higher bending moments and the arch will act less as an arch and more like a curved beam. The thickness of the walls of the arch and tie members need to be increased significantly, as well as the diameter of the hangers, almost doubling the costs of this solution.

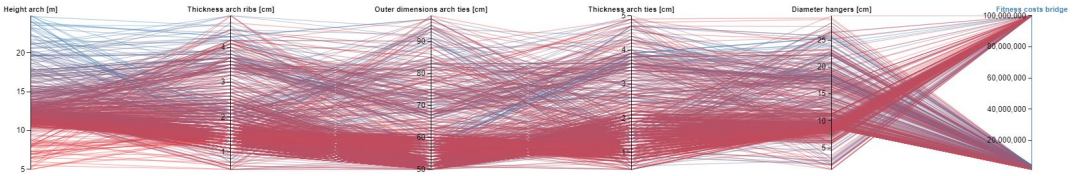

(a) Parallel Coordinate Plot of all solutions produced by Galapagos while optimizing the arch bridge with diagonal hangers

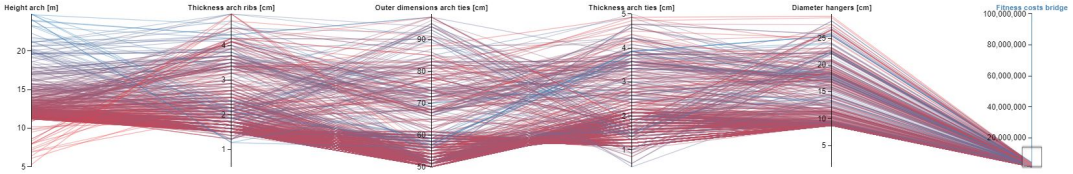

(b) Parallel Coordinate Plot of all solutions meeting the requirements produced by Galapagos while optimizing the arch bridge with diagonal hangers

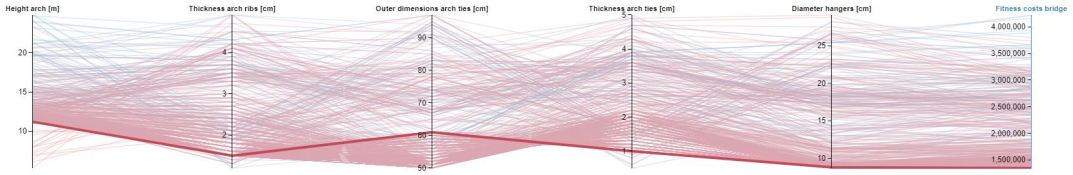

(c) Parallel Coordinate Plot highlighting the lowest cost solution produced by Galapagos while optimizing the arch bridge with diagonal hangers

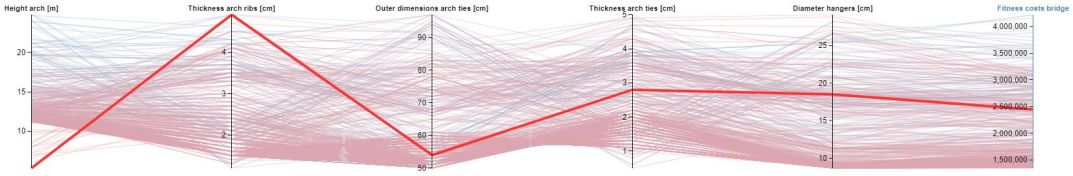

(d) Parallel Coordinate Plot highlighting the solution with the lowest arch height produced by Galapagos while optimizing the arch bridge with diagonal hangers

Figure 4.65: Parallel Coordinate Plots showing different selections of solutions produced by Galapagos while optimizing the arch bridge with diagonal hangers [1]. At (c) and (d) the parameters are rescaled to provide a better overview

4.8. Single Pylon Cable Stayed Bridge

The single pylon cable stayed bridge has two separate concrete columns connected by a cross-beam which is located underneath the deck. This cross-beam provides lateral stability to the columns. All stays have one anchor point near the top of the column, and the height of the pylon is governed by the angle of the outermost stay, which is set to thirty degrees.

The concrete deck is supported by cross-beams, which are connected to the longitudinal girders. These girders span the distance between the supports at the start and end of the bridge and the pylons, and they are elastically supported by the stays. The stays transfer the loads by means of normal force to the top of the pylons, which then transfer the loads towards their support. The last stay of the back span is connected to the support, stabilizing the system in longitudinal direction. The spacing of the cross-beams is kept near the distance of four metres, and defined in such a way that they divide the main or side span in an equal number. The spacing of the cable stays is then set to a multiple of the spacing of the cross-beams, also dividing the main or side span in whole numbers. The dimensions of the cross-section of the pylons, the thickness of the longitudinal girders and the diameter of the stays are variable parameters for optimization, while the outer dimensions of the longitudinal girders, the cross-beams and the deck are kept constant. These input values are visible in Figure 4.66 and the resulting geometry in centre lines and surfaces in Figure 4.68.

4.8.1. Element Properties

The pylons are modelled as concrete hollow box sections of strength class C40/50. The hollow box provides internal access and space for the anchoring of the stays. The deck is a concrete shell element of 40 cm thick with strength C30/37. It is connected to the cross-beams with shear studs, the cross-beams are IPE550 steel

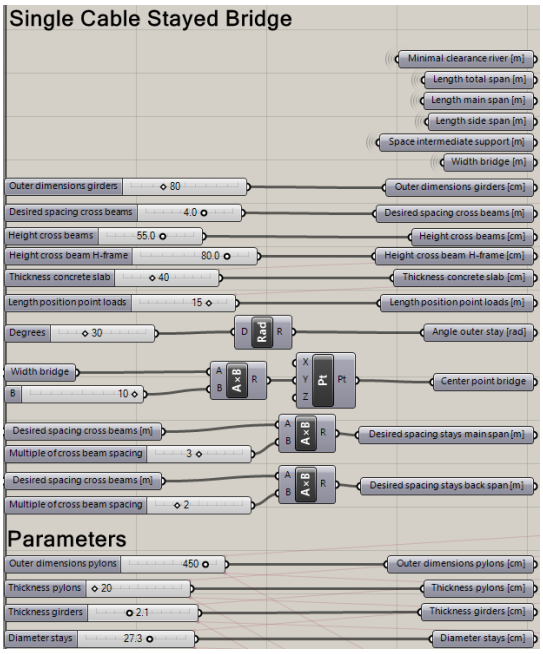

Figure 4.66: Input values and parameters used for the design of the single pylon cable stayed bridge

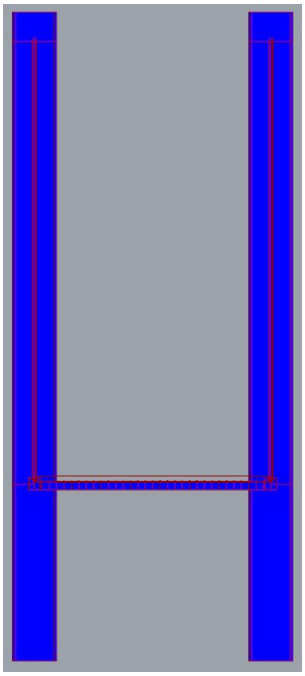

Figure 4.67: Cross-section of the single pylon cable stayed bridge as modelled with Karamba

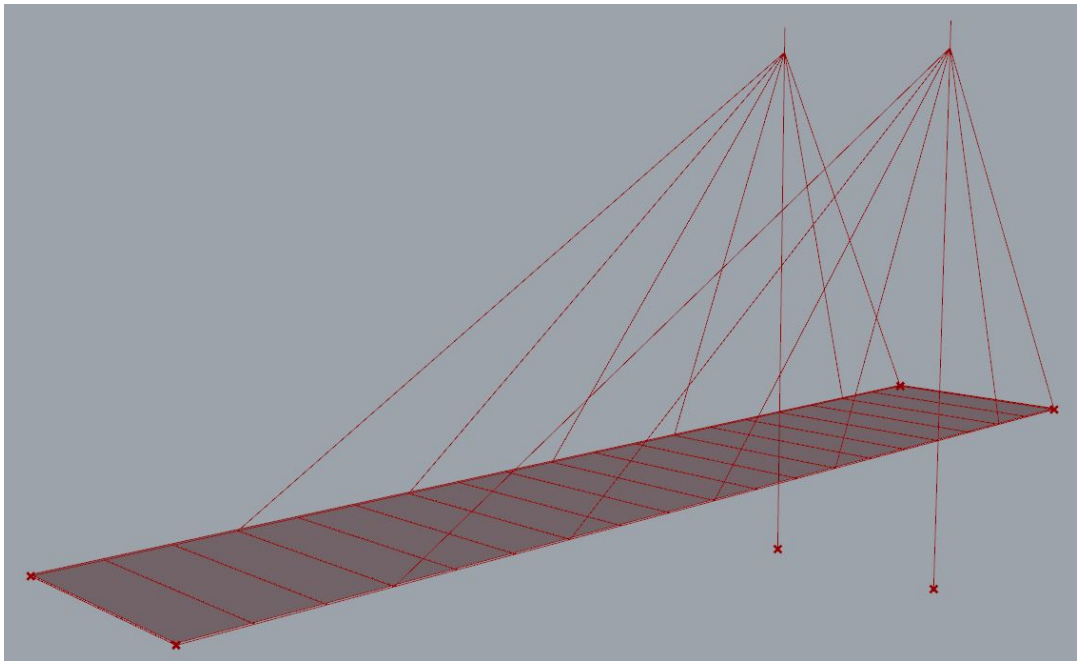

Figure 4.68: Geometry of the single pylon cable stayed bridge in centre lines and surfaces, with location of supports visible

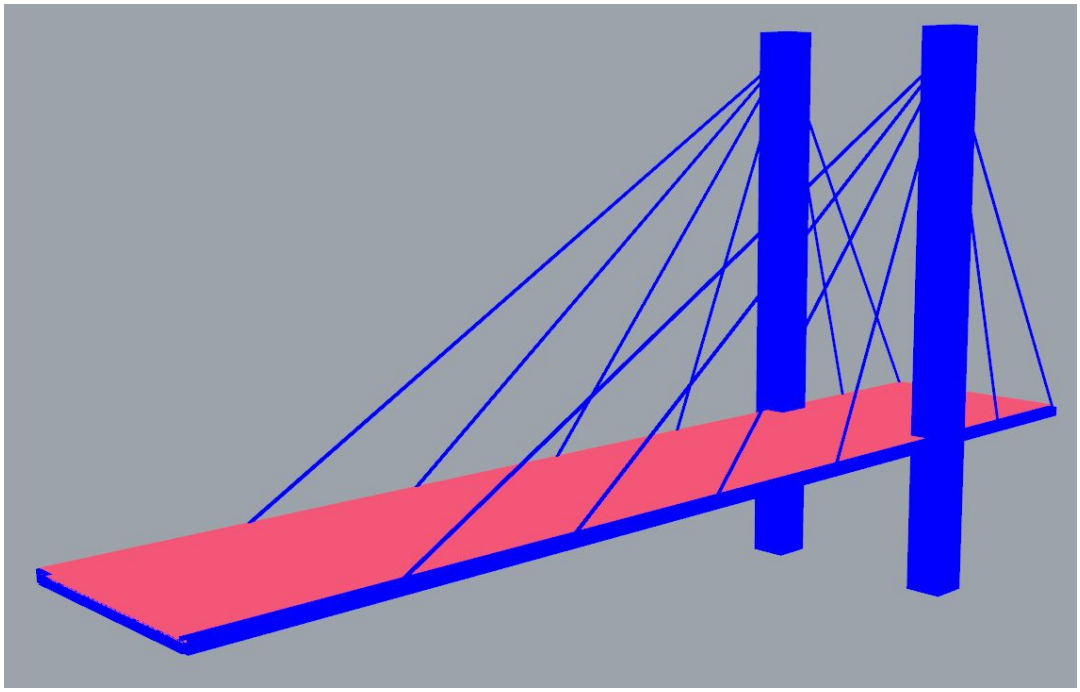

Figure 4.69: Structural model of the single pylon cable stayed bridge with all its properties as modelled with Karamba

beams of strength S355, while the cross-beam between the pylons is an IPE600. The longitudinal girders are steel hollow box sections, also providing space for the connections of the stays. The stays are modelled as steel rods of S235 which cannot take any bending, making their connections hinged. Loads of LM1 are applied to the bridge deck, the supports of the back span and the pylon are pinned and the supports at the end of the main span are sliding. A cross section of this bridge with all its properties is depicted in Figure 4.67 while a 3D overview is visible in Figure 4.69. These figures show that the geometry in centre lines has been given cross-sectional properties, and the elements are not given an eccentricity. The result is that the deck and longitudinal girders seem to pass straight through the pylons. The effect of aligning all elements as they should be by giving each element a local eccentricity has been investigated. The influence on the structural behaviour was small compared to the effort needed to apply all these eccentricities, and therefore it was decided to keep the original structural form.

4.8.2. Structural Analysis

Eurocode 1 states that the point loads from LM1 should be positioned in such a way that they produce the most unfavourable effect. To find the location where the deflection of the bridge is largest, Galapagos is set to find the largest deflection by changing the position of the loads in length direction. This position is at 73% of the main span, measured from the pylon, in between the two outer most stays. The load will be placed on this position for structural analysis and optimization.

For structural analysis, first the behaviour of the pylon is investigated. The stays introduce vertical and horizontal forces at the anchor point near the top of the pylon, which are components of the normal forces in the stays. At the point where the deck is supported by the pylons, horizontal compression forces present in the deck and girders are introduced to the pylon, as well as a vertical load due to self-weight of the deck structure and the UDL of LM1. At the bottom the pylon is supported by a pin support, resulting in horizontal and vertical forces at this point. A schematisation of all forces acting on the pylon, as well as the resultants, are visualised in Figure 4.70. The main span is located on the right side of the pylon in this picture.

From this schematisation of forces, the normal force, shear force and bending moment diagrams can be derived. The normal force diagram is visible in Figure 4.71, where one can clearly see the introduction of the large vertical component of the stay forces at the anchor point near the top. The normal force then gradually increases downwards due to the self-weight of the pylon. Where the deck structure is connected to the pylon, a small increase in normal force is visible and the force keeps increasing towards the support at the bottom.

The bending moment diagram, Figure 4.72, is derived from the horizontal forces acting on the pylon.

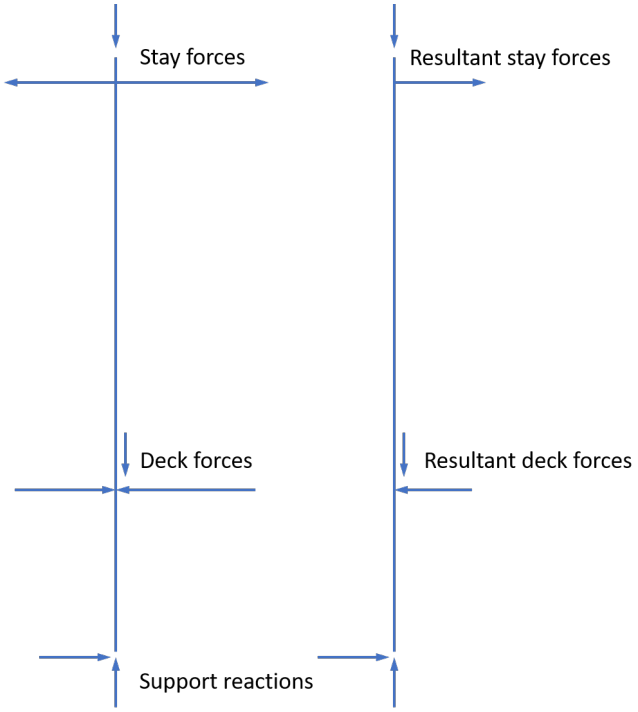

Figure 4.70: Schematised overview of all forces acting on the pylon in longitudinal span direction

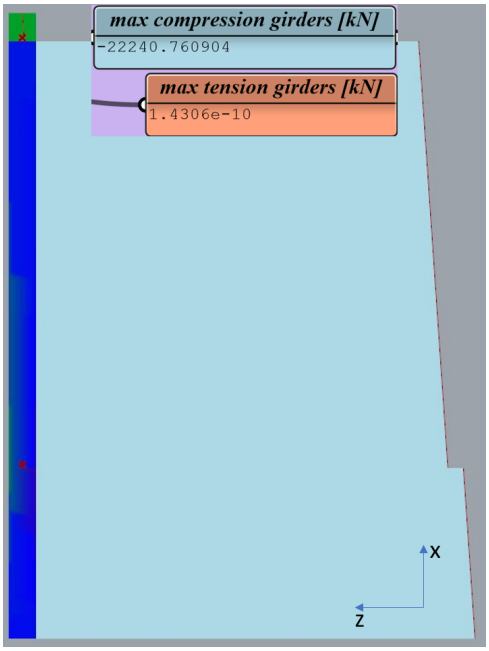

Figure 4.71: Normal force diagram over the height of the bridge pylon, with anchor point of the stays and location of the deck highlighted

The upper part of the diagram, from the anchor point to the deck, is the result of the horizontal stay force component times the height of this part of the pylon. The lower part of the diagram, from the support towards the deck, is the result of the horizontal support reaction times the height of the minimal clearance of the bridge. The jump at the location of the deck is due to the fact that the longitudinal girder is modelled as a continuous beam, thus introducing a bending moment at this point.

The shear force in the part of the pylon above the deck is equal to the resulting horizontal component of the stay forces at the anchor point and is constant over this part, see Figure 4.73. At the location of the deck, the horizontal compression force acting on the pylon causes a jump and change of sign in the diagram. Towards the support the shear force continues to be constant and the value of the shear force in this lower part equals the horizontal support reaction. Since the z-axis is in the opposite direction of what is usually drawn with respect to the x-direction, the positive and negative sign of the shear force values are swapped. Therefore the shear symbols are drawn in the diagram, as to prevent confusion. These symbols also correspond with the slope of the moment diagram.

The normal force in the longitudinal girders in Figure 4.75, shows the expected behaviour. The largest part is under compression due to the horizontal component of the stay forces. The part between the outermost stay and the support at the end of the main span at the right is under tension since the horizontal component of this stay force pulls on this part of the girder. The remaining tensile forces are a result of the external loads acting at this part of the bridge, which tend to bend the girders downwards, resulting in tensile forces. Near the support at the end of the main span, there still is a normal force present. This could imply that the support is pinned and that horizontal forces are introduced to the foundation. The support however, is sliding. The horizontal forces are a result of the deformation of the structure. Because it bends downwards, the concrete deck is under compression and the girders are under tension. At the location of the support, these compression and tensile forces cancel each other, resulting in zero horizontal forces in the support.

Figure 4.74 shows the bending moment diagram in the longitudinal girders. At the far end of the main span there is a large negative bending moment due to the large forces from LM1 acting on this part. All cable stays introduce a positive bending moment in the girder, this can be compared with a girder on multiple supports, where at the supports hogging moments occur.

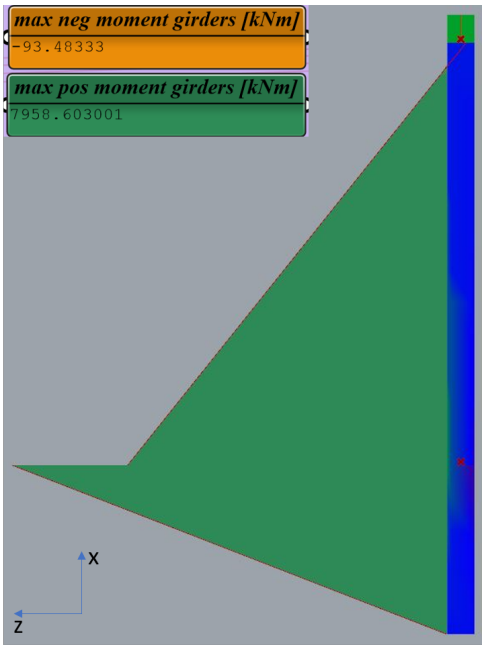

Figure 4.72: Bending moment diagram over the height of the bridge pylon

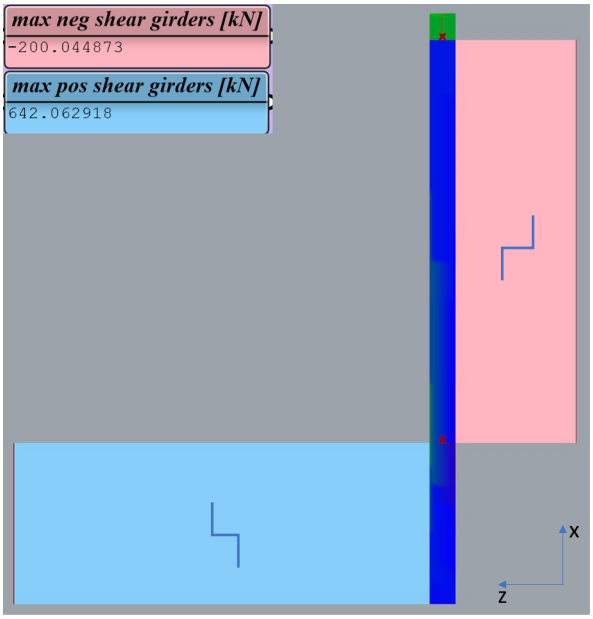

Figure 4.73: Shear force diagram over the height of the pylon including shear symbols

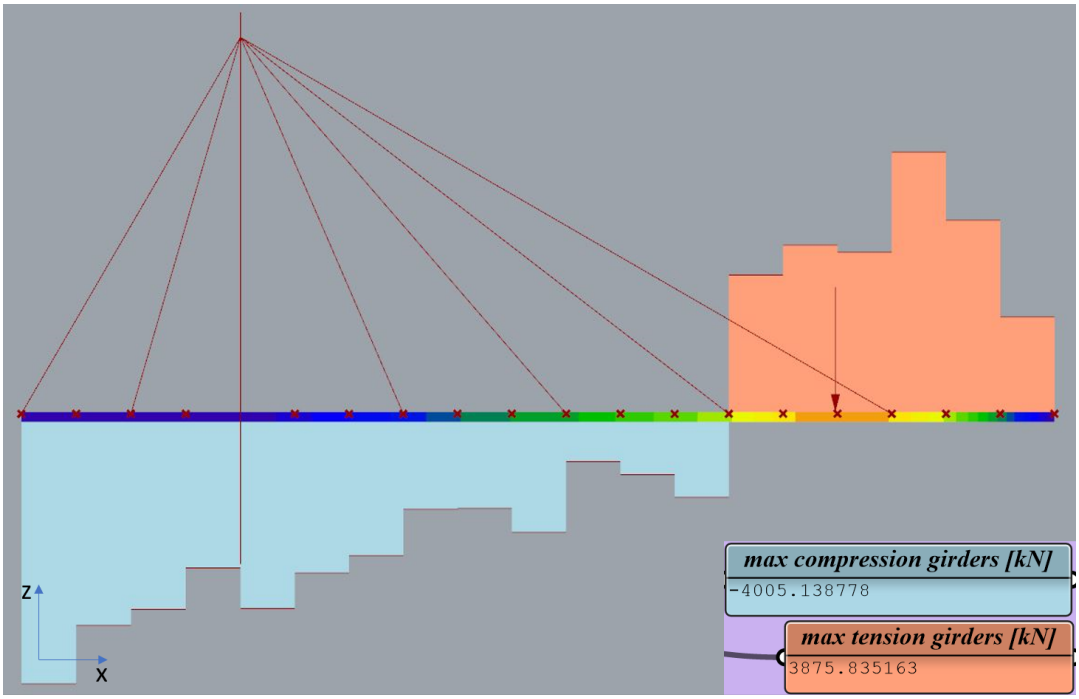

Figure 4.74: Bending moment diagram of the longitudinal girders with the position of the point loads and the location of the cross-beams visible

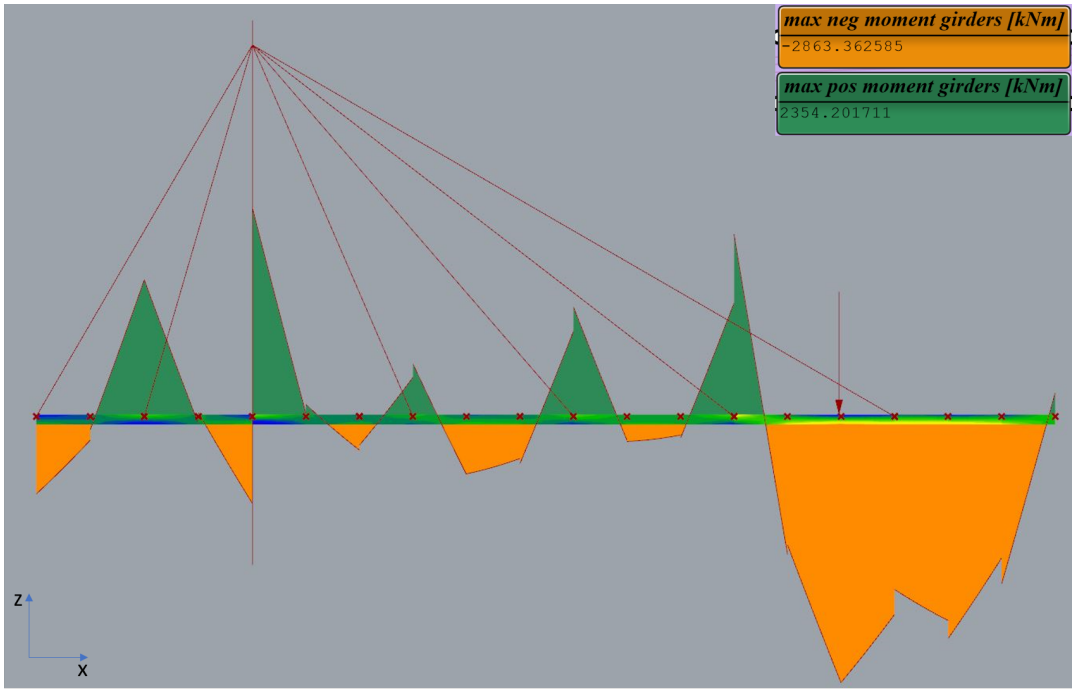

Figure 4.75: Normal force diagram of the longitudinal girders with the position of the point loads and the location of the cross-beams visible

4.8.3. Verification

To verify the behaviour of the bridge structure, the normal forces in the cable stays as well as in the pylon are checked. The stays should carry the external loads applied to the bridge. Each stay carries the part of the load that is acting on the surface consisting of the spacing of the stays times half the width of the bridge. The test load of $10kN/m^2$ is applied and to make sure the loads are mainly carried by the stays into the pylon and towards the support, in stead of by the longitudinal girders and deck, the dimensions of the deck and girders are lowered. The vertical load acting on the stays is $F_v = q * l_s * 1/2b$ with l_s the spacing between the stays. F_v is the vertical component of the normal force in the stays, making the normal force

$$N_{stay} = \frac{F_v}{sin(\alpha)}$$

with α the angle between the stay and the horizontal. Since the last stay of the back-span is connected to the support, this stay will ensure stability in longitudinal direction by making equilibrium of the horizontal components of the stay forces. The force in this stay is calculated with

$$N_{bstay} = \frac{\sum F_h}{cos(\alpha)}$$

with $SUM(F_h)$ being the sum of the horizontal components of all other stay forces. Figure 4.76 shows this verification step in the Grasshopper model and the results are very close to the values obtained from the model

The normal force in the pylon should equal the sum of vertical components of all stay forces. This normal force is calculated with $N = \sum(N_{stay} * sin(\alpha))$, and is only 0.8% larger than the force obtained from the model.

4.8.4. Optimization

For the optimization of the single pylon cable stayed bridge the same setting is used as previously where Galapagos is set to search for the solution with the lowest costs while still fulfilling the requirements. Solutions which do not meet these requirements are penalized with very high costs. For the optimization the outer dimensions and thickness of the concrete hollow box members of the pylon, the diameter of the stays and the thickness of the steel hollow box members of the longitudinal girders are variable parameters. This is the first bridge where the material concrete is part of the optimization, and since the cable stays are a factor

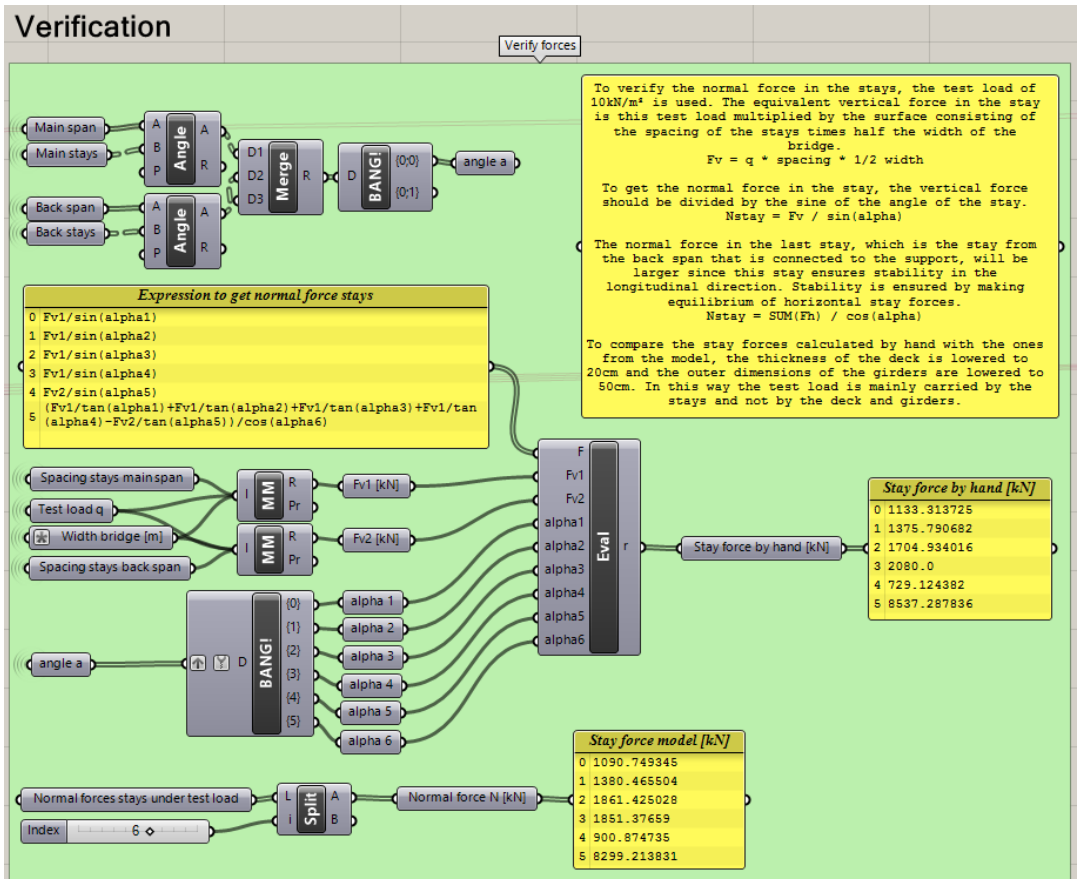

Figure 4.76: Verification of the normal forces in the cable stays of the single pylon cable stayed bridge

60 more expensive, it is expected that the dimensions of the cables will be minimized at cost of the pylon volume.

Different selections of solutions from this optimization are displayed in a PCP in Figure 4.77, where 4.77a shows all solutions produced. A large variety of combinations is explored, but it is clear that Galapagos has focussed on solutions with large outer dimensions of the pylons, mid-range stay diameters and a low thickness of both box members. Zooming in on all solutions which meet the requirements in 4.77b, it is clear that there is a lower bound value for both the thickness of the longitudinal girders and the cable diameters. Any lower value for these parameters means that the either the stresses in these members become too large or the maximum deflection of the bridge is exceeded. There are also only a few solutions which have a relatively small outer pylon dimension.

Looking at the solution which produces the lowest cost, one immediately sees that the outer dimensions of the pylon are maximised to a value of 5 metres, see Figure 4.77c. The thickness of the pylons is close to its minimum and the thickness of the girders and the diameter of the cables are at their minimum value. Such a large pylon has a big influence on the appearance of the bridge and is not really proportional to the rest of the bridge structure. The reason Galapagos produces this outcome is that with such a large column the diameter of the cable stays can be kept to a minimum and therefore also the overall costs are lower. One could argue that a large pylon does not necessarily decreases the cable diameters, since the external load which has to be carried by the cables does not change. In this design however, all cable stays have the same dimension. This means that the cable with the largest force is governing, and this is the one which is connected to the support at the back-span, stabilizing the whole structure. The pylon tends to deflect towards the main span, since that is where most of the loading is. This deflection causes additional elongations in the cables at the back-span, and since the last cable is anchored to the support, large stresses occur. By increasing the dimensions of the pylon, the deflection at the top is reduced, reducing the stresses in the anchored stay and therefore reducing the needed minimum diameter of all cables. Additional effects of this increased pylon dimension and decreased force in the anchored stay, is that the resulting horizontal force component at the anchor point in the top of the pylon is changed. A schematisation of these forces is visible in Figure 4.70. Since the force in the anchored stay is reduced significantly and in all other cables only slightly, a large resulting horizontal force towards main span remains. This causes a large increase in shear force and bending moment in the pylon compared to the design before optimization. This effect results in an increase of wall thickness of the pylon.

The solution which has the lowest outer dimensions of the pylon is highlighted in 4.77d. This solution also has a lower wall thickness of the pylons compared to the lowest cost solution and turns out to also be the solution with the lowest weight. The diameter of the stays has to be increased by 7 centimetres to cope with the increased stresses in the anchored stay due to the reduced bending stiffness of the pylon. This increase in cable dimension results in a solution which is about 1.5 million Euro more expensive.

The design of this bridge could be changed so that the anchored stay can have a different dimension than the other stays. This would be a more realistic design leading to a large cost reduction. Another option would be to use an optimization algorithm which is able to search for the best trade-off between cost- and weight reduction so that the dimension of the pylon will be better proportioned compared to the rest of the bridge.

4.8.5. Improved Design

After the previous optimization, it is concluded that the design of the cable stayed bridge is not very realistic, since all cable stays have the same diameter. By allowing the anchored stay to have a different diameter than all other stays, it is predicted that the total cost of the bridge structure will be significantly lower. This is due to the fact that the cable stays are the most expensive element per unit weight. In this way, the stays will have a diameter that corresponds better with the stress they are subject to. Eventually, this might also lead to a more slender pylon.

A new parameter is added to the model, which is the diameter of the anchored cable stay. All other settings are kept the same and the optimization run is performed. Figure 4.78 shows the results of this optimization, where 4.78a shows all viable solutions and 4.78b highlights the solution with the lowest cost. From these graphs it follows that the diameter of the anchored stay is increased while the diameter of the other stays is decreased. It can be concluded that this minor change in the design results in a reduction of costs of around 700.000 Euro and a weight reduction of 400 metric tonnes. The outer dimensions of the pylon are not reduced as much as expected, but these results are still significant.

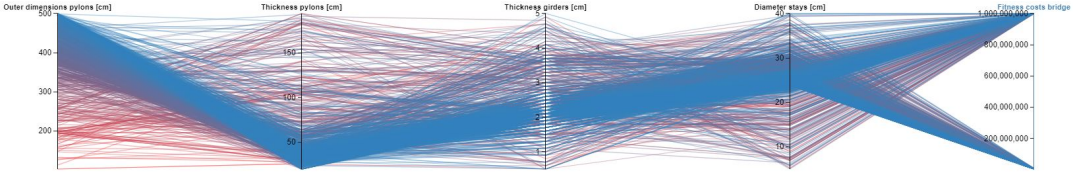

(a) Parallel Coordinate Plot of all solutions produced by Galapagos while optimizing the single pylon cable stayed bridge

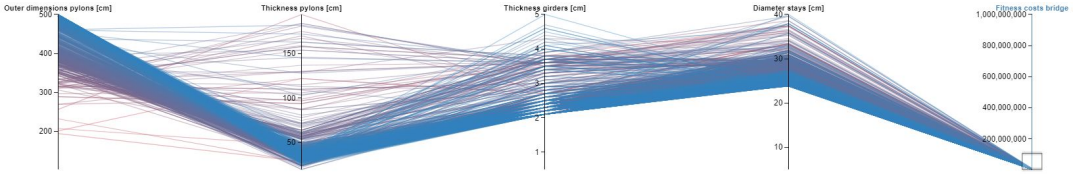

(b) Parallel Coordinate Plot of all solutions meeting the requirements produced by Galapagos while optimizing the single pylon cable stayed bridge

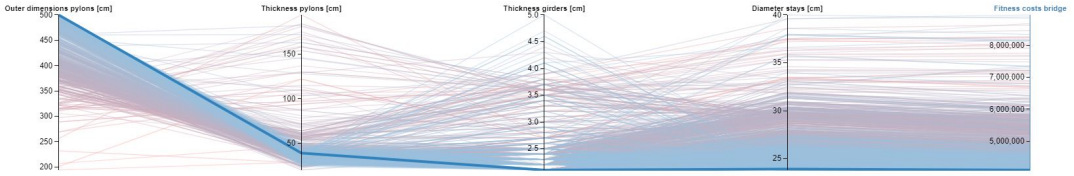

(c) Parallel Coordinate Plot highlighting the lowest cost solution produced by Galapagos while optimizing the single pylon cable stayed bridge

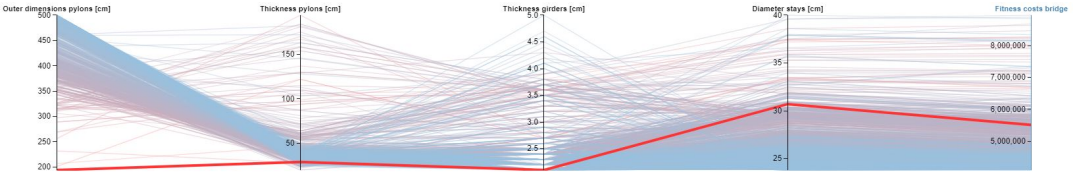

(d) Parallel Coordinate Plot highlighting the solution with the lowest pylon dimensions produced by Galapagos while optimizing the single pylon cable stayed bridge

Figure 4.77: Parallel Coordinate Plots showing different selections of solutions produced by Galapagos while optimizing the single pylon cable stayed bridge [1]. At (c) and (d) the parameters are rescaled to provide a better overview

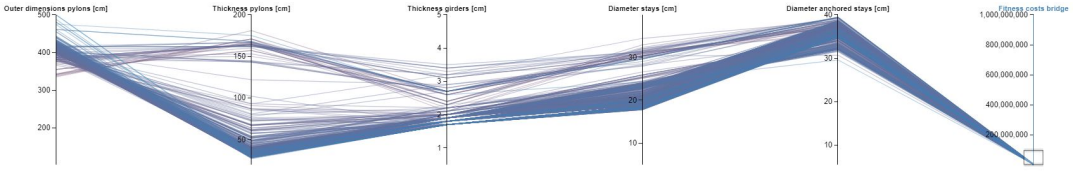

(a) Parallel Coordinate Plot of all solutions meeting the requirements produced by Galapagos while optimizing the improved single pylon cable stayed bridge

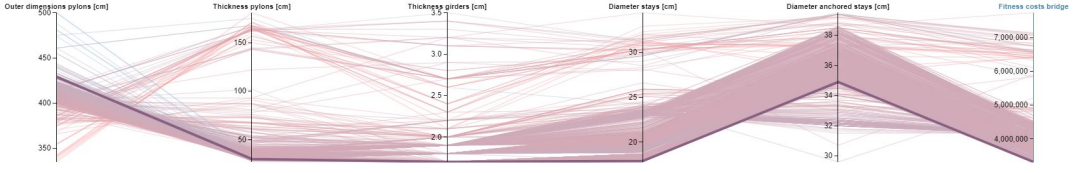

(b) Parallel Coordinate Plot highlighting the lowest cost solution produced by Galapagos while optimizing the improved single pylon cable stayed bridge

Figure 4.78: Parallel Coordinate Plots showing different selections of solutions produced by Galapagos while optimizing the improved single pylon cable stayed bridge [1]. At (b) the parameters are rescaled to provide a better overview

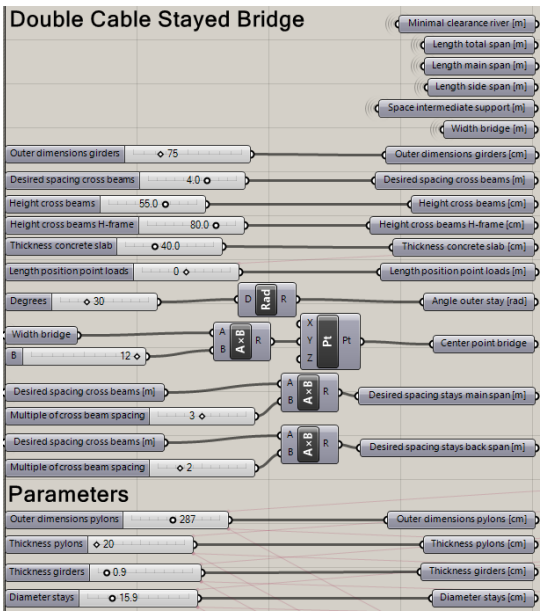

Figure 4.79: Input values and parameters used for the design of the double pylon cable stayed bridge

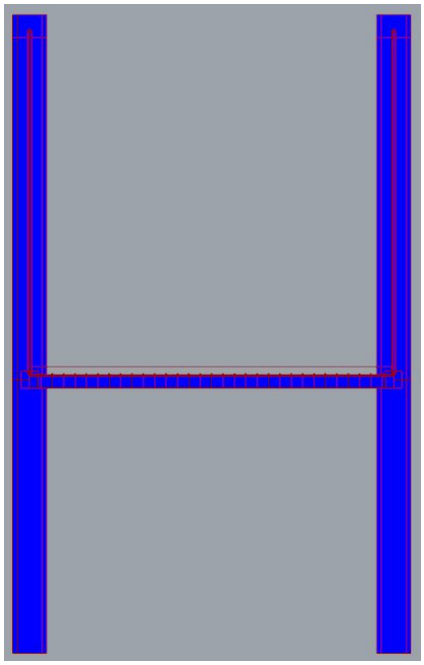

Figure 4.80: Cross-section of the double pylon cable stayed bridge as modelled with Karamba

4.9. Double Pylon Cable Stayed Bridge

The cable stayed bridge with double pylon has the same basis of design as the single pylon, with the difference that at both sides of the main span a pylon is present, making this bridge symmetric. The main span is carried by both pylons and again the height of the pylon is governed by the minimum angle of the cable stays of 30 degrees. Both pylons have one side span as their back-span. At both side spans the outer cable stay is anchored to the support, stabilizing the pylon in longitudinal direction. The deck is supported by cross-beams which are connected to the longitudinal girders. These girders are supported by the supports at the start and end of the bridge and by the pylons. All input values and parameters are visible in Figure 4.79 and they lead to the geometry, in centre lines and surfaces, depicted in Figure 4.81.

4.9.1. Element Properties

All element properties are modelled the same as with the single pylon bridge. The pylons are C40/50 concrete hollow box members, providing internal access and space for anchoring of the stays. The deck is a 40 cm thick C30/37 concrete shell and is supported by IPE550 beams of class S355 and the cross-beams between the pylons are IPE600. The cable stays are steel rods of S235 and modelled that they are unable to take any bending. For the longitudinal girders steel hollow box sections of S355 are used. The pylons, as well as the start and end point of the bridge, are supported by pins. The resulting structure is visible in Figure 4.82 and the cross-section of the bridge is depicted in Figure 4.80.

4.9.2. Structural Analysis

The position of the load which has the worst influence on the deflection of the bridge, is exactly at mid-span. This will therefore be the position for structural analysis and optimization. Taking a look at the forces in one pylon, the same schematisation can be used as with the single pylon bridge. It is depicted in Figure 4.83. The resulting horizontal force in the top of the pylon will cause bending moments and shear forces, and the resulting vertical forces, together with self-weight of the pylon, will cause normal forces. The normal force diagram is visible in Figure 4.84, where the introduction of the vertical force component of the stays is visible at the top, and the introduction of the weight of and external load on the deck causes the jump, located at the height of the deck.

The bending moment diagram of Figure 4.85 shows that the horizontal resulting component of the stay force at the top of the pylon causes a linear increase in bending moment towards the location of the deck. The horizontal support reaction also causes a linear increase in bending moment from the bottom towards

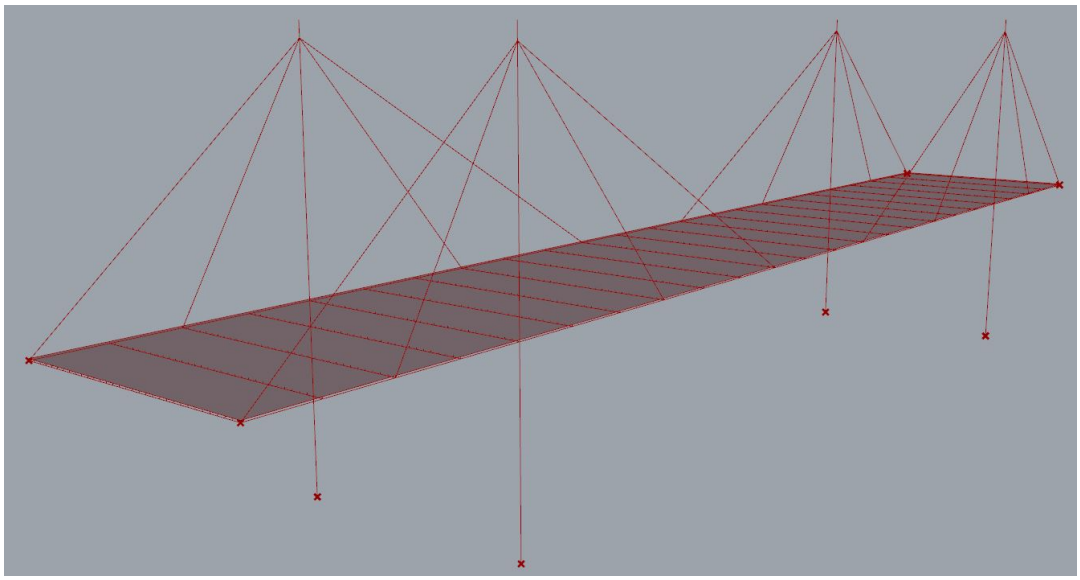

Figure 4.81: Geometry of the double pylon cable stayed bridge in centre lines and surfaces, with location of supports visible

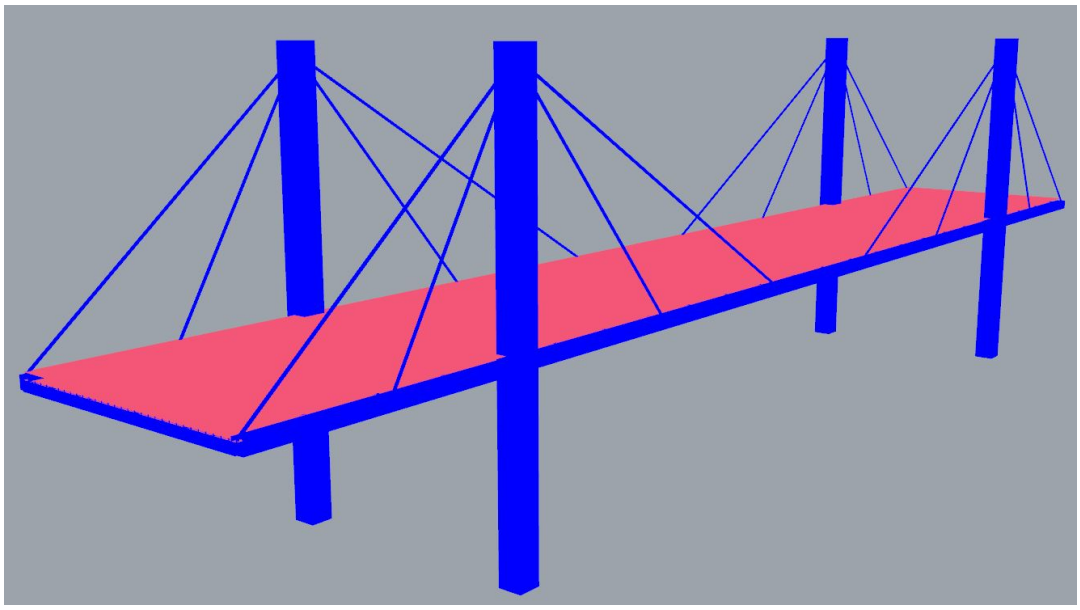

Figure 4.82: Structural model of the double pylon cable stayed bridge with all element properties as modelled in Karamba

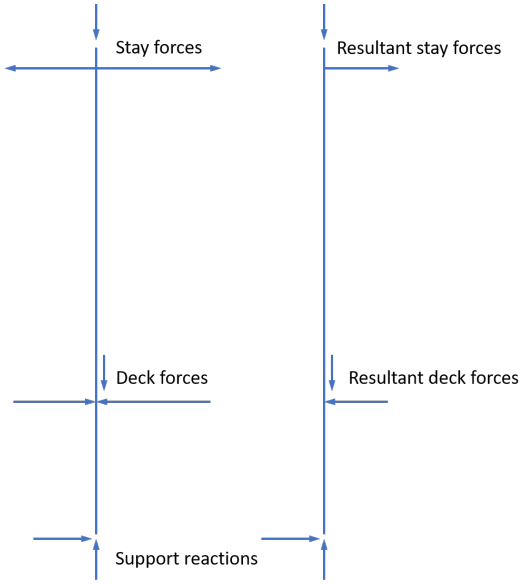

Figure 4.83: Schematised overview of all forces acting on the pylon and on the right the resulting forces

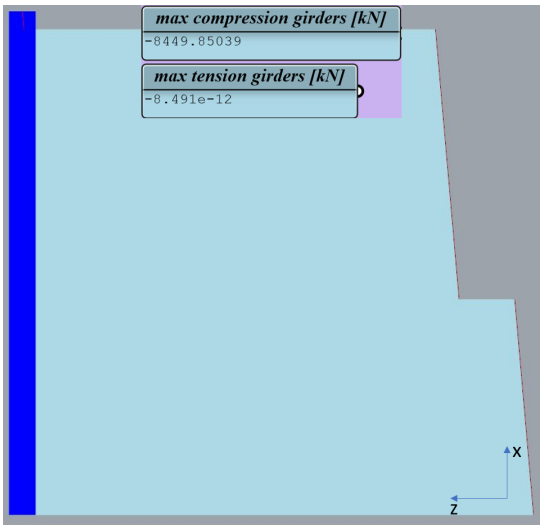

Figure 4.84: Normal force diagram over the height of the bridge pylon

the deck. The jump at the location of the deck is due to the fact that the longitudinal girder is modelled as a continuous beam, thus introducing a bending moment at this point.

The same horizontal forces causing the bending moments, also cause the shear force diagram of Figure 4.86. The part above the deck has the same value as the horizontal stay force component at the anchor point at the top of the pylon. The lower part has the same value as the horizontal component of the support reaction. The jump and change of sign is caused by the resulting horizontal compression force of the girders and the deck acting on the pylon. To prevent confusion about negative and positive values and the used coordinate system, the shear symbols are placed in the diagram.

The normal forces in the longitudinal girders can be seen in Figure 4.87. The load and resulting deflection of the bridge, as well as the stay forces of the outermost stays, cause relatively large tension forces at mid span. The first stay from mid-span brings this back to compression forces, but due to the still present deflection and stay force from the second stay seen from mid-span, this turns to tension towards this second stay. The horizontal component of this stay is responsible for the compression forces towards the pylon, and the first stay from the back span does the same. Since the last stays are anchored, their horizontal force component is taken by the support. The tensile forces in the last part of the girders are due to the horizontal force component of the first stay of the back span.

Figure 4.88 shows the bending moment diagram of the longitudinal girder. Again, this can be seen as a girder on multiple supports, where the vertical component of the stay forces cause hogging moments in the girder. The loads from LM1 and the self-weight of the deck are introduced as point loads at the locations of the cross-beams.

4.9.3. Verification

For the verification of this bridge the same approach as with the single pylon bridge is followed. At first, the normal forces in the cable stays are checked. The test load of $q = 10kN/m^2$ is applied on the whole deck surface. The resulting vertical force that has to be carried by each stay follows from $F_v = q * l_s * 1/2b$ and the normal force in the stay is

$$N_{stay} = \frac{F_v}{sin(\alpha)}$$

Since the last stay of the back span is anchored to the support, this will balance the horizontal forces at the anchor point. The force in this stay is calculated with

$$N_{bstay} = \frac{\sum F_h}{cos(\alpha)}$$

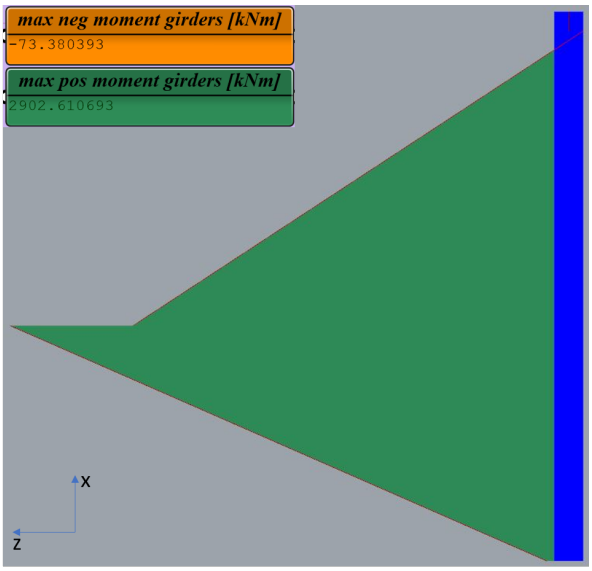

Figure 4.85: Bending moment diagram over the height of the bridge pylon

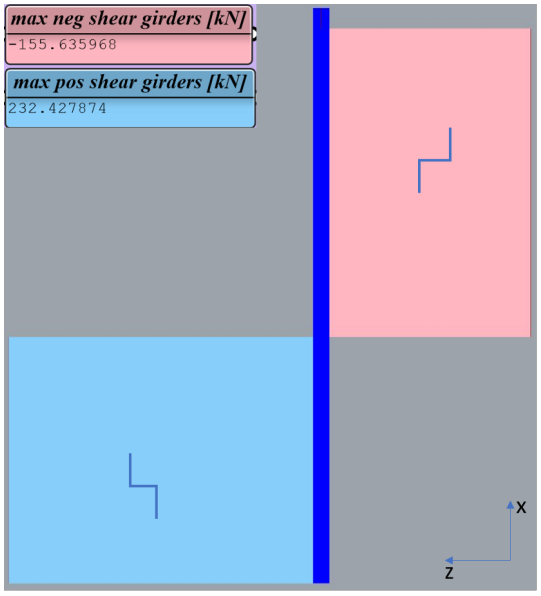

Figure 4.86: Shear force diagram over the height of the pylon, including shear symbols

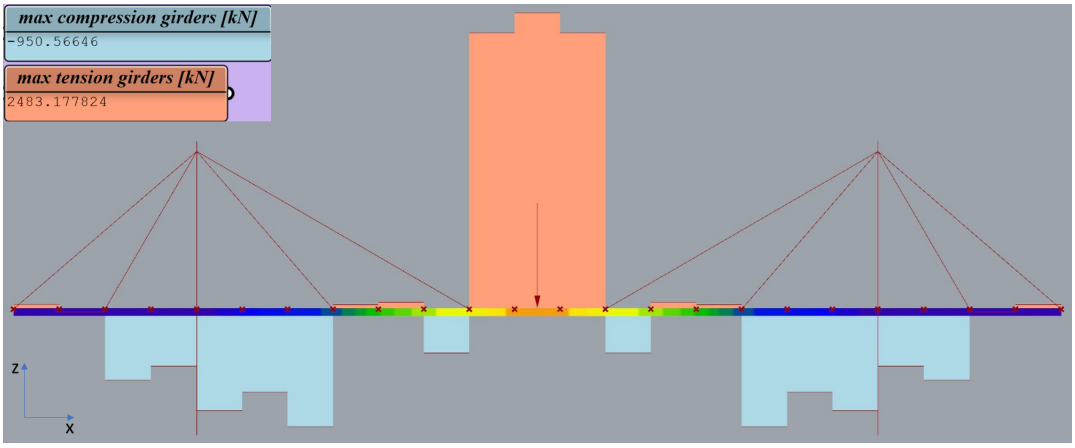

Figure 4.87: Normal force diagram of the longitudinal girders with the point of application of the load and the locations of the cross-beams visible

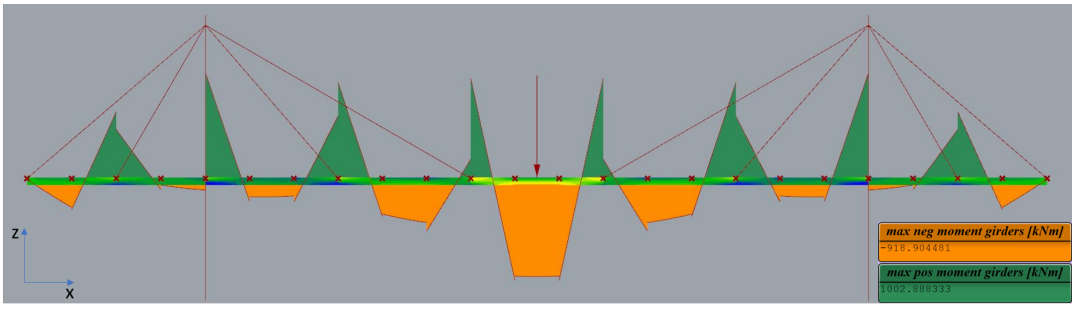

Figure 4.88: Bending moment diagram of the longitudinal girders with the point of application of the load and the locations of the cross-beams visible

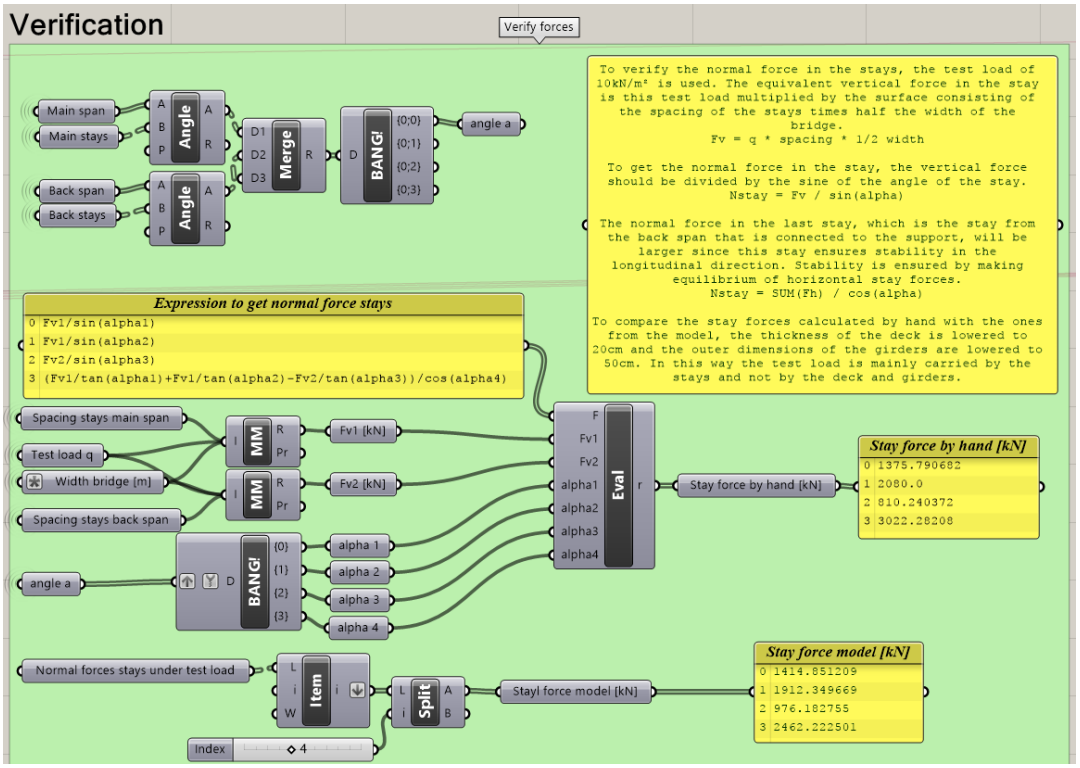

Figure 4.89: Verification of the normal forces in the cable stays under test loading

where α is the angle between the stays and the horizontal. To make sure most of the loads are carried by the cables and not by the girders and the deck, the dimensions of these latter two elements are lowered. Figure 4.89 shows the verification of the stay forces in the Grasshopper model. It shows that the hand calculations do not differ too much from the results of the model.

Following, the normal force in the pylon is checked. At the top of the pylon, below the anchor point, this should be equal to the sum of vertical components of all cable stays. From Figure 4.90 it is clear that with a difference of 5.8% this is the case.

4.9.4. Optimization

After optimization of the single pylon cable stayed bridge, it was noticed that optimizing towards the lowest costs possible produces designs with very large pylons. It would be interesting to use an evolutionary optimization algorithm which is capable of optimizing for more than one fitness parameter. This algorithm is available in Grasshopper and is called Octopus. However, to keep the optimization consistent throughout this research, first Galapagos is used in the same setting as previously to optimize the structure based on

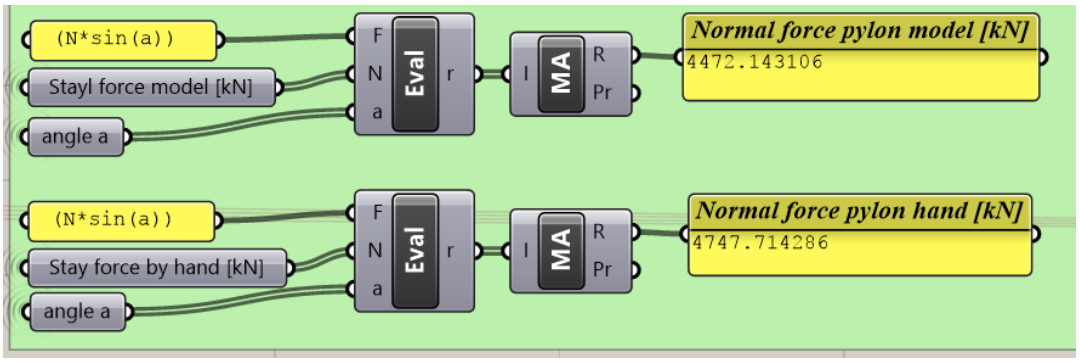

Figure 4.90: Verification of normal force in the pylon under test loading

costs. Solutions which do not meet the requirements are penalized with a very large number. Afterwards, the same optimization set-up for weight reduction is created, where the solver is set to search for the lowest weight possible, and solutions which do not meet the requirements concerning unity check and deflection will be penalized with a very large number.

After Galapagos has optimized the structure for costs, Octopus is set to optimize for both costs and weight. This solver has not been used during the previous cases, since it was found to take a lot more time to produce equal amounts of variants. Octopus returns all solutions in a Pareto front graph where one can choose solutions from this front which resemble the best trade-off between minimum costs and minimum weight. Again the optimization is recorded and all values are plotted in a PCP to analyse the results. The values of the optimization with Octopus are plotted and visualised in Figure 4.91a. In this graph the column 'Fitness mass bridge' is added to the right, since this is now also a fitness to be optimized. For both fitness values the same requirements have to be met, therefore all solutions which are penalized in costs, are also penalized in weight. There are no solutions visible where one fitness is not penalized while the other is, and this should also be the case.

In 4.91b all variants which meet the requirements are selected. As was the case with the single pylon bridge, there are lower bounds for the diameter of the cable stays and for the thickness of the girders. Furthermore, there are two trends visible. One where the outer dimension of the pylons is at the lower range of its domain, and one where these dimensions are at mid-range. This is due to the fact that there are two objectives, minimizing costs and minimizing weight. Minimizing for weight returns the solution trend with lower pylon dimensions.

The solution with the lowest costs is highlighted in 4.91c. Just as with the single pylon bridge, the outer dimensions of the pylons are increased to lower the deflection of the pylon. With lower deflection of the pylon, the elongation and therefore stresses in the anchored stays are decreased. These stays have the largest normal force and since all cables have the same diameter, they are governing. Decreasing the stress in these stays leads to a decrease in cable diameter and since the cables are the most expensive elements in terms of unit costs, this leads to a large cost reduction. The outer dimensions of the pylons are not further increased, because this will probably not reduce the stress in the stays sufficiently to compensate for the increased costs of the larger pylon. All other dimensions of this solution are at their minimum, as to keep the costs low.

Figure 4.91d highlights the solution with the lowest weight. It shows that the outer dimensions of the pylons are decreased to half of the value from the lowest cost solution. The thickness of the pylon members, as well as of the girders, is at their minimum value, just as with the optimization for costs. What is noticeable is that the diameter of the stays only has to be increased with 2.5 cm to obtain a viable solution. With a reduction of weight of 13.5% at an increase of costs of 10.5%, these solutions are not really far apart from each other. The difference in outer pylon diameter of 51% however, is substantial.

4.9.5. Improved Design

As was the case with the single pylon version, in this bridge design all cable stays have the same dimension. This is not realistic since all stays experience different stresses. Especially the anchored stays have much higher stresses, therefore it is more realistic to model the bridge structure with different cable diameters for the anchored stays as for the other stays. It is predicted that this will lead to a large decrease in total costs.

A new parameter for the dimension of the anchored stays is introduced, while all other settings are kept the same. The optimization is started and all results are recorded and collected in a PCP. Figure 4.92 shows these plots, while 4.92a shows all viable solutions and 4.92b highlights the solution with the lowest costs. By comparing this last graph with 4.91c it can be observed that the outer dimensions of the pylon is more than halved, while the diameter of the anchored stays is increased only slightly and the other stays are not changed. Apparently, the cable diameters were already minimized in the previous design. The improved design manages to reduce the pylon dimensions and this leads to an overall cost reduction of 70.000 Euro and reduces the weight with 190 metric tonnes.

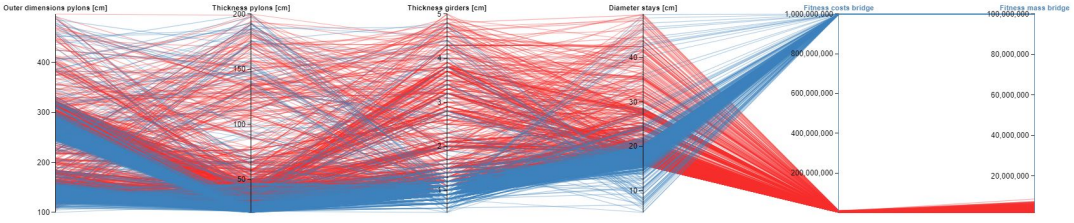

(a) Parallel Coordinate Plot of all solutions produced by Octopus while optimizing the double pylon cable stayed bridge

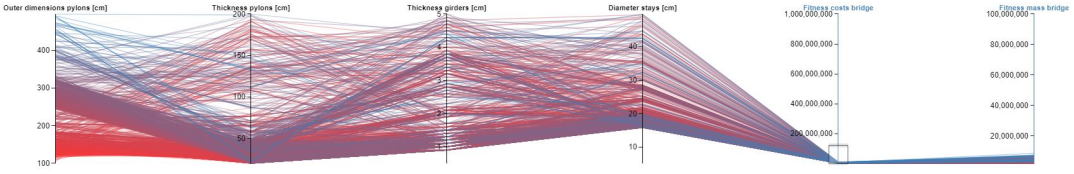

(b) Parallel Coordinate Plot of all solutions meeting the requirements produced by Octopus while optimizing the double pylon cable stayed bridge

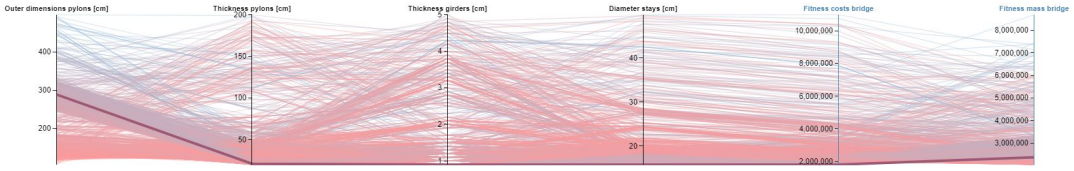

(c) Parallel Coordinate Plot highlighting the lowest cost solution produced by Octopus while optimizing the double pylon cable stayed bridge

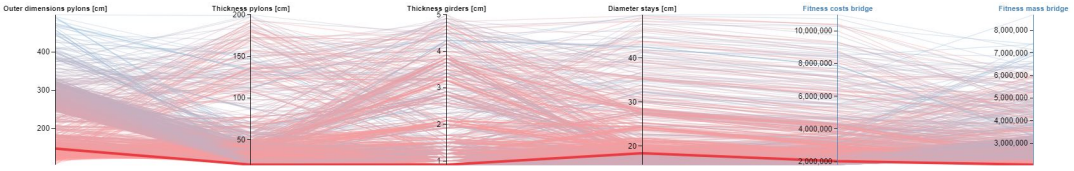

(d) Parallel Coordinate Plot highlighting the solution with the lowest weight produced by Octopus while optimizing the double pylon cable stayed bridge

Figure 4.91: Parallel Coordinate Plots showing different selections of solutions produced by Octopus while optimizing the double pylon cable stayed bridge [1]. At (c) and (d) the parameters are rescaled to provide a better overview

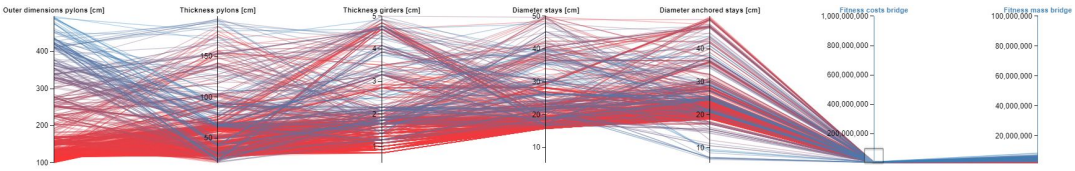

(a) Parallel Coordinate Plot of all solutions meeting the requirements produced by Octopus while optimizing the improved double pylon cable stayed bridge

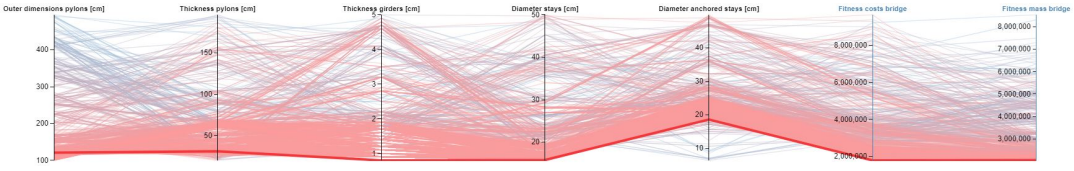

(b) Parallel Coordinate Plot highlighting the lowest cost solution produced by Octopus while optimizing the improved double pylon cable stayed bridge

Figure 4.92: Parallel Coordinate Plots showing different selections of solutions produced by Octopus while optimizing the improved double pylon cable stayed bridge [1]. At (b) the parameters are rescaled to provide a better overview

4.10. Side Span

Some bridges, like the truss and arch bridges, are designed to only cross the main span. Previously, it was explained that for the side spans, one of the two girder bridge typologies would be used for these parts. From the optimization runs it can be concluded that the double-girder bridge typology is less expensive than the multi-girder variant. Therefore it is decided to use the double-girder bridge typology for the side spans of the warren truss bridge, arch bridges and single pylon cable stayed bridge.

The design of the double-girder bridge is changed to a statically determinate, simply supported structure with a span of 17.5 metres. The height of the deck is set to 40 cm and load model 1 is applied, with point loads at mid-span. All other parameters are kept the same as with the double-girder bridge design and the optimization on costs is started.

The result of the optimization is that the girders have a height of 72 cm, while the bottom flanges are 40 cm wide and 3 cm thick. This results in a structure which weighs 290 tonnes and costs slightly more than 120.000 Euros.

The truss and arch bridges have a side span on either side, thus the cost and weight of the side span has to be added twice to the results from the truss and arch bridges. For the single pylon cable stayed bridge these results have to be added once, for it has only one side span. In the next chapter on comparison, this is already accounted for.

5 Comparison

In this chapter all optimized bridge structures will be compared. Primarily this comparison will be based on the overall costs of each typology investigated. Also some insights in the total weight of the structures, as well as other characteristics which are worth noting, will be discussed. The goal is to provide a clear overview of all optimized bridge typologies which can be used as a basis for decision making in early design stages.

5.1. Costs

This section will cover the comparison of the bridges based on their total costs. Only the cost for te bridge itself is taken into account. Large parts of the overall costs consist of the foundations and approach ramps. These fall out of the scope and are therefore not designed, their costs will not be considered. Later on in this chapter the influence of the bridge structure on the foundation and approach ramps will be discussed.

With the cable stayed bridges, the complete pylon is modelled, also the part from the level of the road beneath up to the deck structure. This is necessary for the structural behaviour of the bridge, but for the other bridge typologies this part is not designed and can be seen as the support. To compare the bridges equally, the lower part of the pylons of the cable stayed bridges will not be considered in cost and weight calculation.

The bar chart of Figure 5.1 shows the absolute costs and weight of all bridge typologies which are optimized for costs. All bridges cost between one and two million Euros when calculated with the unit costs of 0.25 euros per kilogram of concrete, 5 euros per kilogram of steel and 15 euros per kilogram of cable. The only exception is the single pylon cable stayed bridge with a cost of 4 million Euros. This is due to the large total amount of cable length and due to the large stresses in the anchored cable, which is governing for the diameter of all cables. The improved design still has a cost of over 3.2 million Euros. The use for concrete as material for the pylon also increases the weight of the cable stayed bridges with respect to the others. The single pylon cable stayed bridge also has larger costs than weight, which is again due to the large total length of the cables.

The only other bridge having larger costs than weight is the multi-girder bridge. This is due to the fact that there is no cross-bracing modelled for the bridge, but in weight and cost calculation an additional weight of 50 kg/m² deck surface is added as bracing of the bridge. This seems to be relatively expensive and might need reconsidering, but even when the weight of the bracing is set to such a number that the total bracing weighs the same as with the double-girder bridge, the costs of the multi-girder bridge stay above 1.7 million Euros, making it slightly less expensive than the double pylon cable stayed bridge.

The double-girder, truss and arch bridges all are very close to each other when it comes to weight. They all have the same deck thickness making the difference in weight and costs all steel related. The slightly higher costs for the arch bridges are on the account of the steel hangers which are expensive. Since the relatively small difference in weight between the Warren truss and double-girder is caused by steel members, which have a unit price of 5 Euros per kilogram, the difference in total costs is still noticeable. This makes the Warren truss bridge design the one with the lowest costs for the considered case in this research. In Figure 5.2 the bar chart shows the costs and weight of the structures relative to the Warren truss, which values are set to 100%.

Although the span is quite short for cable stayed bridges, the double pylon cable stayed bridge is quite

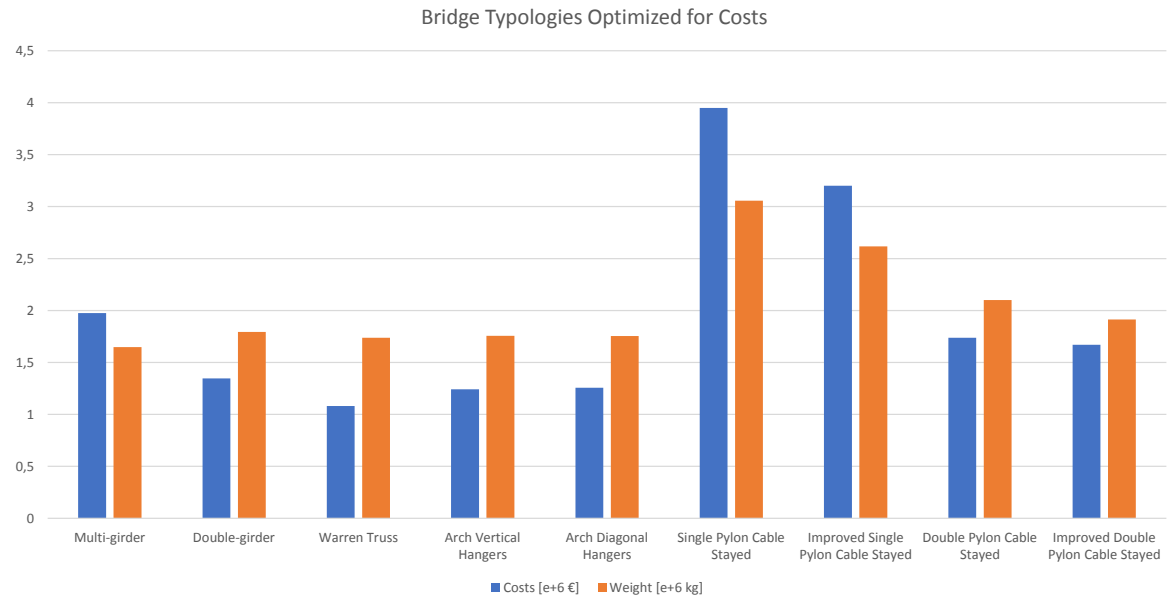

Figure 5.1: Bar chart showing the costs and weight of each for cost optimized bridge typology in absolute values

competitive, especially compared to the single pylon version. This is due to the fact that the total cable length is more than 25% shorter and because the cables can have a smaller diameter since a smaller component of the force is transferred to each pylon and therefore a smaller load is acting on the anchored cable stay. In other words, this symmetric design transfers the loads more efficiently towards the supports.

5.2. Weight

Next to the actual bridge structure, there are other costs involved in the construction of a bridge. One of these costs are the ones for the foundation of the bridge. The foundation is not considered during this research and therefore not designed, this means that no exact values are known for detailed comparison. One can argue however, that the higher the weight of the structure, the larger the foundation has to be designed to transfer all loads into the soil. With the generally weak soil conditions in the Netherlands, deep pile foundations are needed to reach strong sand layers capable of carrying the bridge with all of its loads. This makes the foundation an expensive part of the overall costs and any savings on this regard would be very beneficial.

All bridges, except the cable stayed ones, are very close regarding the total weight of the structure, with values around 1.7 million kilograms. The multi-girder bridge is the one with the lowest weight, this is due to the fact that the concrete deck can be slightly thinner with the small spacing of the longitudinal girders. The fact that there are six girders however, also means that there need to be six supports which all have their own foundation. These supports do carry a smaller part of the load. To be able to get decisive results, the foundation of the bridges should be designed. For now, the results are too close to make any statements.

The cable stayed bridges have a much larger weight, especially the pylons introduce large vertical forces to the foundations. Since the supports of the pylons and of the anchored stays are pinned, also large horizontal forces are introduced to the foundation. This is something that should be avoided when possible. One solution for the anchored stays would be to make the supports sliding and use the deck and girder structure to take up the horizontal forces.

5.3. Height

There are two different heights which can be compared. One is the structural height of the bridge, this mainly has an impact on the appearance of the bridge within its surrounding landscape. The other is the height of the top of the concrete deck, measured from the ground level next to the river of the considered case. These two values are depicted in Figure 5.4.

The bar chart in Figure 5.3 shows these two values for all bridges which are optimized for costs. The structural height shows the height of the structure measured from its support. This support is located at such

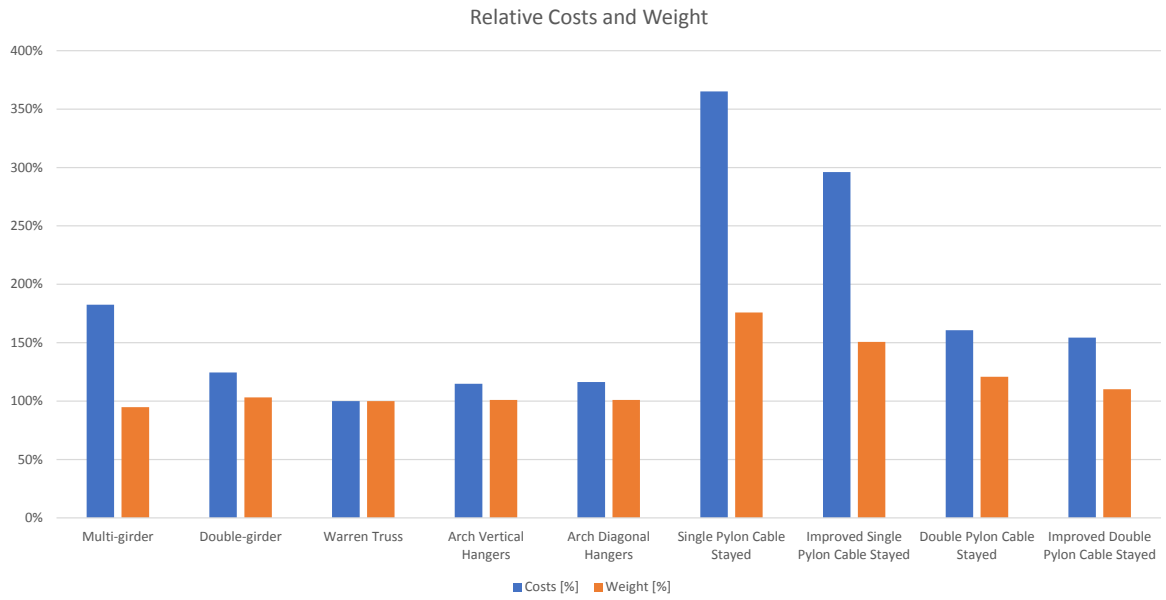

Figure 5.2: Bar chart showing the costs and weight of each for cost optimized bridge typology in relative values, with the warren truss set to 100%

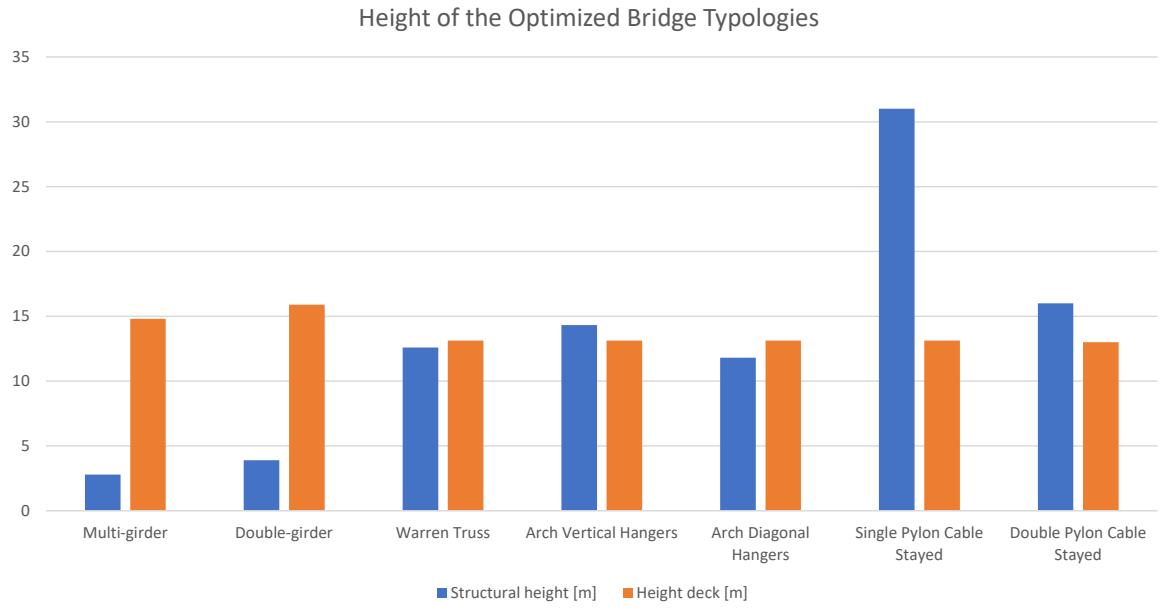

Figure 5.3: Bar chart showing the structural height and height of the road surface of each for cost optimized bridge typology

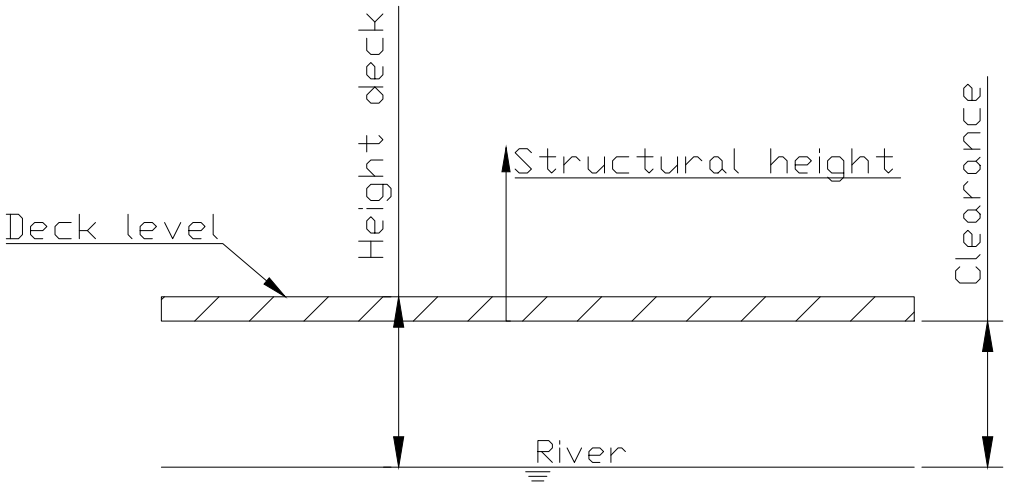

Figure 5.4: Schematisation explaining the structural height and the height of the deck of the bridge structures

a height that the minimal clearance of 12 metres beneath the bridge is reached. For the cable stayed bridges the lower part of the pylon, which is beneath the deck, is therefore not considered. The girder bridges show low structural heights, mostly governed by the height of the girders. The truss and arch bridges are already considerably higher, with values between 11 and 15 metres. What is noticeable is that the arch bridge with diagonal hangers has a lower height than the Warren truss. The Warren truss is a lot higher than the initial design with the rule of thumb of one-tenth of the span. The reasons for this are explained in the previous chapter. The prediction in section 2.1.2 that the diagonal hanger arch bridge could have a more slender design because of the bracing effect of the diagonal arches, is visible in the structural height of the arch bridges. The height of the pylons of the cable stayed bridges are governed by the minimal angle of the outermost stay of 30 degrees. The pylons of the double pylon bridge carry half of the span, making them half the height of the single pylon bridge.

The height of the top of the deck is more interesting for the overall costs of the bridge project. The road which is travelling over the bridge needs approach ramps to reach the height of the deck of the bridge. The higher this height, the larger the approach ramps need to be and the larger their costs will be. Just as with the foundations, these costs are substantial and need to be considered in a bridge project. What the bar chart shows is that the girder bridges have the highest level of the deck. This is due to the fact that the complete bridge structure is located beneath the deck. The higher the longitudinal girders, the higher the deck will be located. With all other bridges, the deck passes through the main load carrying system, only supported by the cross-beams.

5.4. Comparative Overview

To aid the decision making, and to better visualize how the bridge structures look like compared to one another and within the boundaries defined for the considered case, a comparative overview is beneficial.

In Figure 5.5 all optimized bridge structures are visualized from the side, together with the boundary conditions. Their performance regarding costs and weight is also included, with the size of the circles being scaled regarding to the values of the Warren truss bridge. In Appendix C a 3D perspective overview of every bridge structure within its surroundings is included.

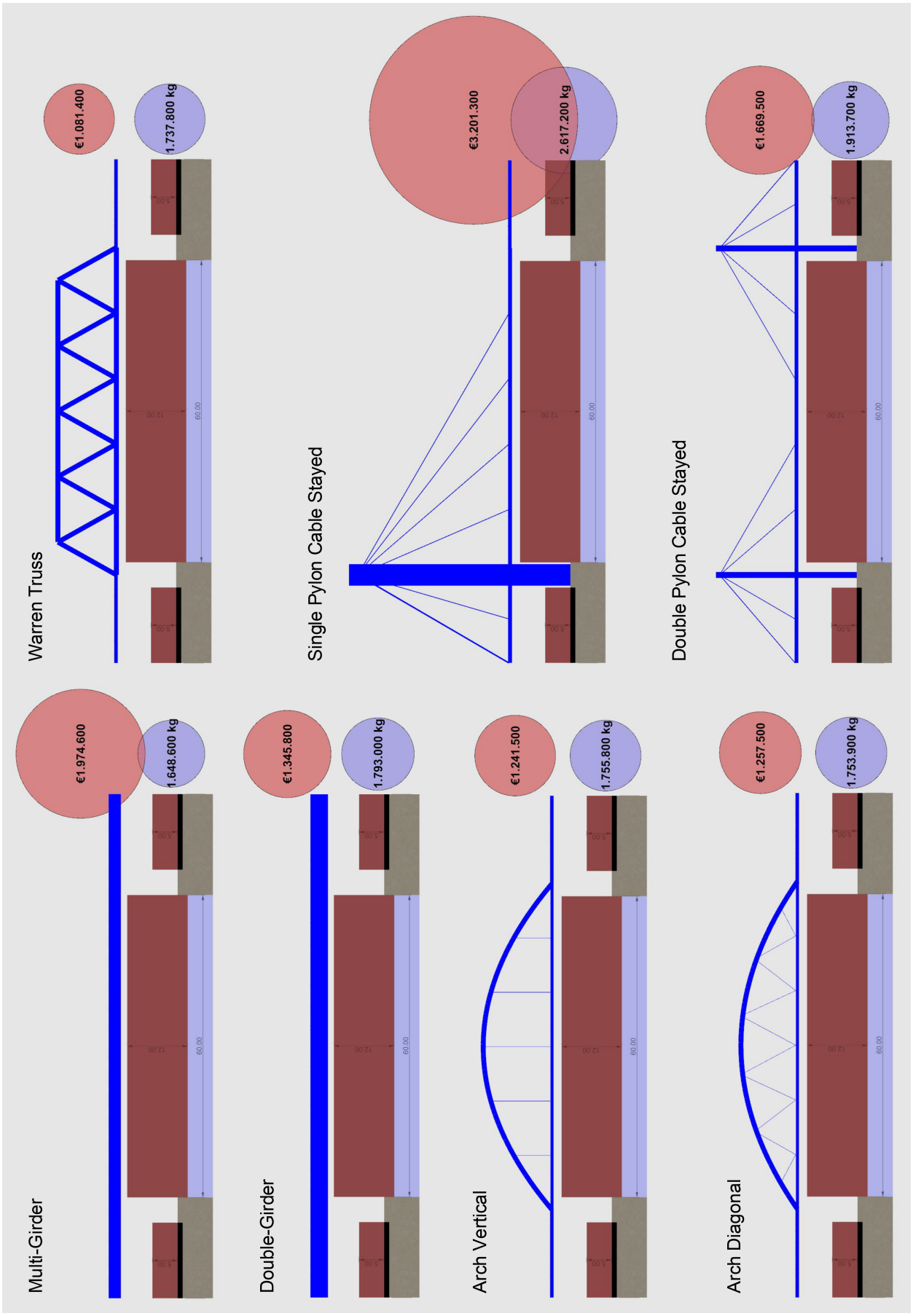

Figure 5.5: Comparative overview of all bridge typologies as seen from the side, including total cost and weight of the structures

6 Discussion

In this closing chapter conclusions regarding the parametric design process and optimization will be drawn, as well as on the obtained results. Furthermore, recommendations regarding improvements and future research will be discussed.

6.1. Conclusions

Conclusions are drawn based on the initial bridge designs and the forthcoming parameters, on the parametric design of the bridges, on the optimization and on the obtained results.

6.1.1. Initial Design and Parameters

Making initial designs and investigating which parameters are important for each different bridge, are important first steps before starting with the parametric model. It provides insight into the bridge behaviour and gives guidelines on how the geometry of the bridge can be described. With these guidelines the parametric model can be built not only quicker but also in a smarter way. The values selected to be parameters seemed to be correct for every bridge typology and were capable of optimizing the structures. There is however a difference in the number of parameters per typology. For the girder bridges the three parameters were sufficient, but for the truss bridge it would be interesting to also add the outer dimensions of the truss members as parameters. The arch bridges already have five parameters, so adding more would lead to a substantial increase in calculation time, but adding the outer dimensions of the arch ribs as parameters would also be interesting, since the arch ribs are one of the main load carrying elements.

The designs do cover the main steel bridge typologies constructed in the Netherlands and give sufficient insight in the differences in behaviour.

6.1.2. Parametric Design

Making use of parametric design software seems crucial to produce large amounts of variants in a short time frame. During optimization of the structure between five to ten thousand different variants were produced, calculated and assessed in a time frame of about one to two hours. But not only for optimization, also for changing boundary conditions and requirements, or for minor alterations or solving problems, the designs are easily adapted. Even the number of bays, hangers or cable stays is quickly changed and the influence of the change is immediately visible.

By making use of a single environment, for both design and structural analysis, all design changes are calculated real-time and results are directly visible. By making use of Karamba as a plug-in within Grasshopper no exchange of files is necessary for calculation of the structure in a different software program. This saves a lot of time, especially during optimization, and also prevents possible loss of data on the way. The single environment is beneficial for a quick and clear overview of the design and structure, and supports fast optimization. The downside of such a large model with seven different bridges is that the parametric model tends to get slower and making changes costs more time. The size and complexity of the parametric model makes it difficult to read and understand for persons not involved in this research.

Over the course of this research, more knowledge about the parametric software used was gained, and certain parts of the model were rewritten to make it more efficient. Due to the nature of parametric design

software, and due to the thought through structuring of the model, this was possible without large efforts.

6.1.3. Optimization

Optimization of the bridge structures was carried out with the evolutionary solver Galapagos. At first, the idea was to use the evolutionary solver Octopus. This solver is able to search for multiple objectives at once, as explained at the douple pylon cable stayed bridge. This solver proved to be slow during the first optimization runs, therefore is was decided to use Galapagos. Since Galapagos can only optimize for one objective, an approach had to be thought of where solutions which did not meet the requirements were discarded. The use of the if-statement with penalization of non-viable solutions seemed to be effective. Within a reasonably short amount of time large amounts of variants were produced and assessed, on average about 5000 per hour. With the right settings the solver was able to converge and find solutions.

In the end, Octopus was used to explore results of the double pylon cable stayed bridge which would be a trade-off between weight and costs. The same if-statements designed for Galapagos were used, and with this approach Octopus was also able to produce more variants in a shorter amount of time compared to the first trials with this solver.

One could argue that in stead of penalizing results which do not meet the requirements, it is desirable to completely exclude these solutions. In this way they will not be processed in the evolutionary solver, and all solutions produced during the optimization are viable ones. In this light, a new optimization procedure has been modelled, where the non-viable results are culled and a null-value is recorded in the solver. Also, a margin on the maximum deflection of +2% is included, since these small values do not significantly influence the structural behaviour nor the safety of the bridge. With this margin more design solutions can be considered.

The new optimization procedure has been tested and produces the same amount of variants per hour, with the beneficial effect that only viable solutions are recorded. This saves one step of manually filtering the results.

6.1.4. Results

After the first optimization runs, it was clear that the design of the cable stayed bridges could be improved to be closer to reality. This mainly concerned the option to include different diameters for the anchored cables.

The results show that, purely based on the costs of the bridge structure, the warren truss without verticals is the best solution for the fictional case considered in this research. For the span of 65 metres, this typology transfers the loads in the most efficient way towards the supports, resulting in minimal material usage. The Warren truss consumes less structural steel compared to the girder beam bridges and it also lacks the presence of expensive cables in the structure, this makes it the solution with the lowest costs. It is closely followed by both arch bridges and the double-girder bridge, however. Both cable stayed bridges are more expensive and due to the large amount of girders also the multi-girder bridge is expensive.

There are numerous other factors influencing the total costs of the whole project, as discussed in the previous chapter. These factors are not included in this research, but looking at how close the obtained results are, they might be decisive. Also the choice of parameters and minor design choices can affect the optimization outcomes in positive or negative favour per typology. These design choices could for instance be the option to have different diameters for all cable stays in the cable stayed bridges. Also considering different loading conditions or construction sequences could have a major impact on the results.

The 2D comparative overview, as well as the 3D overviews of all bridges within their environment, do support quick assessment of all optimized bridge structures.

6.2. Recommendations

For improvements and further research the following recommendations are stated.

6.2.1. Relation Between Parameters

Looking at the results of the optimization, and especially at the parallel coordinate plots (PCP), it might seem interesting to investigate whether there are relations between the parameters of a bridge. If there is a relation between for instance the increase of one parameter and the decrease of another, this relation could be used to guide or steer the optimization process. Certain behaviour could be predicted, or desired end results could be obtained.

6.2.2. Influence Range Parameters

Not only the relation between parameters, but also the influence of the choice for a specific range of parameters could be investigated. Several times the PCP's showed that parameters were at their lower or upper bound of their range. This implies that their range could be improved. There are, however, certain restrictions as a minimum plate thickness for example.

6.2.3. Interactive Visualization of Results

In the end, the goal of the parametric model is to quickly see the basic bridge designs for any specific set of requirements and to compare their performances. In this research the comparative overview is static and manually made. It would be beneficial to make these overviews interactive, so that every design choice is automatically updated in this overview. This could aid the decision making process, but also for sitting with clients or to explain effects of certain decisions, such an interactive visualization could be very helpful.

6.2.4. Height Cable Stayed Bridge Pylon

In this research, the height of the pylons of the cable stayed bridges is governed by the minimum angle of the outermost stays. This angle is set to 30°, as to prevent excessive sag of the cable and therefore loss of structural performance. The size of this angle could be up for debate, and it should be investigated whether this value of 30°can be improved.

6.2.5. Implementation Within the Design Process of Movares

At the start of this research, it was proposed to implement this parametric design in the overall design process of Movares. This could be done by means of programming or by using application programming interfaces (API's). During the course of this project there was not enough time available to learn programming, and therefore this part is less considered than previously desired.

By using API's, or one of the numerous plug-ins available for Grasshopper, it will be possible to implement the parametric model in the design process of Movares. For verification of results, the stresses, deflections and resulting forces in all bridge elements could be exported to a software program of ones liking.

A

Flowchart Parametric Model

In this appendix the flowchart representing the structure of the parametric model is presented. The flowchart resembles the flow of data for one bridge. For every bridge this structure is repeated, all within one single parametric model.

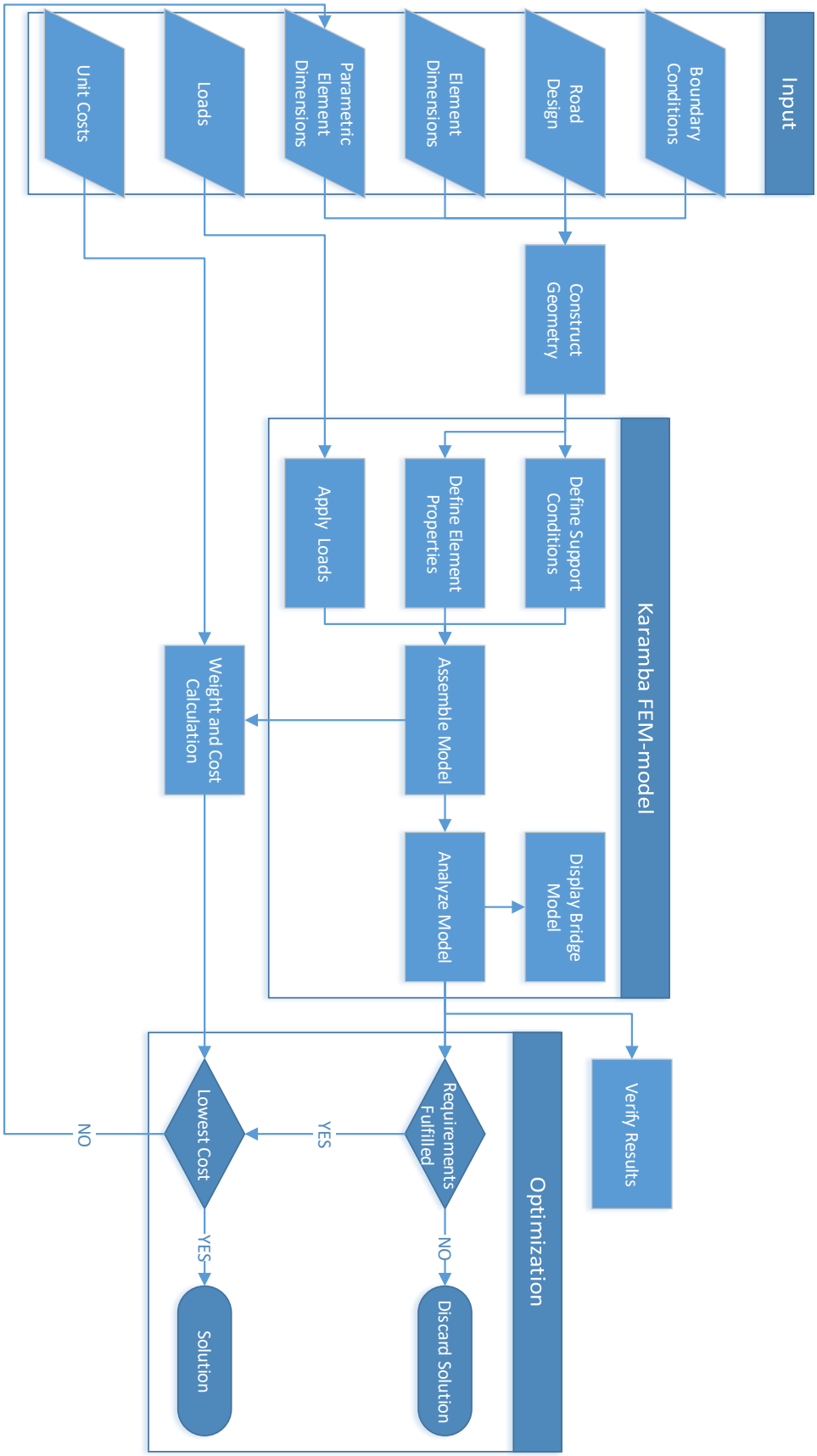

Figure A.1: Flowchart representing the structure of the parametric model, which is repeated for every bridge design

B

Bending Moments in Arches

In this appendix the Maple sheets to calculate the bending moments in both arch structures, the vertical hanger and diagonal hanger arches, are presented.

```
> restart;

Vertical Hanger Arch with ODE:
> L := 65 : f := 14 : q0 := 400 : EI := 2259810 :
> z := -4·f·x·(L - x)/L^2 : q := q0·Dirac(x - 1/4·L) :
> ODE := EI·diff(w(x), x$4) + H·diff(z, x$2) - q = 0;
> w := rhs(dsolve(ODE, w(x))) :
> phi := -diff(w, x) : M := EI·diff(phi, x) :

Boundary Conditions:
> x := 0 : eq1 := w = 0 : eq2 := M = 0 :
> x := L : eq3 := w = 0 : eq4 := M = 0 :
> sol := solve({eq1, eq2, eq3, eq4}, {_C1, _C2, _C3, _C4}) : assign(sol) : x :='x':

Find H with additional expression for zero horizontal displacements:
> eq5 := int(diff(w, x)·diff(z, x), x = 0..L) = 0 :
> H := solve(eq5, H) :
> evalf(H);
> plot(-M, x = 0..L, title = "Moment M");
> plot(-w, x = 0..L, title = "Displacement w");
>
```

Figure B.1: Maple sheet used to calculate the bending moment in the vertical hanger arch with the ODE for arches

```
> restart;

Diagonal Hanger Arch with ODE:
> L := 65 : f := 11 : q0 := 400 : EI := 2005762 :
> z := -4·f·x·(L - x)/L^2 : q := q0·Dirac(x - 0.41·L) :
> ODE := EI·diff(w(x), x$4) + H·diff(z, x$2) - q = 0;
> w := rhs(dsolve(ODE, w(x))) :
> phi := -diff(w, x) : M := EI·diff(phi, x) :

Boundary Conditions:
> x := 0 : eq1 := w = 0 : eq2 := M = 0 :
> x := L : eq3 := w = 0 : eq4 := M = 0 :
> sol := solve({eq1, eq2, eq3, eq4}, {_C1, _C2, _C3, _C4}) : assign(sol) : x :='x':

Find H with additional expression for zero horizontal displacements:
> eq5 := int(diff(w, x)·diff(z, x), x = 0..L) = 0 :
> H := solve(eq5, H) :
> evalf(H);
> plot(-M, x = 0..L, title = "Moment M");
> plot(-w, x = 0..L, title = "Displacement w");
>
>
```

Figure B.2: Maple sheet used to calculate the bending moment in the diagonal hanger arch with the ODE for arches

C

Three-Dimensional Overviews

This appendix covers the three-dimensional overviews of all optimized bridge structures. They are placed within the requirements and boundary conditions specified for the fictitious case which is considered during this research. These overviews help visualizing the structures within their surroundings and could aid the decision making process.

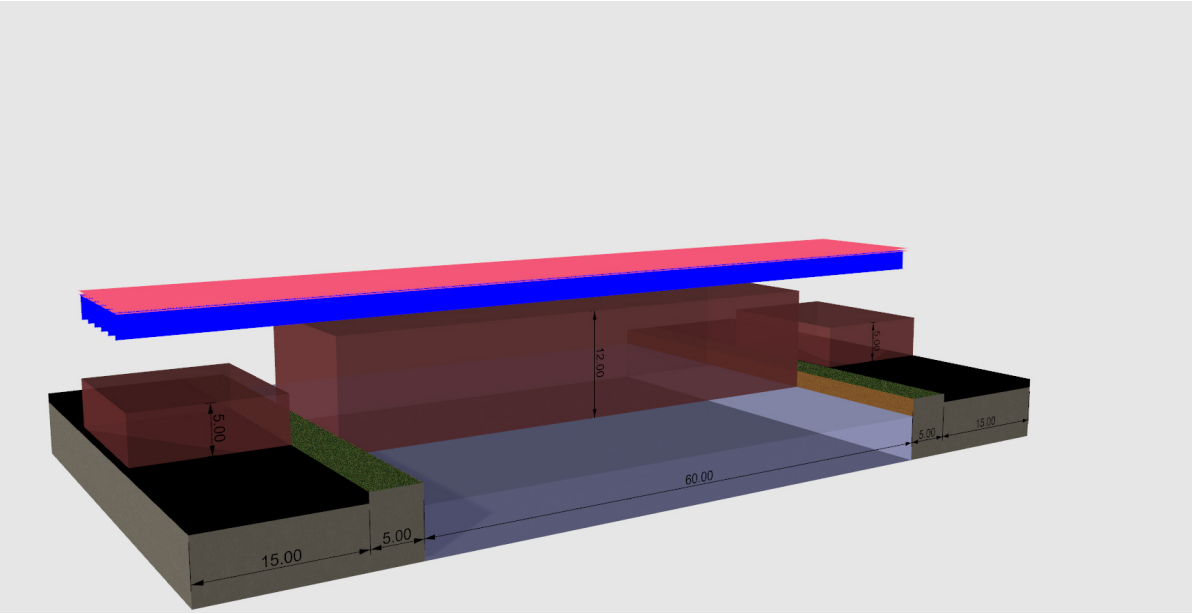

Figure C.1: Perspective overview of the multi-girder bridge design within its surroundings including required clearances

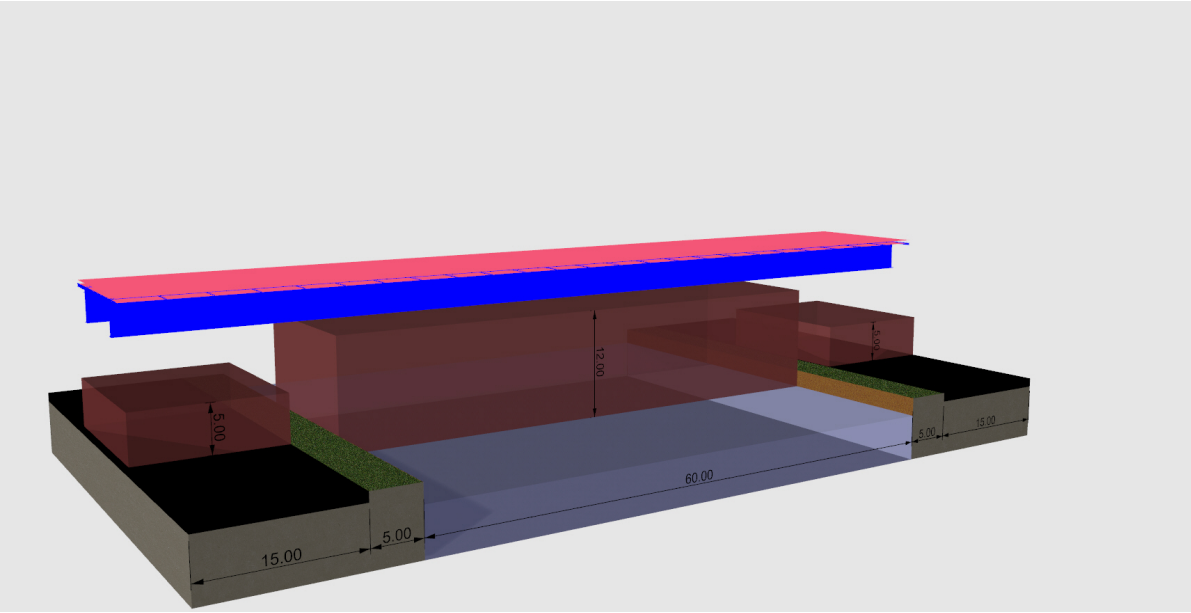

Figure C.2: Perspective overview of the double-girder bridge design within its surroundings including required clearances

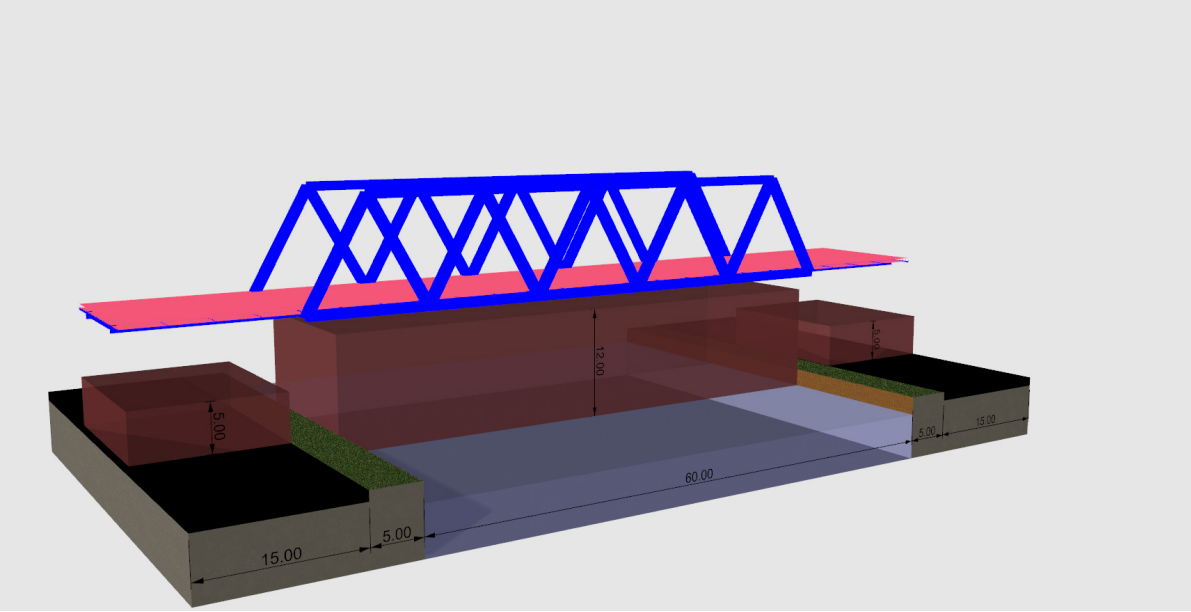

Figure C.3: Perspective overview of the Warren truss bridge design within its surroundings including required clearances

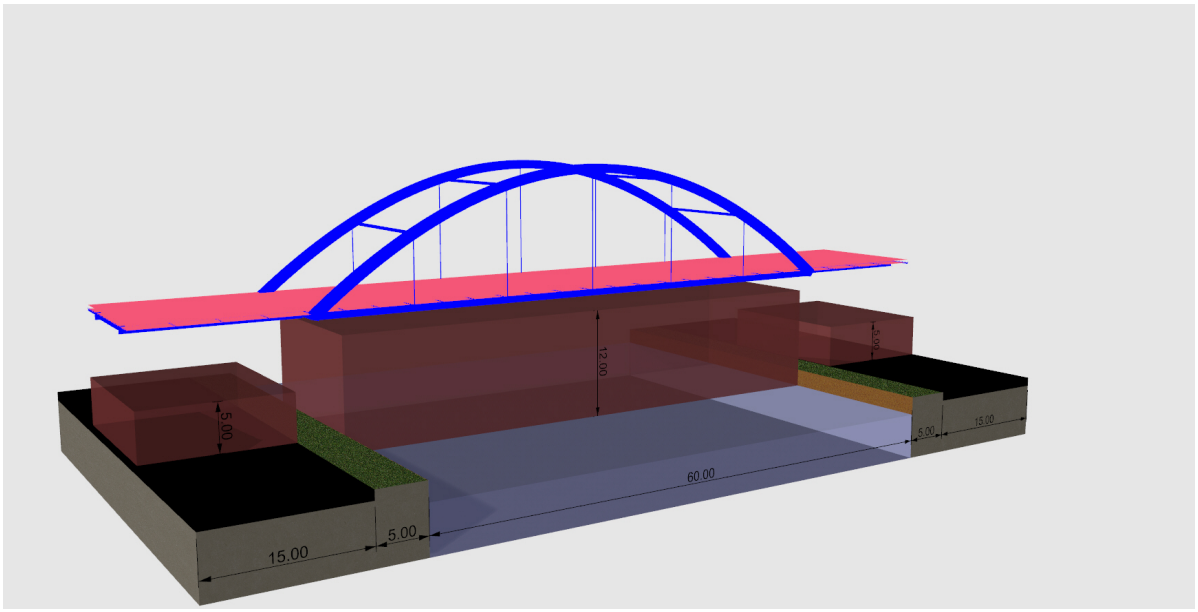

Figure C.4: Perspective overview of the vertical hanger arch bridge design within its surroundings including required clearances

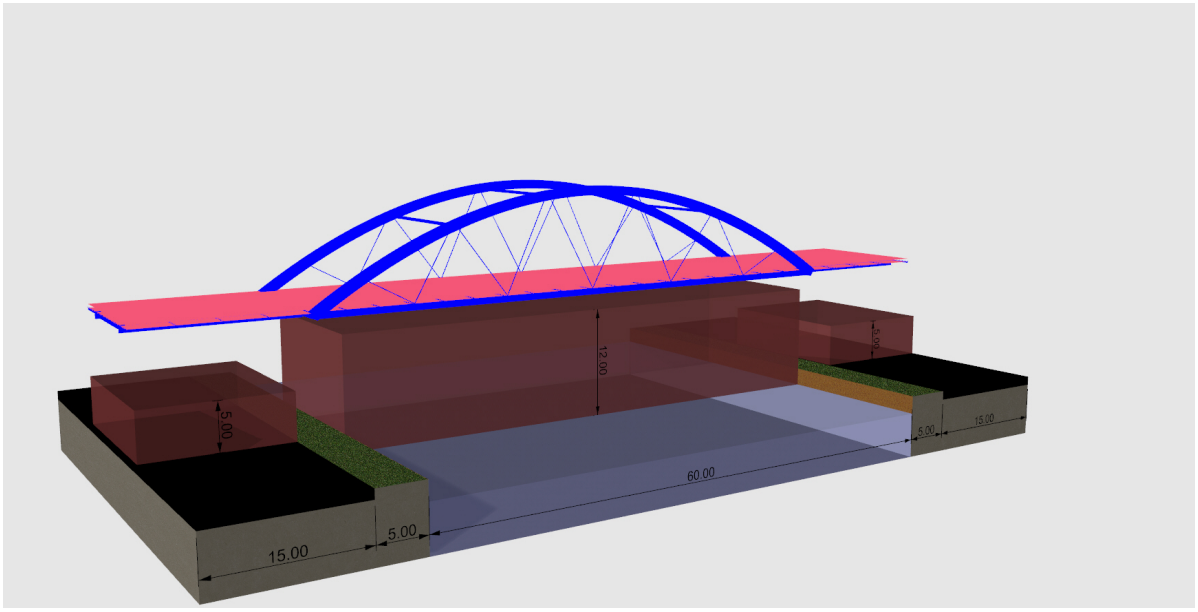

Figure C.5: Perspective overview of the diagonal hanger arch bridge design within its surroundings including required clearances

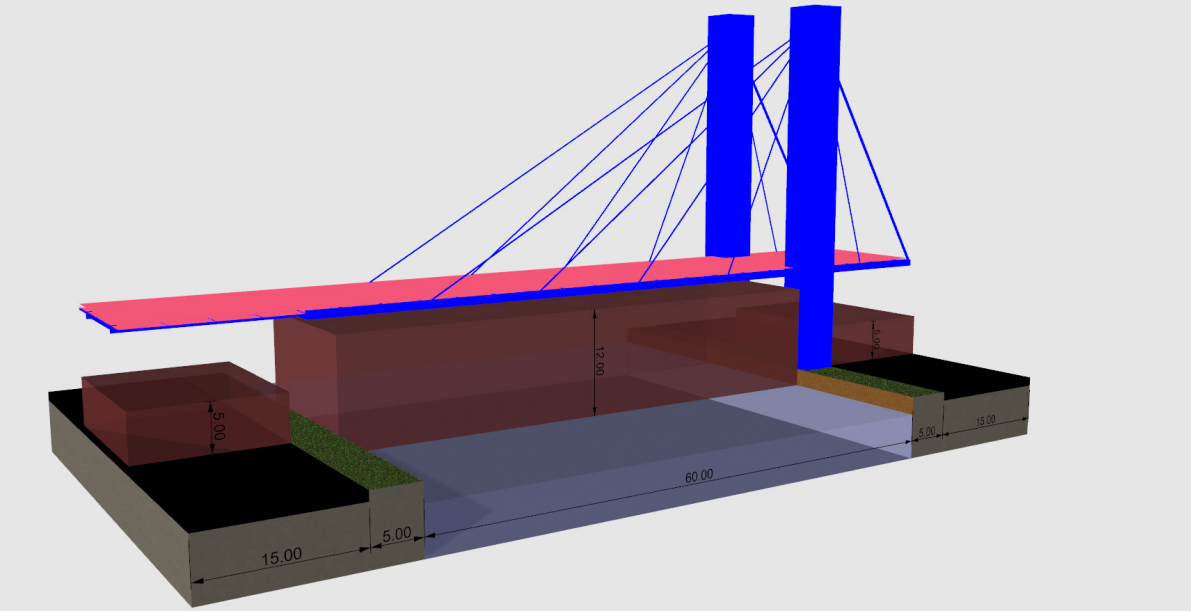

Figure C.6: Perspective overview of the single pylon cable stayed bridge design within its surroundings including required clearances

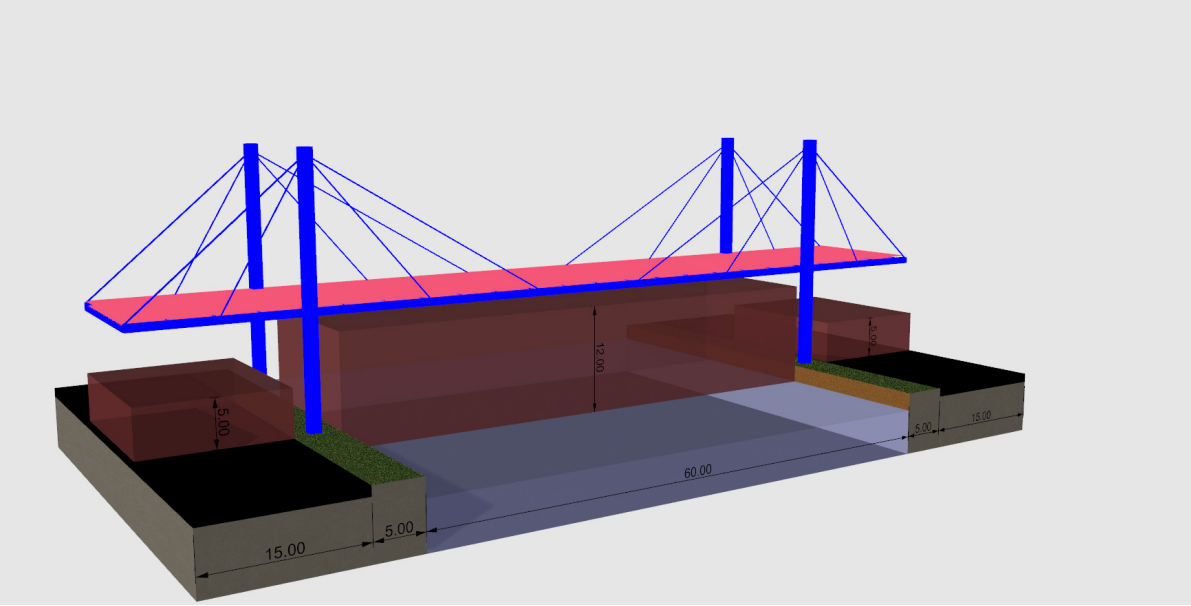

Figure C.7: Perspective overview of the double pylon cable stayed bridge design within its surroundings including required clearances

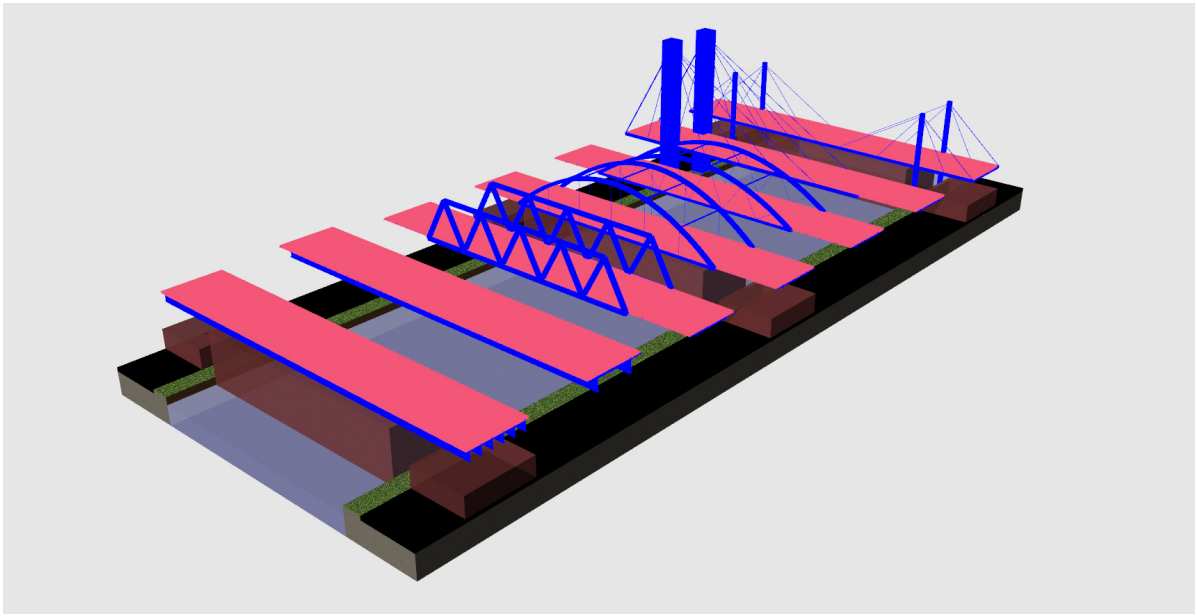

Figure C.8: Perspective overview of all bridge designs within the surroundings including required clearances

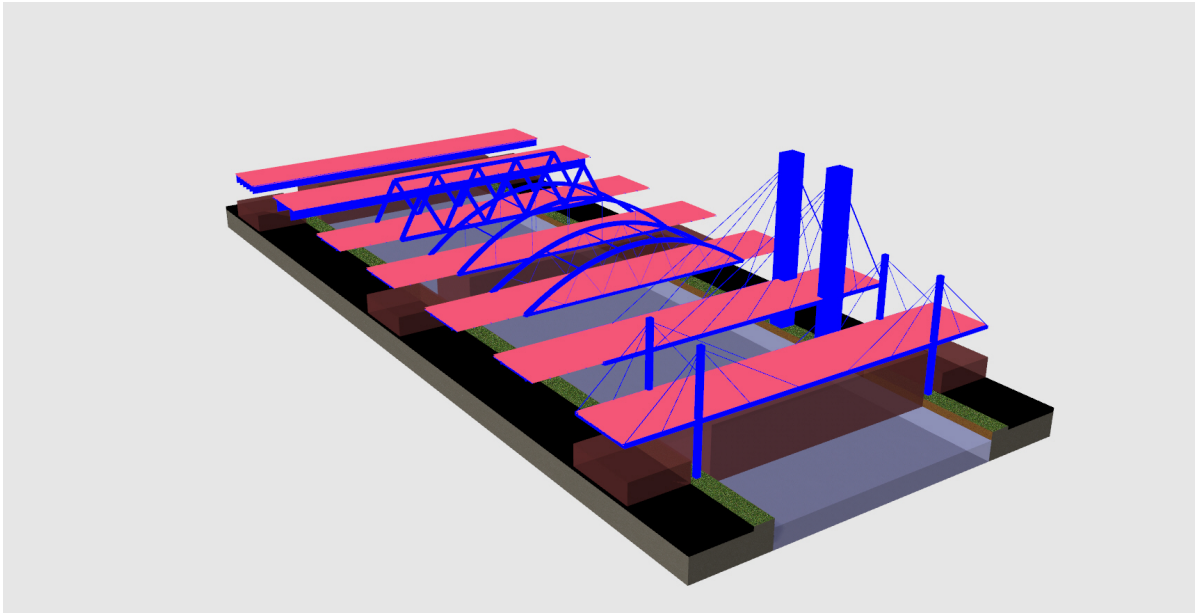

Figure C.9: Perspective overview of all bridge designs within the surroundings including required clearances

Bibliography

[1] Design Explorer. URL tt-acm.github.io/DesignExplorer/.

[2] Grasshopper. URL http://www.grasshopper3d.com/.

[3] NEN-EN 1991-2 + C1. (ICS 91.010.30; 93.040), 2015.

[4] J.U. Brolsma. Rapportage Containerhoogtemetingen. Technical report, Rijkswaterstaat Dienst Verkeer en Scheepvaart, Driebergen, 2015.

[5] Wai-Fah Chen and Lian Duan. *Bridge engineering handbook. Fundamentals.* CRC Press, second edition, 2014. ISBN 9781439852347.

[6] Wai-Fah Chen and Lian Duan. *Bridge engineering handbook. Superstructure design.* CRC Press, second edition, 2014. ISBN 9781439852293.

[7] David Collings. *Steel-Concrete Composite Bridges - Designing with Eurocodes.* 2013. ISBN 9780727758101.

[8] COMSOL. The Finite Element Method (FEM). URL https://www.comsol.com/multiphysics/finite-element-method.

[9] D.J. Farquhar. *Manual of Bridge Engineering.* ICE Publishing, 2000. ISBN 9780727738028.

[10] Glenn Burrows. Bridges 1. URL https://www.emaze.com/@AFCRCLOI/Bridges-1.

[11] Coen Hartsuijker and Hans Welleman. *Module : Non-Symmetrical and Inhomogeneous Cross Sections.* Number October. 2017. ISBN 9039505942.

[12] J.J.M. Haug and F. Schuurman. Voetpaden voor iedereen. Technical report, Bouw Advies Toegankelijkheid, 2017.

[13] Jean-Paul Lebet and Manfred A. Hirt. *Conceptual and Structural Design of Steel and Steel-Concrete Composite Bridges.* 2013. ISBN 9781466572973.

[14] António Leitão, Luís Santos, and José Lopes. Programming Languages for Generative Design: A Comparative Study. *International Journal of Architectural Computing*, 10(1):139–162, 2012. ISSN 1478-0771. doi: 10.1260/1478-0771.10.1.139. URL http://journals.sagepub.com/doi/10.1260/1478-0771.10.1.139.

[15] ParametricCamp. What is Parametric Design? URL http://www.parametriccamp.com/en/what-is-parametric-design/.

[16] Alessio Pipinato. *Innovative bridge design handbook: construction, rehabilitation and maintenance.* Butterworth-Heinemann, imprint of Elsevier, Kidlington, Oxford, UK, 2015. ISBN 9780128000588.

[17] Clemens Preisinger. Linking Structure and Parametric Geometry. *Architectural Design*, 83(2):110–113, 2013. doi: 10.1002/ad.1564.

[18] David Rutten. Evolutionary Principles applied to Problem Solving, 2010. URL http://www.grasshopper3d.com/profiles/blogs/evolutionary-principles.

[19] G. Schermers and J.W.H. van Petegem. Veiligheidseisen aan het dwarsprofiel van gebiedsontsluitingswegen met limiet 80 km/uur. Technical report, Stichting Wetenschappelijk Onderzoek Verkeersveiligheid SWOV, Leidschendam, 2013.

[20] I Vayas and A Iliopoulos. *Design of Steel-Concrete Composite Bridges to Eurocodes.* 2014. ISBN 9781466557451.

[21] T. Zeegers. Over breedtes van fietspaden. Technical report, CROW fietsberaad, 2004.